# U–Pb Dating of Mineral Deposits: From Age Constraints to Ore-Forming Processes

Cyril Chelle-Michou and Urs Schaltegger

**Abstract**

The timing and duration of ore-forming processes are amongst the key parameters required in the study of mineral systems. After more than a century of technical developments, innovations and investigation, the U–Pb system arguably is the most mature radioisotopic system in our possession to conduct absolute dating of a wide range of minerals across geological environments and metallogenic processes. Here, we review the basics of U–Pb geochronology, the key historic developments of the method, and the most commonly used analytical techniques (including data reduction, Pb-correction, uncertainty propagation and data presentation) and minerals while pointing out their respective advantages, weaknesses and potential pitfalls. We also highlight critical aspects that need to be considered when interpreting a date into the age of a geological process (including field and petrographic constraints, open-system behavior, handling and interpretation of uncertainties). While U–Pb geochronology is strongly biased toward zircon dating, we strive to highlight the great diversity of minerals amenable to U–Pb dating (more than 16 mineral species) in the context of mineral systems, and the variety of geological events they can potentially date (magmatism, hydrothermal activity, ore-formation, cooling, etc.). Finally, through two case studies we show (1) how multi-mineral geochronological studies have been used to bracket and decipher the age of multiple geological events associated with the world-class Witwatersrand gold province, and (2) how rather than the absolute age, the duration and rate of the mineralizing event at porphyry copper deposits opens new avenues to understand ore-forming processes and the main controls on the size of such deposits. The improving precision, accuracy and spatial resolution of analyses in tandem with high-quality field and petrographic observations, numerical modelling and geochemical data, will continue to challenge paradigms of ore-forming processes and contribute significant breakthroughs in ore deposit research and potentially to the development of new exploration tools.

C. Chelle-Michou (✉)
Department of Earth Sciences, ETH Zurich, Clausiusstrasse 25, 8092 Zurich, Switzerland
e-mail: cyril.chelle-michou@erdw.ethz.ch

U. Schaltegger
Department of Earth Sciences, University of Geneva, Rue des Maraîchers 13, 1205 Geneva, Switzerland

## 1 Introduction

The knowledge of the timing and duration of ore-forming processes are perhaps one of the most desirable pieces of information that geologists



D. Huston and J. Gutzmer (eds.), *Isotopes in Economic Geology, Metallogenesis and Exploration*, Mineral Resource Reviews, https://doi.org/10.1007/978-3-031-27897-6_3

require to draw a complete picture of the deposit and to put its genesis into a coherent regional or even global geological framework. In many cases, it represents an essential parameter for establishing detailed genetic models, and can critically impact on exploration strategies. This necessarily requires a reliable, precise and accurate geochronometer.

In the past two decades, U–Pb dating has seen a remarkable success across the Earth Sciences to become the most commonly used absolute isotopic geochronometer. This great success results from considerable improvements in the analytical techniques and in advances of our understanding of the U–Pb system in the geological environment. The paramount advantage of U–Pb dating relies on the coexistence of two chemically identical but isotopically distinct radioisotopes of U ($^{238}$U and $^{235}$U), both of which have their very own decay chain and decay rates. Furthermore, their half-lives are particularly suitable for geologically relevant ages. This allows the determination of two independent dates of which equivalence (concordance) can usually be taken as a sign of the meaningfulness of the date, while discordant dates can be either geologically irrelevant or may be extrapolated to a meaningful date if the cause(s) of this discordance can be identified.

The recent success of U–Pb geochronology is the result of numerous stepwise improvements over the last decades (see detailed history in Davis et al. 2003; Corfu 2013; Mattinson 2013), but has experienced a boost due to coordinated community efforts (EARTHTIME for isotope dilution analysis: http://www.earth-time.org; PLASMAGE for laser ablation analysis: http://www.plasmage.org).

Geochronology was born out of the U–Pb system. Radioactivity was discovered at the dawn of the nineteenth century by H Becquerel, M and P Curie in their work with various uranium compounds (U-salts, U-metal, pitchblende) (Becquerel 1896a, b; Curie et al. 1898; Curie and Skolodowska Curie 1898; Skolodowska Curie 1898). Soon after, E Rutherford first suggested that the Pb/U ratio of geological materials could be used to date them (Rutherford 1906). The next year, B Boltwood applied this method to 43 uranium ore samples and obtained the first absolute total-U and total-Pb ages ranging from 410 to 2200 Ma (Boltwood 1907). This revolution conclusively supported the suggestion made by Charles Darwin half a century prior, that the earth was several hundred million years old, and was about to provide absolute age calibrations for the geological timescale of A Holmes (1911, 1913). However, it was not until the turn of 1930 that the existence of two radioactive U isotopes and their respective Pb daughter isotopes was recognized in U ores (Rutherford 1929; Aston 1929; von Grosse 1932), paving the way for modern U–Pb geochronology. Ever since, improvements in mass spectrometry, laboratory procedures and advances in nuclear physics have permitted the analysis of increasingly smaller quantities of U and Pb with improved precision and accuracy. This in turn, enabled a switch from the analysis of U ore minerals, to low-U bearing minerals such as zircon, titanite and apatite in the second half of the last century (Larsen et al. 1952; Tilton et al. 1955, 1957; Webber et al. 1956). However, dating still involved multigrain mineral fractions which typically show discordance between $^{206}$Pb/$^{238}$U and $^{207}$Pb/$^{235}$U dates, and render their interpretation subjected to debate, assumption and uncertainty. The 1970s to 1980s period arguably marks the turning point of U–Pb geochronology. At that time, the development of low blank single grain zircon dating (Mattinson 1972; Krogh 1973; Krogh and Davis 1975; Lancelot et al. 1976; Michard-Vitrac et al. 1977; Parrish 1987), air-abrasion techniques (Krogh 1982) and in-situ ion probe dating (Hinthorne et al. 1979; Hinton and Long 1979; Froude et al. 1983) concurred to routinely produce concordant U–Pb ages and triggered an expansion in the range of application of U–Pb dating across various minerals, geological terrains and planetary materials. The 1990s saw the advent of the chemical abrasion technique (Mattinson 1994) and of laser-ablation inductively coupled plasma mass spectrometry (Fryer et al. 1993; Horn et al. 2000) that are now

common practices in many laboratories around the world. This is the time when U–Pb dating was embraced by the Earth Sciences community, and became an essential tool of geological mapping and mineral exploration. Perhaps as a sign of a mature discipline, the last decade has seen U–Pb practitioners around the world collaborating in a community driven effort to push precision, accuracy and inter-laboratory reproducibility of dates toward unprecedented limits, the EARTHTIME initiative (http://www.earthtime.org).

This century of development of U–Pb dating has left us with a powerful tool for ore deposit studies. While zircon is arguably the most commonly used and understood mineral due to its robustness and minimal amount of Pb it can incorporate in its lattice during crystallization (so-called "common" Pb), a number of other U-bearing minerals are amenable to U–Pb dating (e.g., titanite, apatite, monazite, xenotime, rutile, baddeleyite, perovskite, columbo-tantalite, cassiterite, allanite, calcite, etc.). While most minerals can date their crystallization, a handful of them (e.g., apatite, rutile, titanite) actually date their arrival below their respective closure temperature for the U–Pb system. This diversity of minerals allows a variety of ore deposit types and related geological processes (magmatic, hydrothermal, metamorphic, sedimentary and supergene) to be dated. As we write, U–Pb dates have been published on almost the full spectrum of deposit types and an increasing number of minerals are being tested and improved for U–Pb geochronology. However, the systematics of the U–Pb system are only really well-known in zircon and possibly monazite, followed by titanite, apatite, rutile, baddeleyite, and xenotime.

Geochronology can illuminate the apparent geological chaos at some deposits or districts, as well as support, refute or generate hypotheses for ore-forming processes. Nevertheless, only in rare cases does the dated mineral directly date the ore itself (e.g., columbo-tantalite, cassiterite, uraninite). As examples, zircon from a porphyry stock dates magma intrusion and not the cross-cutting copper mineralization, titanite in a skarn dates the high temperature metasomatism and not the deposition of the polymetallic ore at lower temperature. Some minerals may date magmatic crystallization (e.g., zircon, baddeleyite), or metamorphic reactions (e.g., monazite, titanite) and some may date their precipitation from hydrothermal fluids (e.g., monazite, xenotime, calcite, uraninite). In fact, the meaning of any date remains deeply anchored into proper field observations and sample characterization. Some minerals and dating methods (e.g., fission tracks in apatite and zircon, $^{40}Ar/^{39}Ar$ in micas and K-feldspar, etc.) can also record low-temperature events that that post-date ore formation, allowing a fuller understanding of the coupled temperature–time evolution of mineral systems.

While U–Pb geochronology has been extensively used to determine the age of geological events, it remains to current and future generations of scientists to give increasingly more added value to increasingly more precise and accurate dates, feeding quantitative and numerical models or ore-forming processes. For example, when combined with numerical models, the duration of magmatic-hydrothermal events or the probability density distribution of a population of dates may be interpreted in terms magmatic-hydrothermal flux and volume (Caricchi et al. 2014; Chelle-Michou et al. 2017). This will be a critical step if we want to uncover the processes at play during ore formation, and provide mineral exploration professionals with innovative and efficient tools that may help locating a distant or deeply buried deposit, or that could provide early information on the potential size of the explored deposit (e.g., Chelle-Michou et al. 2017).

This chapter reviews the basics of the U–Pb geochronology and the most commonly used dating techniques and minerals while pointing out their respective advantages, weaknesses and potential pitfalls. Through a series of case studies, we illustrate the various usages of U–Pb dating for the study of mineral deposits. Admittedly, U–Pb geochronology is a field that is strongly biased toward the use of zircon and this chapter is not an exception. Nevertheless,

we will also shed light on U–Pb dating applied to less commonly encountered and dated minerals.

## 2 Basics of U–Pb Geochronology

### 2.1 The U–Pb System

On first approximation, both naturally occurring long-lived parent uranium isotopes ($^{238}$U and $^{235}$U) decay to stable lead isotopes ($^{206}$Pb and $^{207}$Pb, respectively) at distinct rates, and thus have different half-lives and decay constants ($\lambda_{238}$ and $\lambda_{235}$). Details of the U decay to Pb are actually more complex and involve a long chain of alpha or beta decays with the production of a number of intermediate daughter isotopes (Fig. 1a). This allows the formulation of two generalized age equations:

$$\left(\frac{^{206}\mathrm{Pb}}{^{204}\mathrm{Pb}}\right) = \left(\frac{^{206}\mathrm{Pb}}{^{204}\mathrm{Pb}}\right)_0 + \left(\frac{^{238}\mathrm{U}}{^{204}\mathrm{Pb}}\right)\left(e^{\lambda_{238}t} - 1\right), \quad (1)$$

$$\left(\frac{^{207}\mathrm{Pb}}{^{204}\mathrm{Pb}}\right) = \left(\frac{^{207}\mathrm{Pb}}{^{204}\mathrm{Pb}}\right)_0 + \left(\frac{^{235}\mathrm{U}}{^{204}\mathrm{Pb}}\right)\left(e^{\lambda_{235}t} - 1\right), \quad (2)$$

where $^{204}$Pb is the only non-radiogenic isotope of Pb and the subscript 0 indicate the initial isotopic composition of lead at the time (t) when the system closed. In cases where the proportion of initial to radiogenic Pb is negligible, which is common for zircon, monazite, and xenotime, Eqs. (1) and (2) can be simplified:

$$\left(\frac{^{206}\mathrm{Pb}^*}{^{238}\mathrm{U}}\right) = e^{\lambda_{238}t} - 1, \quad (3)$$

$$\left(\frac{^{207}\mathrm{Pb}^*}{^{235}\mathrm{U}}\right) = e^{\lambda_{235}t} - 1, \quad (4)$$

where the superscript * indicate the amount of radiogenic Pb that has formed since the system closed. If the system has remained closed since the mineral crystallized, the $^{206}$Pb/$^{238}$U and $^{207}$Pb/$^{235}$U dates should be identical. Dividing Eqs. (1) and (2) yield a third age equation:

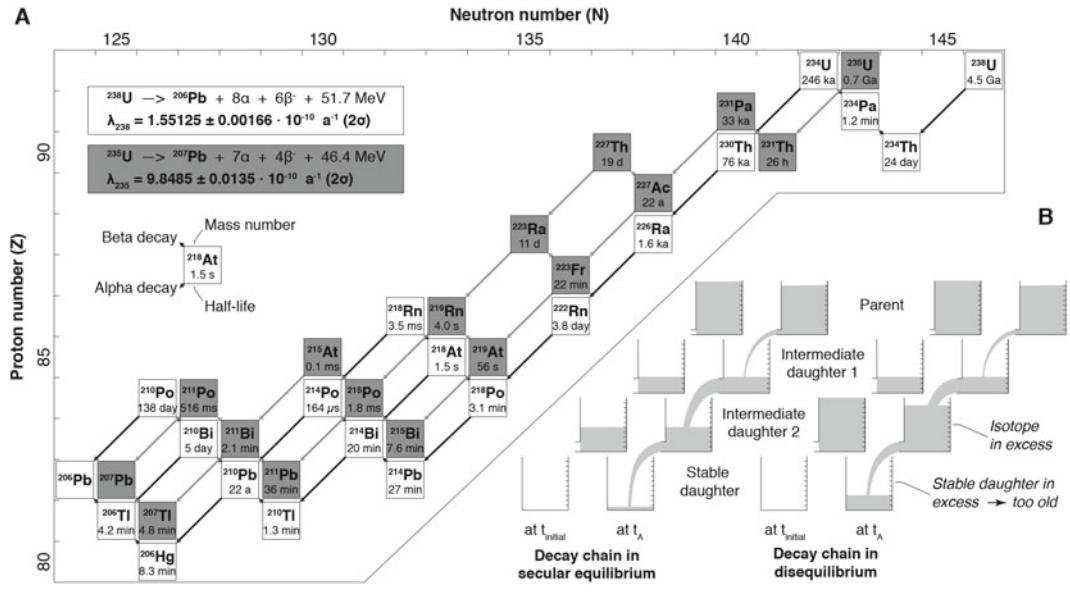


**Fig. 1** **a** Decay chains of $^{238}$U and $^{235}$U with the approximate half-life indicated for each radionuclide. **b** Cartoon illustrating the difference between a decay chain in secular equilibrium and one in disequilibrium. $t_{initial}$ and $t_A$ refer to the time immediately after and some time after mineral crystallization, respectively

$$\frac{\left(\frac{^{207}Pb}{^{204}Pb}\right) - \left(\frac{^{207}Pb}{^{204}Pb}\right)_0}{\left(\frac{^{206}Pb}{^{204}Pb}\right) - \left(\frac{^{206}Pb}{^{204}Pb}\right)_0} = \left(\frac{^{207}Pb}{^{206}Pb}\right)^* = \left(\frac{^{235}U}{^{238}U}\right)\frac{\left(e^{\lambda_{235}t} - 1\right)}{\left(e^{\lambda_{238}t} - 1\right)}. \quad (5)$$

This equation has the advantage that the determination of the age does not require measurement of the U isotopes because the present-day $^{238}U/^{235}U$ ratio is mostly constant in U-bearing accessory minerals and equal to 137.818 ± 0.045 (2σ; Hiess et al. 2012). However, in practice, $^{207}Pb/^{206}Pb$ dates are relevant only for ages older than ca. 1 Ga (see below). The constancy of this ratio and the low abundance of $^{235}U$ further allow the measurement of the $^{235}U$ to be neglected, which is common practice in many laboratories.

Decay constants for $^{238}U$ and $^{235}U$ are by far the most precisely determined ones among those used in geochronology. Recommended values are those determined by Jaffey et al. (1971) and are $\lambda_{238} = 1.55125 \pm 0.00166 \cdot 10^{-10}$ $a^{-1}$ and $\lambda_{235} = 9.8485 \pm 0.0135 \cdot 10^{-10}$ $a^{-1}$ (2σ) (Schoene 2014). However, these constants have been suggested to be slightly inaccurate (Schoene et al. 2006; Hiess et al. 2012), but always within their reported 2σ uncertainties. More accurate values may be available in the future providing further counting experiments are done.

## 2.2 Data Presentation

The trinity of age equations presented above (Eqs. 3–5) has promoted the emergence of U–Pb specific plots, the concordia diagrams, that provide a convenient and elegant representation of the data. By far, the most common visual representations of U–Pb data use either the Wetherill concordia plot (Fig. 2a; Wetherill 1956) or the Tera-Wasserburg concordia plot (Fig. 2b; Tera and Wasserburg 1972a, b). These concordia diagrams are bivariate plots where each axis corresponds to one of the three isotopic ratios used in eqs. 3–5 or their inverse (i.e., $^{206}Pb/^{238}U$, $^{238}U/^{206}Pb$, $^{207}Pb/^{235}U$ and $^{207}Pb/^{206}Pb$). On each diagram, the curve represents the line where both isotopic ratios (in abscissa and ordinate) correspond to the same dates, it is the so-called concordia curve. The curvature of the concordia simply reflects the contrasted decay rates of $^{238}U$ and $^{235}U$. If the U–Pb system has remained closed since the crystallization of the mineral and no common Pb is present, the three dates will be the same and plot on the Concordia line, meaning they are be concordant.

For both diagrams (Fig. 2a, b), each analysis is represented by an ellipse where the center is the measured isotopic ratios and the size of the ellipse depicts the analytical uncertainties at a given level of confidence (usually 2σ). Additionally, uncertainties of isotopic ratios plotted on both axis of the concordia diagram are not fully independent from each other and often correlated (e.g., York 1968; Ludwig 1980). This is either due to the use of the $^{206}Pb$ measurement on both ratios of the Tera-Wasserburg plot or to the use of $^{238}U$ to calculate $^{235}U$ for the Wetherill diagram. Thus, the orientation of the uncertainty ellipse reflects the correlation (or covariance) of the errors.

For data that are concordant, it is also convenient to use only the most precise of the three isotopic dates (usually the $^{206}Pb/^{238}U$ or $^{207}Pb/^{206}Pb$ date) and plot them as ranked bars of which the center represents the date and the length reflect the associated uncertainty (Fig. 2c). For a population of dates, the same information can also be presented as a probability density function (Fig. 2c) or a kernel density estimate. The latter is particularly suitable for detrital studies (e.g., Vermeesch 2012).

Because the production of these specific diagrams can be quite labor intensive and calculations in geochronology involve advanced statistical methods, it is recommended to use available software packages dedicated to isotopic geochronology. The most popular and versatile package is the Isoplot Microsoft Excel VBA add-in of K Ludwig (Ludwig 2012) that has served isotope geochronologists for nearly two decades. However, Isoplot is no longer being updated for later versions of Microsoft Excel (last versions

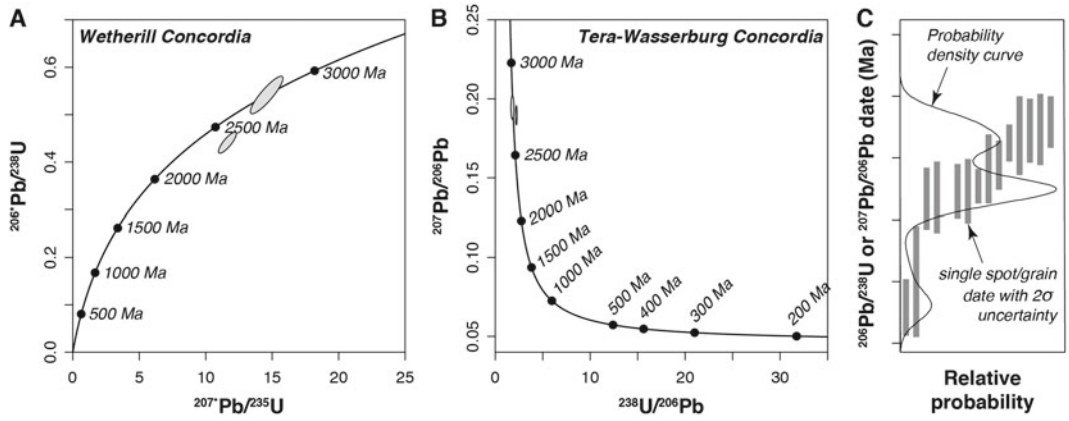


**Fig. 2** Classical plots used to present U–Pb geochronological data. **a** Wetherill concordia plot with one concordant and one discordant analysis shown as example, **b** Tera-Wasserburg concordia plot with the same analyses, **c** ranked isotopic date plot for synthetic concordant data together with the corresponding probability density curve. Note that the while the y-axis is valid for both the data bars and the density curve, the x-axis labelled "relative probability" is only relevant for the probability density curve. Single spot/grain dates are ranked only to facilitate the reading of the figure

working on Excel 2010 on PC and Excel 2004 on Mac). This was the incentive for the development of the multiplatform replacement geochronological application IsoplotR. IsoplotR is a package developed for the R statistical computing and graphics software environment by P. Vermeesch (University College London, UK) and can be used through the command line in R or as an online RStudio Shiny applet at http://isoplotr.london-geochron.com (Vermeesch 2018).

## 2.3 Causes of Discordance

Since the beginning of isotopic dating, discordance has been the main concern of U–Pb geochronologists. Ultimately, understanding the causes of discordance and trying to eliminate it has been the most powerful driving force to advance U–Pb dating during the second half of the twentieth century (Corfu 2013). It is now established that discordance can have a number of origins including: mixing of various age domains, Pb-loss during physical and chemical changes in the crystal lattice (partially opened system), initial intermediate daughter isotopic disequilibrium, incorrect or no correction for non-radiogenic Pb, or a combination of these (Fig. 3). Nevertheless, one should keep in mind that the recognition of some dates as being discordant is intimately tied to the uncertainty of the data. Indeed, low-precision data might appear perfectly concordant, while high-precision ones would actually reveal otherwise (e.g., Moser et al. 2009). This means that any method is blind to discordance at a degree that is inferior to the best age resolution of that method. Below we present the classical causes of discordance and the most appropriate ways to avoid, mitigate or value them.

### 2.3.1 Mixing Multiple Age Domains

A number of minerals (e.g., zircon, monazite, xenotime) often record multiple growth events. The recognition of different growth zones is crucial for the analysis and interpretation of any dating result. Imagery using transmitted and reflected light together with cathodoluminescence (CL) and back-scattered electron (BSE) microscopy greatly aids in this process but is not always definitive. These images can reveal that a mineral grain can be made up of a sequence of growth zones starting in the center, and mantled by sequential zones towards the rim, all of which can have distinct U–Pb ages. Bulk (whole grain) dating of such multi-domain

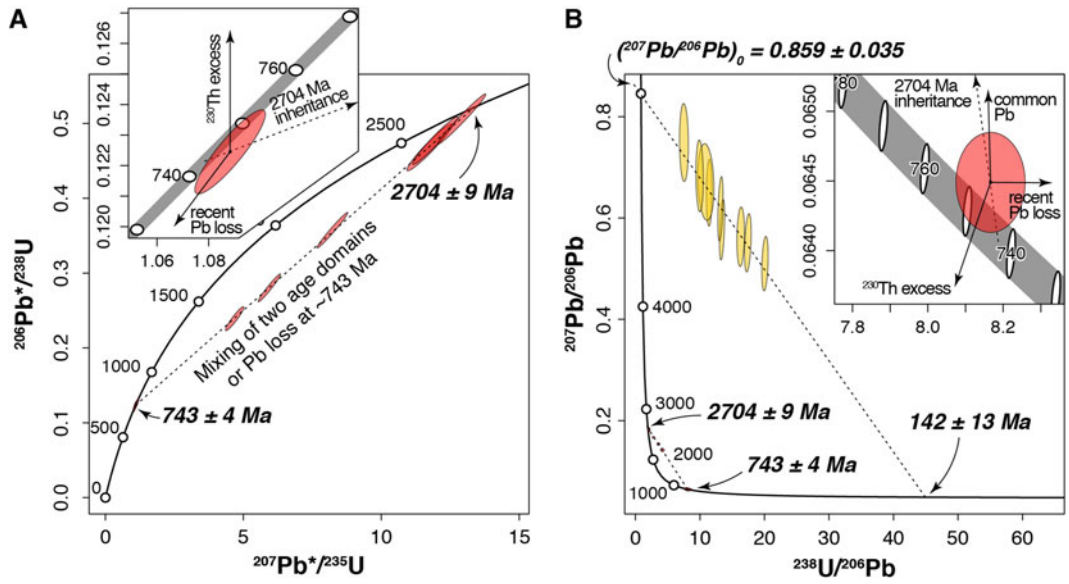


**Fig. 3** Main causes of discordance plotted on **a** Wetherill concordia diagram and **b** on a Tera-Wasserburg concordia diagram. Discordance of the red ellipses group is caused by either mixing of two age domains (one at 2704 ± 9 Ma and one at 743 ± 4 Ma) or by Pb-loss of 2704 ± 9 Ma minerals at 743 ± 4 Ma. Discordance of the yellow ellipses group is caused by the presence of common lead in minerals crystallized at 142 ± 13 Ma ($Pb_c$ uncorrected data). Insets shows the possible vectors of discordance

mineral grains could result in discordant dates, if the age differences are sufficiently large. A similar effect can arise from dating multigrain mineral fractions if they include grains with different isotopic ages. In the case of a simple two component mixture of two different age domains, several analyses could plot along a linear array (a so-called discordia line) in concordia diagrams, of which the lower and upper intercept dates would correspond to the respective ages of the two components (red ellipses on Fig. 3). However, multicomponent mixtures may show more scattered distribution or even plot along artificial, and often poorly correlated discordia arrays of which the upper and lower intercept dates have no geological significance, therefore inhibiting meaningful interpretation of the data.

In order to avoid problems arising from mixing several age domains, imagery of the minerals has become a necessary prerequisite to any dating (either in-situ or whole grain) in order to accurately place the spot of the analysis (for in-situ dating) or to select only those grains (or grain fragment) that have one age domain (for whole grain dating). However, small cores or domains with distinct ages can still go unrecognized if they are present below the imaged surface or have a similar chemistry to the surrounding zones. This effect may be monitored on the time-resolved signal for in-situ measurements (changing isotopic ratio) but would hinder the interpretation of whole grain dates.

### 2.3.2 Open System Behavior

It has long been recognized that the crystallographic lattice of minerals can, under certain conditions, behave as an open system with respect to the U–Pb system (e.g., Holmes 1954; Tilton 1960) through the partial or complete loss of radiogenic Pb. Radiogenic intermediate daughter products of the U decay chains experience a recoil during ejection of the highly energetic alpha particle. The final radiogenic $Pb^{2+}$ is thus situated in a decay-damaged area with enhanced fast pathway diffusion characteristics and could tend to leave this site when appropriate conditions are met. Mechanisms of Pb-loss have been studied extensively, but no simple process

can be universally put forward to explain it. Leaching of metamict (radiation-damaged) crystal domains, metamorphic recrystallization, crystal plastic deformation and thermally activated volume diffusion are the most commonly advocated causes of Pb-loss, in decreasing order of importance (see Corfu 2013; Schoene 2014 and references therein). At the sample scale, all these processes will result in discordance of the $^{206}Pb/^{238}U$ and $^{207}Pb/^{235}U$ dates if the age difference is large enough. By calculating by a linear regression through a series of discordant analyses, upper and lower intercepts ages can be reconstructed, corresponding to the age of crystallization of the mineral and to the age of the Pb-loss event, respectively (Fig. 3). Multiple Pb-loss events are notoriously difficult to unravel and may present as excess data scatter or even spurious discordia lines. Furthermore, highly metamict crystal domains may also experience U loss or U gain that would result in inversely (i.e., above the Wetherill concordia) or normally discordant data, respectively. In such cases, no age interpretation can be made. Complete recrystallization of a grain may lead to complete loss of all accumulated radiogenic Pb and reset the age to zero. The extremely low diffusion constants for Pb and U in zircon (Cherniak et al. 1997; Cherniak and Watson 2001, 2003) means that volume diffusion is a very inefficient process to remove radiogenic Pb from an undisturbed zircon lattice. It is for this reason that cases of U–Pb system survival have been reported in granulite facies rocks (e.g., Möller et al. 2003; Kelly and Harley 2005; Brandt et al. 2011; Kröner et al. 2015).

Open-system-related discordance is caused by several distinct processes that cause fast diffusion pathways in the zircon lattice, and such discordant data may be difficult to interpret. Features like multiple growth zones, overgrowth rims, dissolution-reprecipitation textures, or metamorphic recrystallization can be recognized in BSE or CL images (Geisler et al. 2007). Furthermore, recrystallized domains have distinct trace element compositions that can be identified by in-situ chemical analysis (Geisler et al. 2007). Pb-loss through fluid leaching of metamict domains can result in the deposition of minute amounts of 'exotic' elements that normally would not be able to enter the mineral structure (e.g., Fe or Al in zircon; Geisler et al. 2007). Additionally, the degree of metamictization, crystal ordering and ductile crystal reorientation can be evaluated with Raman spectroscopy, electron backscatter diffraction (EBSD), and transmission electron microscopy (TEM), respectively. Finally, for the specific case of zircon, the chemical abrasion technique (Mattinson 2005) has proven to be a powerful method for removing zircon domains that have suffered Pb-loss due to fission tracks, metamictization or other fast diffusion pathways.

### 2.3.3 Common Pb

Common Pb is a generic name for the fraction of Pb that is not radiogenic in origin and results from a mixture of initial Pb (i.e., Pb incorporated during mineral crystallization) and/or Pb contamination (both in nature and in the lab). The measurement of $^{204}Pb$ (the only non-radiogenic Pb isotope) undoubtedly pinpoints the presence of common Pb. However, $^{204}Pb$ measurement can be very challenging for low concentrations of common Pb, or may be prone to isobaric interference with $^{204}Hg$, inherent to the LA-ICPMS technique (see analytical methods). On a Tera-Wasserburg plot, analyses containing common Pb typically display a linear array of discordant ellipses defining an upper intercept date older than 4.5 Ma which points to the $^{207}Pb/^{206}Pb$ common Pb composition on the ordinate axis, and a lower intercept providing the age of the mineral (2D isochron; Fig. 3b). If $^{204}Pb/^{206}Pb$ can be measured, it can be plotted on a third axis and the data regressed to estimate the common Pb composition, the age of the mineral and to evaluate the relative contributions of common Pb and Pb-loss on the cause of discordance (3D isochron; Wendt 1984; Ludwig 1998). This approach has been shown to provide better precision for the common Pb composition than the 2D isochron method (Amelin and Zaitsev 2002; Schoene and Bowring 2006). Another Pb-correction practice in LA-ICPMS and SIMS analysis consists of deducing the common Pb correction from measurement of $^{208}Pb$ (stable

decay product of $^{232}$Th) and by assuming concordance of the U and Th systems. However, these correction methods may result in overcorrection of some data that are discordant for reasons other than common Pb only. When possible, it is therefore ideal to apply a more robust correction based on the direct measurement of the sample $^{204}$Pb. The Pb isotopic composition from laboratory contamination ("blank") is also an important consideration in high-precision U–Pb geochronology using isotope-dilution TIMS, and is obtained through repeated measurement of blank aliquots.

The isotopic composition of initial Pb incorporated during the crystallization of a mineral is best obtained from measurements of cogenetic low-U minerals such as feldspars, galena or magnetite. Alternatively, initial Pb compositions for a known age may be estimated from bulk Earth evolution models (Stacey and Kramers 1975). However, this last approach is less reliable compared to the measurement of a cogenetic low-U mineral (Schmitz and Bowring 2001; Schoene and Bowring 2006). Finally, for the specific case of zircon where the presence of common Pb is essentially limited to inclusions, fractures and metamict domains (see Sect. 6.1), the chemical abrasion technique (Mattinson 2005) has proven to be a powerful method for removing initial Pb from the crystal, leaving only the need for a laboratory blank correction.

### 2.3.4 Intermediate Daughter Disequilibrium ($^{230}$Th and $^{231}$Pa)

The age equations presented above (Eqs. 1–5) are valid under the assumption that the decay chains are in secular equilibrium, that is, one atom of Pb is created for every decay of one atom of U (Fig. 1b). However, elemental fractionation during mineral crystallization or partial melting would likely disrupt a previously established secular equilibrium (Fig. 1b). This effect should ideally be accounted for in geochronology. Nevertheless, most intermediate decay products of the U series have half-lives of many orders of magnitude smaller (microseconds to years) than the half-lives of U (Ga; Fig. 1a) and potential disequilibrium would have negligible effect on the U–Pb dates even at the best of current analytical capabilities (i.e., 0.5‰ uncertainty on the date). However, intermediate daughters $^{230}$Th ($^{238}$U decay chain) and $^{231}$Pa ($^{235}$U decay chain) have half-lives that are long enough (75.6 ka and 32.8 ka, respectively; Fig. 1a; Robert et al. 1969; Schärer 1984; Parrish 1990; Cheng et al. 2013) to critically impact on the accuracy of the calculated date if disequilibrium is not accounted for (Schärer 1984; Parrish 1990; Anczkiewicz et al. 2001; Amelin and Zaitsev 2002; Schmitt 2007). For example, during monazite crystallization, Th (of which $^{230}$Th) is preferentially incorporated into the crystal lattice compared to U, thus resulting in excess $^{206}$Pb (e.g., Fig. 1b) and in erroneously old $^{206}$Pb/$^{238}$U dates if the excess $^{230}$Th is not accounted for (Figs. 3, 4a). In turn, the Th-uncorrected $^{207}$Pb/$^{206}$Pb date for the same crystal would be too young (Fig. 4b). Conversely, zircon preferentially incorporates U over Th, rendering $^{230}$Th-uncorrected $^{206}$Pb/$^{238}$U dates typically too young (Fig. 4a). Similarly, the $^{207}$Pb/$^{235}$U isotopic system is potentially affected by $^{231}$Pa excess as has been reported for zircon (e.g., Anczkiewicz et al. 2001).

The magnitude of the correction that needs to be applied to correct the isotopic dates for initial $^{230}$Th and $^{231}$Pa disequilibrium depends on the distribution coefficient of Th/U and Pa/U between the dated mineral and the liquid from which it crystallized (a melt or an aqueous fluid), respectively (Schärer 1984). For the $^{207}$Pb/$^{206}$Pb date, it also depends on the age of the mineral (Parrish 1990). Figure 4 shows the effect of initial $^{230}$Th and $^{231}$Pa disequilibrium has on the $^{206}$Pb/$^{238}$U, $^{207}$Pb/$^{206}$Pb and $^{207}$Pb/$^{235}$U dates. It shows that for low mineral/liquid distribution coefficients ($D_{Th}/D_U < 1$) date offsets converge to a minimum of − 109 ka and − 47 ka for the $^{206}$Pb/$^{238}$U and $^{207}$Pb/$^{235}$U dates, respectively. However, if the distribution coefficients are high (> 1), excess $^{206}$Pb/$^{238}$U and $^{207}$Pb/$^{235}$U dates up to few Ma can be expected. Conversely, Th/U distribution coefficient < 1 causes excess $^{207}$Pb/$^{206}$Pb dates of few ka to ca. 0.5 Ma (depending on the age of the mineral), and distribution coefficient > 1 causes a deficit

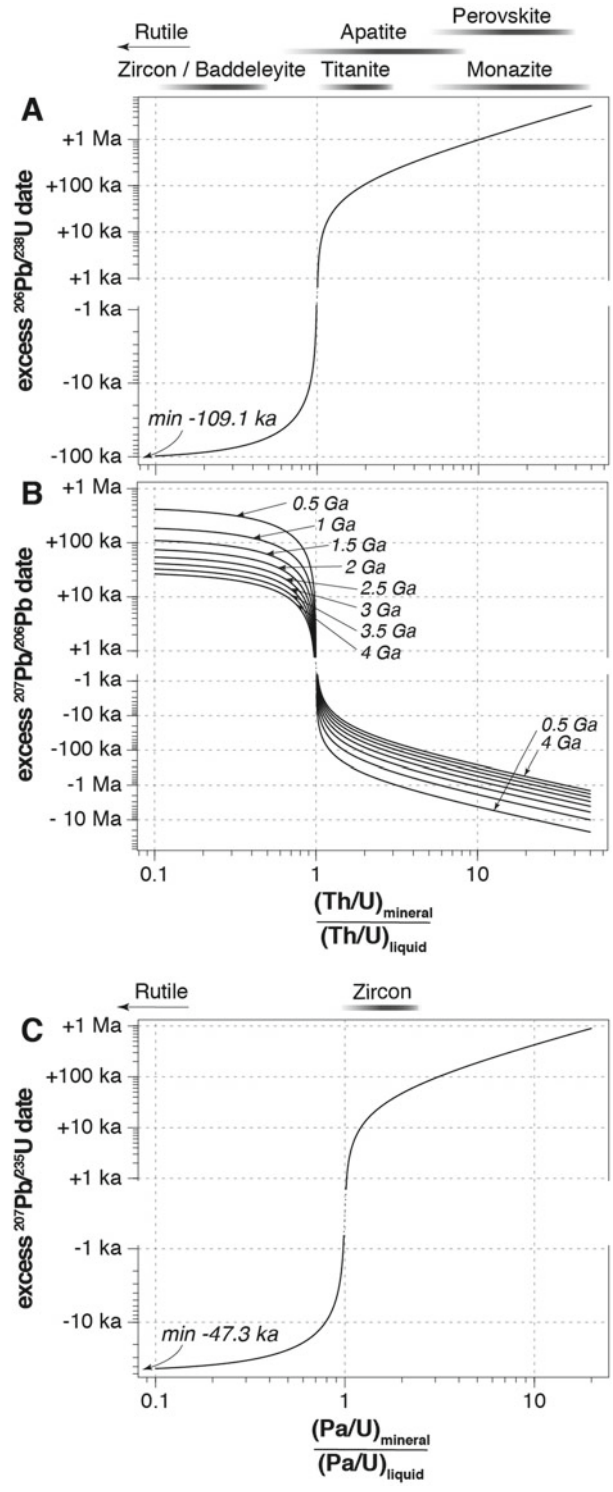


**Fig. 4** Excess in **a** $^{206}Pb/^{238}U$ and **b** $^{207}Pb/^{206}Pb$ dates due to initial $^{230}Th$ disequilibrium, and **c** excess in $^{207}Pb/^{235}U$ date due to initial $^{231}Pa$ disequilibrium as a function of Th/U and Pa/U mineral/liquid distribution coefficients, respectively (modified after Schärer 1984; Parrish 1990). Typical ranges of mineral/melt distribution coefficients for commonly dated minerals are shown for reference

in $^{207}Pb/^{206}Pb$ dates up to few Ma for Precambrian samples (Fig. 4b).

In practice, the Th/U ratio of the mineral is measured as $^{232}Th/^{238}U$ or estimated from the measured amount of its stable daughter isotope $^{208}Pb$ by assuming concordance of the U–Pb and Th–Pb dates. For minerals crystallized from a melt, available Th/U mineral-melt distribution coefficients (Fig. 4a) can then be used to reconstruct the Th/U of the melt needed for the Th-disequilibrium correction (e.g., adopting the values from Tiepolo et al. 2002; Klemme and Meyer 2003; Prowatke and Klemme 2005, 2006; Klemme et al. 2005; Rubatto and Hermann 2007; Stepanov et al. 2012; Beyer et al. 2013; Chakhmouradian et al. 2013; Stelten et al. 2015). Alternatively, direct measurement of melt inclusions hosted in the dated mineral, of glass or of whole rock Th/U ratio are also commonly used. Choosing the most appropriate estimate of the melt Th/U ratio at the time of mineral crystallization (using partition coefficient or direct measurement on whole rock or melt inclusions) should be done at the light of all possible information concerning the crystallization conditions of the dated mineral (e.g., temperature, crystallinity, co-crystallizing Th-bearing mineral phases, etc.; see examples in Wotzlaw et al. 2014, 2015).

In essence, $^{230}Th$- and $^{231}Pa$-corrections are based on the assumption that the dated mineral crystallized from a liquid in secular equilibrium with respect to the U-series. While this might be an acceptable assumption for some magmatic systems (at least for $^{238}U$ and $^{230}Th$) (Condomines et al. 2003), it should not be regarded as a rule, especially for hydrothermal systems in which Th and U have distinct solubilities (Porcelli and Swarzenski 2003; Drake et al. 2009; Ludwig et al. 2011). Indeed, the contrasted partitioning behavior of U and Th into a hydrothermal fluid causes isotopic disequilibrium in the fluid ($^{230}Th$ excess or deficit). In cases where the existence of this fluid is very short (e.g., for magmatic-hydrothermal systems) no time is given for radiogenic ingrowth in the fluid which would remain out of secular equilibrium. Finally, the fractionation of U and Th promoted by the crystallization of U- and Th-bearing hydrothermal minerals may further enhance isotopic disequilibrium. In such cases, the Th-correction (or Pa) should aim at determining the Th/U ratio of the last medium where the decay chain was in secular equilibrium before the crystallization of the mineral. This equates to determining the bulk source (in secular equilibrium) to sink (dated mineral) distribution coefficient of Th/U, regardless of the intermediate process(es), assuming short transport timescales and a unique source of U and Th. For example, Chelle-Michou et al. (2015) used the Th/U ratio of the porphyries (same as for magmatic zircons; Chelle-Michou et al. 2014) to correct the dates obtained on hydrothermal titanite from the Coroccohuayco skarn deposit. In this case, the U-series elements (mainly U and Th) were likely sourced from the magma which was assumed to be in secular equilibrium and transported to the site of deposition by a magmatic fluid in a short period of time.

## 2.4 A Note on Th–Pb Geochronology

Although less commonly used than U–Pb geochronology, Th–Pb dating may, in some cases, be advantageous and complementary to U–Pb dating. Due to comparable ionic radii of U and Th and similar valence (tetravalent except for oxidized systems where U in mostly hexavalent), most minerals hosting U into their structure will also incorporate Th (if it is available in the system), and vice versa. The single long-lived isotope of Th, $^{232}Th$, decays to $^{208}Pb$ through a chain of alpha and beta decays. The Th–Pb decay offers the possibility of a third independent geochronometer embedded within the mineral allowing for a further assessment of the robustness and meaningfulness of the obtained date. In addition, the nearby masses of $^{235}U$, $^{235}U$ and $^{232}Th$ on one side, and of $^{204}Pb$, $^{206}Pb$, $^{207}Pb$, and $^{208}Pb$ on the other side, allows for simultaneous measurement of U–Th–Pb isotopes from the same volume of analyte (ablated volume or dissolved grain). The generalized age equation writes as follow:

$$\left(\frac{^{208}Pb}{^{204}Pb}\right) = \left(\frac{^{208}Pb}{^{204}Pb}\right)_0 + \left(\frac{^{232}Th}{^{204}Pb}\right)\left(e^{\lambda_{232}t} - 1\right), \quad (6)$$

where $\lambda_{232}$ is the $^{232}$Th decay constant. If common Pb is negligible Eq. (6) can be simplified to:

$$\left(\frac{^{208}Pb^*}{^{232}Th}\right) = e^{\lambda_{232}t} - 1. \quad (7)$$

The $^{232}$Th decay constant is much smaller to that of $^{235}$U (half-life of 14 Ga) and is commonly considered to be $4.947 \pm 0.042 \cdot 10^{-11}$ $a^{-1}$ ($2\sigma$; Holden 1990). Despite a good accuracy of the $^{232}$Th decay constant as suggested by the common concordance of Th–Pb and U–Pb dates (e.g., Paquette and Tiepolo 2007; Li et al. 2010; Huston et al. 2016), its precision is an order of magnitude lower than those of $^{238}$U and $^{235}$U. This can represent the main source of systematic uncertainty on Th–Pb dates and the main limitation of this system when working below the percent precision level. However, unlike uranium, intermediate daughter isotopes of the $^{232}$Th decay chain have short half-lives such that any isotopic disequilibrium formed during mineral crystallization will fade within few decades only. Therefore, the $^{232}$Th decay chain can be considered to have remained in secular equilibrium on geological timescale. It results that on cases where U–Pb dates require a large initial $^{230}$Th-disequilibrium correction and parameters required for this correction are difficult to estimate (e.g., hydrothermal minerals), Th–Pb dates may be much more accurate than U–Pb ones (but often of lower precision).

Due to the very long half-live of $^{232}$Th, the optimal use of Th–Pb geochronology (highest analytical precision) is achieved for old sample and/or minerals with high Th concentrations so that large amount of $^{208}$Pb have been accumulated. In the case of Th-rich minerals (e.g., monazite and perovskite, and, to a lesser extent, xenotime, apatite, titanite and allanite), thorogenic $^{208}$Pb (i.e., $^{208}$Pb*) would typically be so abundant than common Pb correction may not introduce significant uncertainties into the computed $^{208}$Pb*/$^{232}$Th ratio or may even be neglected.

$^{208}$Pb/$^{232}$Th dates are most commonly presented in rank-order plots such as Fig. 2c, the center of each bar representing the date and the length reflecting the associated uncertainty. To evaluate the concordance of the Th–Pb and U–Pb systems, concordia diagrams ($^{208}$Pb*/$^{232}$Th vs. $^{206}$Pb*/$^{238}$U or $^{207}$Pb*/$^{235}$U) offer a convenient graphical representation of the data.

## 3 Analytical Methods (Including Data Reduction, Pb-Correction, Uncertainty Propagation and Data Presentation)

Currently, three methods are commonly used to measure isotopic ratios necessary for U–Pb geochronology: (1) laser ablation-inductively coupled plasma mass spectrometry (LA-ICPMS); (2) secondary ion mass spectrometry (SIMS); and (3) isotope dilution-thermal ionization mass spectrometry (ID-TIMS). Each of these methods have particular strengths and weaknesses (see summary in Table 1). In most cases, U–Pb geochronology involves the separation of the mineral of interest through gravimetric and magnetic techniques (e.g., heavy liquids, Wilfley shaking table, Frantz magnetic separator) and the selection of individual grains (picking) under binocular microscope. However, in-situ dating with LA-ICPMS and SIMS can also be done directly on polished thin section, thus preserving the petrographic context of the dated mineral, which may be key for the interpretation of the data in some cases.

The main difference between these three techniques resides in the way the dated material is prepared, ionized and introduced into the mass spectrometer. Below, we present an overview of the main aspects of the state-of-the-art procedures for these methods, while highlighting their respective advantages and disadvantages and the handling of uncertainties. For more details on the technical aspects of mass spectrometry, the interested reader is referred to a number of good textbooks and papers (e.g., Ireland and Williams 2003; Parrish and Noble 2003; Gehrels et al.

**Table 1** Comparison of the three analytical techniques used for U–Pb dating

| | LA-ICPMS | SIMS | CA-ID-TIMS |
|---|---|---|---|
| Spatial resolution | Spot diameter typically of 10–50 µm, depth of 15–40 µm | Spot diameter typically of 10–15 µm, depth of 1–2 µm | Whole mineral grain or grain fragment. Mixing of age domains is hard to avoid |
| Standardization | External with a known reference material and accuracy controlled with a secondary standard | External with a known reference material and accuracy controlled with a secondary standard | Internal with tracer solution (preferably double Pb—double U isotope tracer) |
| Sample preparation | Mineral separate mount or thin section, Imagery (CL, BSE, …) | Mineral separate mount or thin section, Imagery (CL, BSE, …) | Mineral separation, imagery, chemical abrasion (for zircon only) and washing, digestion, column chemistry |
| Time required for sample preparation | Few days for mineral separation, sample mount preparation and imagery | Few days for mineral separation, sample mount preparation and imagery | Few days for mineral separation and imagery; 1 day for chemical abrasion of zircon; $\geq$ 3 days for acid digestion; 1 day for chemical separation of Pb and U |
| Time required for one analysis (sample or standard) | 2–3 min | 15–30 min | 3–4 h |
| Analytical precision (reference for typical zircon: see Fig. 5) | 2–5% on single spot date and ~0.2–2% on weighted mean date | 1–5% on single spot date and ~0.1–1% on weighted mean date | 0.1–0.05% on single grain $^{206}Pb/^{238}U$ date and ~0.02% on weighted mean date |
| Accuracy | ~1–5% | ~1–5% | 0.03–0.3%; fully traceable to SI units |
| Preferred geologic application | Large scale survey, detrital geochronology, in-situ dating, minerals with inherited cores | In-situ dating, complexely zoned minerals | Used when highest temporal resolution or highest accuracy are necessary |
| Limitations | Imprecise common Pb correction, matrix matched standard material | Matrix matched standard material required for $^{206}Pb/^{238}U$ and $^{207}Pb/^{235}U$ dates, but not required for $^{207}Pb/^{206}Pb$ dates | Only very limited spatial resolution (microsampling) |

2008; Arevalo et al. 2010; Arevalo 2014; Carlson 2014; Ireland 2014; Schoene 2014; Schaltegger et al. 2015).

## 3.1 Laser Ablation-Inductively Coupled Plasma Mass Spectrometry (LA-ICPMS)

LA-ICPMS is an efficient U–Pb dating technique that allows high spatial resolution and high sample throughput. Analysis is done directly from a thin section or from polished grains mounted in epoxy resin that have been imaged by transmitted and reflected light, CL and/or BSE techniques prior to analysis. Typical analytical uncertainties for zircon dates are on the order of 3–5% for single spot and of 0.2–2% for the weighted mean dates (Fig. 5). However, accuracy may not be better than 3% (Klötzli et al. 2009; Košler et al. 2013), which should be considered when comparing LA-ICPMS U–Pb dates

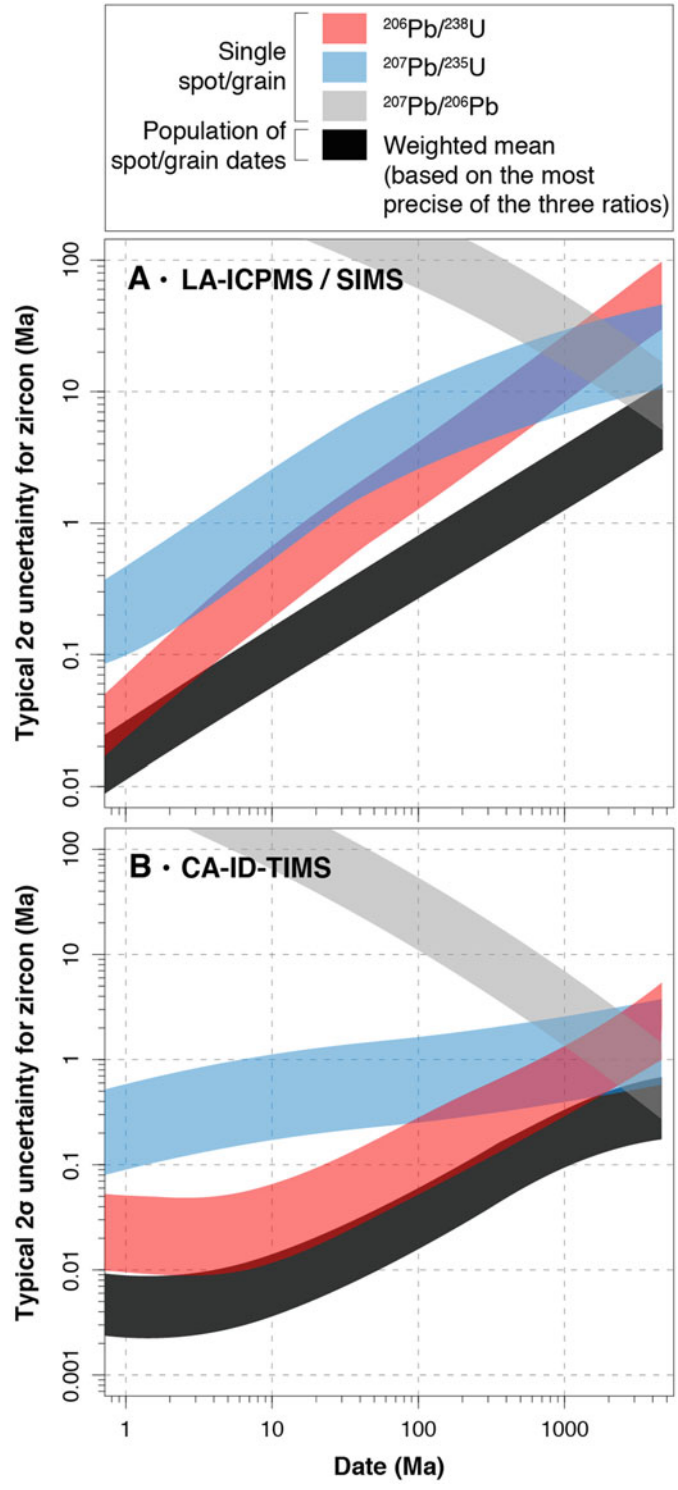


**Fig. 5** Typical analytical uncertainties for zircon $^{206}Pb/^{238}U$, $^{207}Pb/^{235}U$, $^{207}Pb/^{206}Pb$ single spot/grain dates for modern **a** LA-ICPMS, SIMS and, **b** CA-ID-TIMS dating techniques. Weighted mean dates refers to the weighted mean of a set of statistically equivalent single spot/grain dates based the most precise isotopic ratio (typically $^{206}Pb/^{238}U$ for dates younger than ca. 1 Ga and $^{207}Pb/^{206}Pb$ for dates older than 1 Ga)

from different studies or with dates from other isotopic systems.

The LA-ICPMS setup consists of a laser of short wavelength in the UV range (typically 193 nm), an ablation cell and an ICPMS instrument. The sample is placed into the ablation cell along with several standards. During ablation, repeated laser pulses are focused on the surface of the dated mineral. The resulting ablated aerosol is subsequently transported by a carrier gas (usually $He \pm Ar \pm N_2$) toward the Ar-sourced plasma torch at the entry of the mass spectrometer where it is ionized and transferred into the ion optics of the mass spectrometer. LA-ICPMS U–Pb dating is mostly carried out on single-collector sector-field ICP-MS instruments that offer sequential measurement of individual Pb and U isotopes in a mixed ion-counting – Faraday cup mode.

The spot size used for LA-ICPMS geochronology mainly depends on target size and the U concentration of the dated mineral. As a reference, 25–35 μm spots are commonly used for zircon and can be as low as 5 μm for monazite (Paquette and Tiepolo 2007). Crater depth for a 30–60 s analysis is on the order of 15–40 μm depending on the fluence of the laser and on the ablated material. However, laser-induced U–Pb fractionation increases with crater depth during ablation, which negatively impacts on the analytical uncertainty of the measured Pb/U ratio. Ultimately, this is an important limiting factor for precision and accuracy in LA-ICPMS geochronology (Košler et al. 2005; Allen and Campbell 2012). The technique requires a laser setup that yields reproducible ablation with small particles (subsequently more efficiently ionized in the plasma torch) and that limits crater depth to no more than the spot diameter by minimizing the laser fluence (e.g., Günther et al. 1997; Horn et al. 2000; Guillong et al. 2003).

Another important limitation of LA-ICPMS U–Pb dating is the imprecise common Pb correction due to the difficulty of precisely measuring common $^{204}Pb$ caused by an isobaric interference with $^{204}Hg$ (traces of Hg are contained in the Ar gas). Common Pb correction protocols using $^{208}Pb$ may be employed and are preferred over simple rejection of discordant analyses. It results that age interpretation of minerals with elevated common Pb contents (e.g., titanite, rutile) may be hampered by large age uncertainties due, in part, to the large uncertainties associated with the common Pb-correction.

LA-ICPMS and SIMS (see below) U–Pb dating are comparative techniques that require analysis of a reference material, which is as close as possible to the chemical composition and the structural state of the unknown (sample). It is analyzed under identical ablation conditions to the sample to determine the machine fractionation factor of any measured element concentration; this fractionation factor is then applied to the element ratios and concentrations of the unknowns. A series of analyses unknown ($\sim$10) is typically bracketed by analyses of a reference material ($\sim$2–4) to correct for elemental fractionation and monitor for machine drift. In addition, at least one secondary standard should be repeatedly analyzed during the same session in order to demonstrate the accuracy of the fractionation correction. This enables an estimate of the long-term excess variance of the laboratory that is required in the uncertainty propagation protocol (see below). A list of commonly used reference materials and their reference values is provided in Horstwood et al. (2016). Standards for LA-ICPMS and SIMS U–Pb dating should be homogenous in age, trace element composition, and have comparable trace element concentration and structural state (matrix match) as the unknowns (Košler et al. 2005). Failure to match the matrix of the unknown results in different ablation behavior (rate, stability, fractionation) and ultimately compromises the accuracy of the date (Klötzli et al. 2009). Therefore, a mineral of unknown age should be standardized using a reference material from the same mineral. Furthermore, different degrees of metamictization also impact on the matrix match between standards and unknowns and can be an important source of inaccuracy for zircon dates (as much as 5% inaccurate; Allen and Campbell 2012; Marillo-Sialer et al. 2014) and possibly for other minerals as well (e.g., titanite, allanite, columbo-tantalite).

Interlaboratory comparisons for LA-ICPMS and SIMS U–Pb dating have highlighted discrepancies of U–Pb ages for a series of standards measurements which is sometimes outside of the reported 2σ uncertainties (Košler et al. 2013). This is thought to reflect different data reduction strategies in different laboratories (e.g., Fisher et al. 2010) and uncertainty propagation protocols, that are not always thoroughly documented. This has triggered a community driven effort to establish standard data reduction workflow, uncertainty propagation protocols, and data reporting templates (Horstwood et al. 2016) that should be embraced by the LA-ICPMS community. New community-derived standards for LA-ICPMS dating suggest the use of the *x/y/z/w* notation for uncertainty reporting where: *x* refers to the analytical (or random) uncertainty, *y* includes the variability of standards measured in the same lab, *z* includes the systematic uncertainty of the primary standard isotopic composition (and of the common Pb correction if appropriate), and *w* includes the decay constant uncertainty (Horstwood et al. 2016; McLean et al. 2016). Comparing LA-ICPMS U–Pb data with data from other LA-ICPMS, SIMS or ID-TIMS laboratories should be done at the *z* uncertainty level, while comparison with geochronological data from other isotopic systems have to include decay constant uncertainties (Chiaradia et al. 2013). Raw data processing, visualization and uncertainty propagation protocols for LA-ICPMS U–Pb dating have been implemented in the freely available *ET_Redux* software (McLean et al. 2016) and allow more robust interlaboratory data comparison and collaborative science.

## 3.2 Secondary Ion Mass Spectrometry (SIMS)

Compared to LA-ICPMS, SIMS U–Pb analysis has greater spatial resolution and sensitivity, allowing for the analysis of microscopic rims or domains in zircon, monazite, xenotime or other minerals. SIMS analysis involves the ablation of sample with a high-energy $O^-$ or $O_2^-$ ion beam within a high vacuum chamber. A small fraction of the ablated material forms atomic ions or molecular ionic compounds that are subsequently accelerated into a mass spectrometer. Typical SIMS craters are 10–15 μm in diameter and 1–2 μm deep, therefore this technique has higher spatial resolution and is by far less destructive than LA-ICPMS and permit subsequent isotopic analysis (e.g., O, Hf–Lu) to be done on the same spot (slight repolishing would be required before SIMS analysis). Analysis is done directly from a thin section, polished grains mounted in epoxy resin, or from entire grains pressed into indium when analyzing U and Pb isotopes along a profile from the surface to the interior of a grain (depth profiling). The accuracy of the obtained result depends on extrinsic factors such as the position of standard and unknowns in the mount and the quality of the polishing. SIMS analysis of zircon typically yields U–Pb dates of 0.1–1% precision and accuracy (Fig. 5); it is the preferred method when analyzing complex minerals (e.g., thin metamorphic rims), very small grains (e.g., xenotime outgrowths on zircon; McNaughton et al. 1999) or valuable material.

Pb isotopic fractionation in SIMS is subordinate when compared to LA-ICPMS techniques. Therefore, $^{207}Pb/^{206}Pb$ dates can be calculated directly from counting statistics. In contrast, there is a significant difference in the relative sensitivity factors for $Pb^+$ and $U^+$ ions during SIMS analysis. The fractionation of the $^{206}Pb^+/^{238}U^+$ ratios is highly correlated with simultaneous changes in the $^{254}UO^+/^{238}U^+$ ratios which forms the basis of a functional relationship that enables the calibration of the $^{206}Pb/^{238}U$ dates. Although the $^{206}Pb^+/^{238}U^+$ versus $^{254}UO^+/^{238}U^+$ calibration is the most widely used, other combinations of $^{238}U^+$, $^{254}UO^+$ and $^{270}UO_2$ have proved successful. As in the case of LA-ICPMS, the SIMS $^{206}Pb/^{238}U$ calibration is carried out with reference to a matrix matched reference material (e.g., Black et al. 2004). This is quite straightforward for zircon and baddeleyite ($ZrO_2$), but more difficult for chemically and structurally more complex minerals (e.g., phosphates, complex silicates, oxides). In the latter cases, matrix correction procedures using a

suite of reference materials accounting for the effect of highly variable amount of trace elements have been developed (e.g., Fletcher et al. 2004, 2010). Calibration biases are also introduced through different crystal orientation (Wingate and Compston 2000) or different degrees of structural damage from radioactive decay (White and Ireland 2012). It is highly recommended to analyze a reference zircon as unknown again to control the accuracy of the technique (validation or secondary standard; Schaltegger et al. 2015).

The common Pb correction is carried out via measurement of $^{204}$Pb, $^{207}$Pb or $^{208}$Pb masses. The main challenge of SIMS analysis is the resolution of molecular interferences on the masses of interest (Ireland and Williams 2003), which requires careful consideration when analyzing phosphates or oxides.

No standard data treatment protocol exists for SIMS dates. In fact, the two types of equipment (SHRIMP from Australian Scientific Instruments and IMS 1280/90 from CAMECA) provide very differently structured data that require different data treatment software.

### 3.3 Isotope Dilution-Thermal Ionization Mass Spectrometry (ID-TIMS)

The U–Pb method that offers the highest precision and accuracy is Chemical Abrasion, Isotope Dilution, Thermal Ionization Mass Spectrometry (CA-ID-TIMS; Table 1, Fig. 5). This method involves the dissolution and analysis of entire zircon grains and other accessory minerals, and, hence, disregards any protracted growth history recorded in this grain. Zircon imaging prior to dating can be taken to increase the chances of analyzing a single-aged grain or grain population. The ID-TIMS community is organized as a part of the EARTHTIME consortium (Bowring et al. 2005), which is working together to improve precision and accuracy of U–Pb dating.

It is now standard to pre-treat zircons with the "chemical abrasion" procedure of Mattinson (2005). This process involves heating the zircon at 900 °C for 48 h, followed by partial dissolution in HF + $HNO_3$ at 180–210 °C for 12 to 18 h (Widmann et al. 2019). The heating re-establishes the zircon crystalline structure by annealing any radiation-related structural damage in slightly affected domains. The partial dissolution procedure then only removes domains with more severe structural damage and leaves a proportion of the original grain behind. The surviving zircon fragment is then considered to be perfectly crystalline and is used for isotope ratio analysis. Chemically abraded zircon grains are recognized to be more concordant and provide more reproducible U–Pb results. This treatment is not currently applied for SIMS or LA-ICPMS analysis techniques, but initial experiments have yielded positive results (Kryza et al. 2012; Crowley et al. 2014; von Quadt et al. 2014). The procedure has been tested on other accessory phases including baddeleyite (Rioux et al. 2010), but without clear evidence of improving concordance.

The dissolved grains are mixed with a ($^{202}$Pb–)$^{205}$Pb–$^{233}$U–$^{235}$U tracer solution (e.g., as provided by EARTHTIME; ET535 and ET2535; Condon et al. 2015; McLean et al. 2015), and the Pb and U isotopes isolated from other trace elements through chromatography. Isotopic compositions are most commonly measured as $Pb^+$ and $UO_2^+$ on a thermal ionization mass spectrometer from the same filament either by ion counting methods (using a secondary electron multiplier or a Daly-based photomultiplier device), or by a combination of ion counters and high-sensitivity, high-resistance Faraday collectors. Uranium may also be measured separately as $U^+$ by solution MC-ICP-MS utilizing a mixed ion counting—Faraday measurement setup, or as $U^+$ on a double or triple filament assembly in a TIMS.

An important part of high-precision, high-accuracy U–Pb geochronology is the correct treatment of all sources of uncertainty and their correct propagation into the final age. The ID-TIMS community has been adopting the *x/y/z* notation for uncertainty reporting (e.g., 35.639 ± 0.011/0.014/0.041 Ma) where: *x* is the random uncertainty (or analytical; including

counting statistics, common Pb and Th-disequilibrium corrections), *y* includes the systematic uncertainty from tracer calibration and, *z* includes the decay constant uncertainty (Schoene et al. 2006; Schoene and Bowring 2006; McLean et al. 2011). Comparison of ID-TIMS U–Pb data with U–Pb data from SIMS or LA-ICPMS techniques should consider the *y* uncertainty level, while comparison with data from other isotopic systems (e.g., Re-Os, $^{40}Ar/^{39}Ar$) should include both decay constant and systematic uncertainties (*z* level). Final age precision is mainly defined by the ratio of radiogenic to common Pb ($Pb^*/Pb_c$), which is, in the case of zircon, a function mainly of procedural Pb blank. Total blank levels of < 0.5 pg of Pb are currently state-of-the-art.

The EARTHTIME community has generally accepted and adopted a software package consisting of *Tripoli* raw data statistics and *U–Pb_Redux* data treatment and visualization (Bowring et al. 2011; McLean et al. 2011).

## 4 Guidelines for Interpreting U–Pb Dates

### 4.1 Date and Age

Isotopic dating makes a distinction between a *date* and an *age*. The term 'date' refers to a number in time unit (usually Ga, Ma or ka) calculated from an age equation (Eqs. 1–5). The term 'apparent age' is sometimes used as a synonym for 'date'. A 'date' becomes an 'age' as soon as in can be interpreted in terms of a geological process (Schoene 2014). Both terms may be appropriate for single grain/spot or weighted mean data and may be accurate or inaccurate. This semantic distinction reflects the clear distinction that should be made between data and their interpretation, which is at the core of scientific rigor and integrity.

As discussed in the preceding sections, the interpretation of U–Pb dates is not straightforward, even for concordant data. It requires a close and quantitative control of the way how an analytical result has been produced, including the knowledge of sources of error and their correct propagation into the final result (metrology), a good characterization of the sample material, and finally a good knowledge of the geological context. The lack of considering these aspects may very well lead to over-interpretations and erroneous conclusions.

### 4.2 Geochronology Versus Thermochronology

All minerals used for U–Pb dating can be theoretically subjected to some degree of thermally activated volume diffusion of U and Pb. The measured date reflects the time elapsed since closure of the isotopic system. While geochronology corresponds to dating of a mineral that has crystallized, rapidly cooled or remained below it closure temperature, thermochronology deals with minerals that have crystallized and/or spent some time above their respective closure temperatures, or in the partial retention temperature window of their daughter nuclide. As discussed above (causes of discordance) partial resetting of the U–Pb system by diffusion is a possible source of discordance. While the effect of post crystallization diffusion can usually be neglected for zircon, monazite and most other minerals due to their high closure temperature for Pb (> 700 Cherniak and Watson 2001, 2003; Cherniak et al. 2004); Fig. 6), Pb diffusion in minerals such as titanite, rutile and apatite is more likely to occur and should carefully be evaluated before interpreting U–Pb dates as they might record the age of closure rather the age of crystallization. Ultimately, thermochronological U–Pb data on these minerals may be used to constrain the high-temperature (> 350 °C) thermal history of the studied geological object (Schoene and Bowring 2007; Kooijman et al. 2010; Blackburn et al. 2011; Cochrane et al. 2014). Nevertheless, it appears that most minerals used for U–Pb dating can be used as geochronometers, of which partial resetting of the U–Pb system is often controlled by the stability of the mineral phase itself or Pb-loss along fast diffusion pathways (cracks, metamict domains), rather by volume diffusion (Fig. 6).

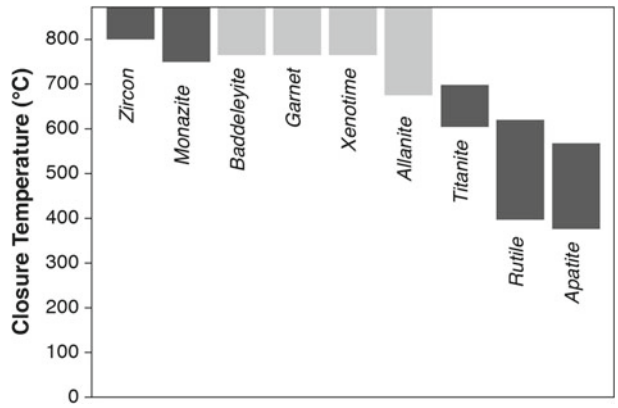


**Fig. 6** Typical range of closure temperature for minerals used for U–Pb dating. Dark grey bars indicate robust closure estimates while light grey bars indicate approximate estimates. Modified from Chiaradia et al. (2014), with additional data for apatite (Cochrane et al. 2014), rutile (Vry and Baker 2006), baddeleyite (Heaman and LeCheminant 2001), garnet (Mezger et al. 1989), xenotime and allanite (Dahl 1997)

## 4.3 Precision and Weighted Mean

The weighted mean age is the most common representation of the age of a relatively short-lived geological event recorded at the scale of the sample (e.g., magma emplacement, hydrothermal fluid circulation) and is usually interpreted as the best age estimate. Weighted mean calculations are applied to a set of individual analyses in order to reduce the uncertainty of the population. It implicitly assumes that the data correspond to repeated analyses (samples) of the exact same value and that the uncertainties are only due to analytical scatter. In this case, the mean square of the weighted deviates (MSWD or reduced chi-squared) of a data population to the weighted mean should be around to 1. In turn, MSWD >> 1 would suggest excess scatter of the data given their respective uncertainties (i.e., they are unlikely to represent a single population), and values << 1 suggest that the reported uncertainties are larger than what would be expected from a single population. In detail, acceptable MSWD values actually depend on the number of points pooled together (Wendt and Carl 1991; Spencer et al. 2016). For example, values between 0.5 and 1.5 are acceptable for a population of 30 points (at $2\sigma$).

However, the accuracy of weighted mean ages has been repeatedly questioned (Chiaradia et al. 2013, 2014; Schoene 2014). Indeed, the advent of high precision dating techniques (CA-ID-TIMS) has highlighted that data that might look statistically equivalent at the level of their uncertainties, can actually hide a spread of data that can only become apparent with more precise dating methods. An illustration of this is provided in Fig. 7 which shows LA-ICPMS and CA-ID-TIMS $^{206}Pb/^{238}U$ zircon dates from a porphyry intrusion from the Coroccohuayco porphyry-skarn deposit, Peru (Chelle-Michou et al. 2014). It is noteworthy that those grains analyzed by CA-ID-TIMS have previously been analyzed with LA-ICPMS (with 1 to 3 spots each) before being removed from the epoxy mount for further processing. Data points are plotted at the level of their analytical uncertainties and weighted mean dates include additional dispersion and standard/tracer calibration uncertainties (see caption of Fig. 7 for more details) so that they can be compared at their right level of uncertainties (i.e., neglecting only decay constant uncertainties). Both the LA-ICPMS ($36.05 \pm 0.25$ Ma, n = 30, MSWD = 1.3) and CA-ID-TIMS ($35.639 \pm 0.014$ Ma, n = 7, MSWD = 1.8) weighted means yield acceptable MSWDs (in agreement with their respective number of data points), thus suggesting they could correspond to statistically equivalent data populations, respectively. Independently from each other, these weighted dates would be

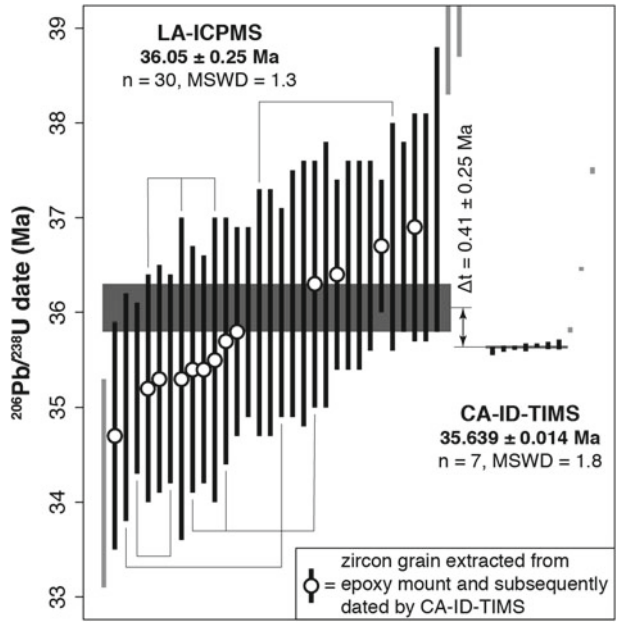


**Fig. 7** Ranked LA-ICPMS and CA-ID-TIMS $^{206}Pb/^{238}U$ zircon dates and weighted means for the hornblende-biotite porphyry (sample 10CC51) from the Eocene Coroccohuayco porphyry-skarn deposit, Peru. Data from Chelle-Michou et al. (2014). Single spot/grain analyses are plotted at the level of their analytical uncertainties (2σ) and weighted mean dates include the analytical uncertainties and: (i) an additional excess variance obtained from repeated measurement of the secondary standard (91,500) and the systematic uncertainty in the standard mineral isotopic composition, for LA-ICPMS data; (ii) the systematic uncertainty related to the composition of the isotopic tracer, for CA-ID-TIMS data. Data bars in black are included in the calculation of the weighed mean date. Multiple LA-ICPMS dates from the same zircon grain are connected with thin lines

interpreted as the age of the porphyry intrusion at the Coroccohuayco deposit. However, Fig. 7 highlights that these ages do not overlap within uncertainties ($\Delta t = 0.41 \pm 0.25$ Ma), therefore indicating that at least one of them is inaccurate. In this case, the more precise single grain CA-ID-TIMS ages highlight more than 1 Ma of zircon crystallization in deep-seated crystal mushed (or proto-plutons) before their incorporation into felsic melts, ascent and emplacement of the porphyry intrusion at an upper crustal level (Chelle-Michou et al. 2014). These older zircon crystallization events cannot be resolved at the uncertainty level of LA-ICPMS dating for which data points pool together that are actually not part of the same population and therefore include data older than the emplacement age, resulting in a weighted mean age that is too old. While it is common practice in zircon CA-ID-TIMS dating to take the youngest point as best representative of the age of magma emplacement or eruption, this practice is not appropriate for in-situ or CA-free ID-TIMS dating techniques where the weighted mean date of the youngest cluster having an acceptable MSWD remains the best option, although it might sometimes be slightly inaccurate.

This example highlights the limitations of the weighted mean approach to complex and protracted natural processes. The statistical improvement in precision may be done at the cost the accuracy of the dated process. The calculated weighted mean date can be either too old (e.g., if grains crystallized from an earlier pulse of magma are included), too young (e.g., if several grains have suffered similar amounts of unrecognized Pb-loss) or just right by coincidence. In fact, the time resolution of geochronology is ultimately limited by the precision of single data points, rather than by the

number of data that are pooled together to statistically reduce the age uncertainty.

### 4.4 Accuracy of Legacy U–Pb Data and Misinterpretation

Cases where the same rock has been dated several times using the same isotopic system and the same mineral are rare but necessary examples to put some perspective of the accuracy of legacy U–Pb data. Ore-related porphyry intrusions at the Miocene Bajo de la Alumbrera porphyry copper deposit have received much attention over the past decade. These rocks have been repeatedly dated by U–Pb zircon geochronology using different analytical methods (LA-ICPMS and CA-ID-TIMS) at different times (Harris et al. 2004, 2008; von Quadt et al. 2011; Buret et al. 2016). The early LA-ICPMS zircon dating survey of Harris et al. (2004, 2008) concluded that the deposit formed on a million-year time scale. However, subsequent high precision CA-ID-TIMS studies have decreased this duration by almost two orders of magnitude, to a maximum duration of 29 ka (Buret et al. 2016).

Available data for three porphyries are compiled Fig. 8 with their respective weighted means. Single LA-ICPMS date broadly range from 8.5 to 6.5 Ma while those obtained by CA-ID-TIMS are significantly less scattered between 8.2 and 7.1 Ma. Weighted mean dates can show as much as ~1 Ma of age difference for the same porphyry between LA-IPCMS and CA-ID-TIMS which is far outside the reported analytical uncertainties (see P2 porphyry on Fig. 8). The same is true for high-precision CA-ID-TIMS data, which show differences up to ~0.1 Ma in excess of the analytical uncertainty. Furthermore, these discrepancies persist even when systematic uncertainties are taken into account (i.e., 3% reproducibility for LA-ICPMS, calibration of the primary standard or of the tracer solution). Similar age discrepancies up to ~0.8 Ma between LA-ICPMS and SIMS U–Pb zircon weighed mean ages have been noted by Ballard et al. (2001) on porphyries from the Eocene Chuquicamata Cu deposit, Chile.

It would be presumptuous to name the causes of these discrepancies without having the entire set of original technical and analytical data at our disposal. Nevertheless, we can make some conjectures. Potential causes may be: (1) that different populations of zircons grains or domains (within a single grain) where hand-picked and dated; (2) the use of inappropriate data reduction, common Pb correction, initial Th-correction and error propagation protocols; (3) a distinct difference in ablation rate between sample and standard zircon resulted in inaccurate correction for fractionation (for LA-ICPMS data); (4) inaccurate isotopic tracer calibration (for ID-TIMS data); and/or (5) unidentified concordia parallel Pb-loss (for the LA-ICPMS data).

In the case of Bajo de la Alumbrera, the most recent data by Buret et al. (2016) are deemed to be the most accurate (in addition of being the most precise) and tightly constrain the age of porphyry emplacement and zircon crystallization. This example illustrates the difficulty of dealing with legacy U–Pb data which might or might not be accurate. Obviously, there are published ages that are inaccurate, but they would remain unnoticed until new dating is done with state-of-the-art techniques. In particular, reporting of *x/y/z* (for ID-TIMS) and *x/y/z/w* (for LA-ICPMS) uncertainties and comparison of disparate U–Pb dates at the level of their *y* uncertainty should be systematic. Again, these potential biases should be carefully accounted for when interpreting short time differences on the order of the analytical uncertainty of single dates. This also highlight the need for thorough reporting of analytical and data handling procedures, or even, using common analytical procedures and data reduction platforms (Košler et al. 2013).

## 5 What Mineral Can We Date with the U–Pb System and What Does It Date?

As of today, a great number of minerals have been used for U–Pb dating, many of which in the context of mineral deposits. A non-exhaustive list of these minerals is provided in Table 2

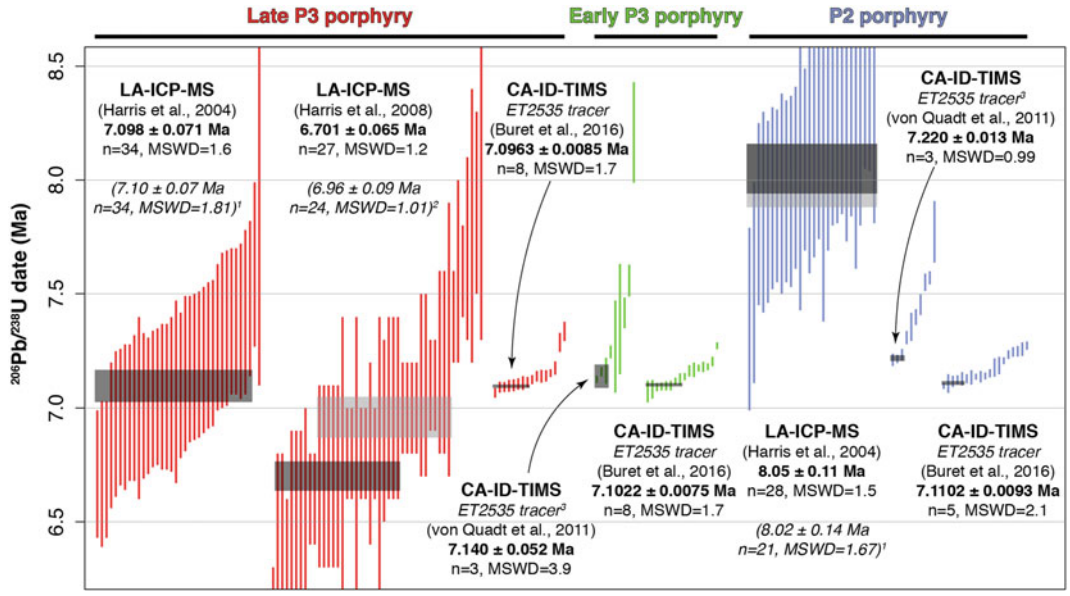


**Fig. 8** Compilation of $^{206}Pb/^{238}U$ Th-corrected dates acquired with different methods for three porphyry intrusions at the Bajo de la Alumbrera porphyry copper deposit, Argentina. Data are from Harris et al. (2004), Harris et al. (2008), von Quadt et al. (2011), and Buret et al. (2016). The horizontal grey bands represent the weighted mean dates recalculated by us and include analytical uncertainties based on U–Pb dates from tables provided in the aforementioned publications. [1]weighted mean date reported in Harris et al. (2004). [2]weighted mean date reported in Harris et al. (2008). [3]tracer used in von Quadt et al. (2011) (written communication to the authors). All uncertainties are given at 2σ (95% confidence)

which presents their main characteristics and usefulness for dating ore deposits. It is noteworthy that this table only presents a selection of some useful minerals, but others might also be amenable to U–Pb dating. Furthermore, ongoing and future developments will likely improve our understanding of the U–Pb system in these and new mineral species while allowing better precision, accuracy and interpretation of the dates.

Ideal minerals for U–Pb dating should necessarily contain traces of U, and as little common (initial) Pb as possible. They should also have a low diffusivity for Pb so as to accurately record the radiogenic Pb ingrowth. Many minerals used for U–Pb dating are accessory minerals (zircon, baddeleyite, titanite, monazite, xenotime) but a handful of them are major rock forming minerals (calcite, garnet) or even ore minerals (cassiterite, columbo-tantalite, uraninite, wolframite) (see Table 2). This exceptional mineralogical diversity allows most types of ore deposit and ore forming processes to be dated directly or indirectly with the U–Pb method. However, in detail, all minerals do not provide equally precise, accurate and/or meaningful dates. In Table 2, we have classified the minerals in three categories depending on the average quality of the date that they can provide. Nevertheless, we stress that this classification should only be taken as a 'rule of thumb' and that each case would be different. For example, zircon might give very imprecise and discordant dates while xenotime from the same sample would return more precise and concordant dates (e.g., Cabral and Zeh 2015).

## 5.1 Low Common Pb, High U and Structurally Robust Minerals

The most dated mineral is arguably zircon. This is mainly due to its virtual ubiquity in the geological environment, its chemical and mechanical

**Table 2** Minerals suitable for U–Pb dating in the context of mineral deposits (as of year 2017)

| Mineral | Formula | Main types of mineral deposit where U–Pb dating can be done (non-exhaustive list) | Event dated | Principal limitations | Additional comments | Average quality of U–Pb dating[a] | Some references with application to mineral deposits |
|---|---|---|---|---|---|---|---|
| Allanite | $(Ca, Ce, La, Y)_2(Fe^{2+}, Fe^{3+}, Al)_3O(SiO_7)(SiO_4)(OH)$ | Skarn; IOCG: Fault-related U (±REE) | Hydrothermal activity, metasomatism; magmatism | Low to moderate amount of common Pb; No matrix-matched standard available; High amount of excess $^{206}Pb$ (initial $^{230}Th$ excess)[b]; | Possibility of Th–Pb dating | XX | Pal et al. (2011); Chen and Zhou (2014); Deng et al. (2014) |
| Apatite | $Ca_5(PO_4)_3(F, OH, Cl)$ | IOCG; REE(±U, P) vein; Magmatic Ni–Cu-PGE(±Co) sulphide; | Cooling; hydrothermal activity | Low to high amount of common Pb; low U concentration; No matrix-matched international standard available (zircon or in-house standard; see Chew et al., 2011); Can be sensitive to initial $^{230}Th$ excess[b] | No metamictization; Possibility of Th–Pb dating | X | Romer (1996); Amelin et al. (1999); Gelcich et al. (2005); Stosch et al. (2010); Seo et al. (2015); Huston et al. (2016) |
| Baddeleyite | $ZrO_2$ | Magmatic Ni–Cu-PGE(±Co) sulphide; Banded iron formation; Orogenic Au; Diamond-bearing kimberlite; Rare-metal carbonatite | Alkaline and mafic to ultramafic magmatism, hydrothermal activity | Crystal orientation affects $^{206}Pb/^{238}U$ ratios and dates measured with SIMS (Wingate and Compston, 2000); | Limited common Pb, no metamictization | XXX | Corfu and Lightfoot (1996); Schärer et al. (1997); Amelin et al. (1999); Wingate and Compston (2000); Müller et al. (2005); Li et al. (2005); Wu et al. (2011); Zhang et al. (2013); Bjärnborg et al. (2015); Wall and Scoates (2016) |
| Brannerite | $(U, Ca, Ce)(Ti, Fe)_2O_6$ | Fault-related U(±REE-F-Ba-Th); Magmatic-hydrothermal/epithermal U (± Ni-Co-As-Mo-Pb-PGE-Au); Archean Au paleoplacer | Hydrothermal activity | Moderate to high amount of common Pb; easy resetting of the U–Pb system (Pb loss) with hydrothermal fluids; no matrix-matched standard available | | X | Frei (1996); Zartman and Smith (2009); Oberthür et al. (2009); Bergen and Fayek (2012) |
| Calcite | $CaCO_3$ | MVT Pb–Zn ± F | Hydrothermal activity, diagenesis | Moderate to high amount of common Pb; easy resetting of the U–Pb system (Pb and U | Date sometimes determined with the isochron method; | X | DeWolf and Halliday (1991); Brannon et al. (1996); Coveney et al. (2000); |

(continued)

**Table 2** (continued)

| Mineral | Formula | Main types of mineral deposit where U–Pb dating can be done (non-exhaustive list) | Event dated | Principal limitations | Additional comments | Average quality of U–Pb dating[a] | Some references with application to mineral deposits |
|---|---|---|---|---|---|---|---|
| | | | | mobility) with hydrothermal fluids; difficulty to interpret the event being dated; No international matrix-matched standard available (in-house standard) | Inverse discordance is not uncommon (U loss). Mostly $Pb_c$ uncorrected $^{238}U/^{206}Pb$ dates | | Grandia et al. (2000); Rasbury and Cole (2009); Burisch et al. (2017) |
| Cassiterite | $SnO_2$ | Granite-related Sn(± Mo–W–Cu–Pb–Zn–Sb–Ag) greisen, skarn and lode; Supergene Sn | Hydrothermal activity, supergene alteration (?) | High amount of common Pb; No international matrix-matched standard available (in-house standard) | Date often determined with the isochron method | X | Gulson and Jones (1992); Yuan et al. (2011); Chen et al. (2014); Zhang et al. (2014); Li et al. (2016) |
| Colombo-tantalite | $(Mn, Fe^{2+})(Nb, Ta)_2O_6$ | Rare-metal (± Sn–W) pegmatite, greisen and granite | Late magmatic stage, hydrothermal resetting | Low to moderate amount of common Pb; in-situ dating often standardized to zircon mineral, the use of Coltan-139 standard is suggested by Che et al. (2015); can be highly metamict | Inverse discordance is not uncommon (maybe related to inclusions); possible inclusions of uraninite; chemical abrasion is possible | XXX | Romer and Wright (1992); Romer and Smeds (1994); Romer and Smeds (1996); Romer et al. (1996); Romer and Smeds (1997); Glodny et al. (1998); Smith et al. (2004); Baumgartner et al. (2006); Dewaele et al. (2011); Melleton et al. (2012); Melcher et al. (2015); Che et al. (2015); Van Lichtervelde et al. (2016) |
| Garnet | $(Ca, Ce, La, Y)_2(Fe^{2+}, Fe^{3+}, Al)_3O(SiO_7)(SiO_4)(OH)$ | Skarn; Metamorphosed deposit | Metasomatim, metamorphism | Moderate to high amount of common Pb; low U content; no matrix-matched standard available | Andradite garnet tend to have higher U content. Date sometimes determined with the isochron method | X | Mezger et al. (1989); Mueller et al. (1996); Glodny et al. (1998); Jung and Mezger (2003); Seman et al. (2017) |
| Perovskite | $CaTiO_3$ | Diamond-bearing kimberlite; Rare-metal carbonatite | Alkaline and ultramafic magmatism | Moderate to high amount of common Pb; prone to Pb loss; in-situ dating often | Possibility of Th–Pb dating | X | Smith et al. (1989); Heaman (2003); Lehmann et al. (2010); Donnelly et al. |

(continued)

**Table 2** (continued)

| Mineral | Formula | Main types of mineral deposit where U–Pb dating can be done (non-exhaustive list) | Event dated | Principal limitations | Additional comments | Average quality of U–Pb dating[a] | Some references with application to mineral deposits |
|---|---|---|---|---|---|---|---|
| | | | | standardized to zircon mineral, perovskite standard described in Heaman (2009) | | | (2012); Zhang et al. (2013); Rao et al. (2013); Wu et al. (2013a, 2013b); Griffin et al. (2014); Heaman et al. (2015); Castillo-Oliver et al. (2016) |
| REE-Phosphate (Monazite and Xenotime) | (Ce, La, Th) $PO_4$ | Rare-metal (± Sn–W) pegmatite, greisen and granite; Orogenic Au; Banded iron formation; Archean Au paleoplacer; Stratabound polymetallic (Co, Cu, Pb, Zn, Fe, Au, Ag, Bi, W, REE); Unconformity-related U; MVT Pb–Zn; IOCG; granite-related U–Mo; Cordilleran polymetallic | Hydrothermal activity, metamorphim, magmatism | High amount of excess $^{206}Pb$ (initial $^{230}Th$ excess)[b]; strong matrix effect due to trace elements needs to be taken in consideration for SIMS dating (e.g., Fletcher et al. 2010) | Limited common Pb. No metamictization. Possibility of Th–Pb dating | XXX | Glodny et al. (1998); Torrealday et al. (2000); Petersson et al. (2001); Pigois et al. (2003); Tallarico et al. (2004); Salier et al. (2004, 2005); Fletcher et al. (2004); Schaltegger et al. (2005); Vallini et al. (2006); Michael Meyer et al. (2006); Rasmussen et al. (2007a, b, 2008); Lobato et al. (2007); Mueller et al. (2007); Kempe et al. (2008); Vielreicher et al. (2010, 2015); Fletcher et al. (2010); Sarma et al. (2011); Muhling et al. (2012); Aleinikoff et al. (2012a,b); Mosoh Bambi et al. (2013); Moreto et al. (2014); Cabral and Zeh (2015); Zi et al. (2015); McKinney et al. (2015); Taylor et al. (2015); Catchpole et al. (2015); Huston et al. (2016); Van Lichtervelde et al. (2016) |
| | $YPO_4$ | | | Moderate excess $^{206}Pb$ (intial $^{230}Th$ excess)[b]; strong matrix effect due to trace elements needs to be taken in consideration for SIMS dating (e.g., Fletcher et al. 2010) | | | |

(continued)

**Table 2** (continued)

| Mineral | Formula | Main types of mineral deposit where U–Pb dating can be done (non-exhaustive list) | Event dated | Principal limitations | Additional comments | Average quality of U–Pb dating[a] | Some references with application to mineral deposits |
|---|---|---|---|---|---|---|---|
| Rutile | $TiO_2$ | Metamorphic and magmatic Ti; Porphyry Cu–Au; Orogenic Au | Cooling; hydrothermal activity | Low U concentration in most cases, but rutiles from high-grade metamorphic rocks tend to have higher U contents (Meinhold 2010); moderate amount of common Pb | | XX | de Ronde et al. (1992); Norcross et al. (2000); von Quadt et al. (2005); Kouzmanov et al. (2009); Morisset et al. (2009); Shi et al. (2012) |
| Titanite (Sphene) | $CaTiOSiO_4$ | Skarn; IOCG; Orogenic Au; VMS | Late magmatic stage, hydrothermal activity; metasomatism; metamorphism; (cooling) | Low to moderate amount of common Pb; Titanites BLR-1 and MKED-1 proposed as matrix-matched standards (Aleinikoff et al., 2007; Spandler et al., 2016), common use of zircon or in-house standards | Possibility of Th–Pb dating | XX | Corfu and Muir (1989); Romer and Öhlander (1994); Romer et al. (1994); Eichhorn et al. (1995); Mueller et al. (1996, 2007); Norcross et al. (2000); Salier et al. (2004); Bucci et al. (2004); Wanhainen et al. (2005); De Haller et al. (2006); Skirrow et al. (2007); Chiaradia et al. (2008); Smith et al. (2009); Li et al. (2010); Dziggel et al. (2010); Chelle-Michou et al. (2015); Deng et al. (2015a,b); Seo et al. (2015); Fu et al. (2016); Poletti et al. (2016) |
| Uraninite | $UO_2$ | U(±Au, REE,…) deposits; Stratiform polymetallic (Co, As, Pb, Zn, Cu, Mo, …) epithermal | Hydrothermal activity; Metamorphism | Prone to U and Pb mobility (loss and gain) and recrystallization; low to high amount of common Pb; no international matrix-matched standard available (in-house standard) | Chemical dating (EMP) is common | X | Hofmann and Eikenberg (1991); Hofmann and Knill (1996); Fayek et al. (2000); Polito et al. (2005); Alexandre et al. (2007); Ono and Fayek (2011); Carl et al. (2011); Philippe et al. (2011); Dieng et al. (2013); Decree et al. (2014); Luo et al. (2015); Skirrow et al. (2016) |

(continued)

**Table 2** (continued)

| Mineral | Formula | Main types of mineral deposit where U–Pb dating can be done (non-exhaustive list) | Event dated | Principal limitations | Additional comments | Average quality of U–Pb dating[a] | Some references with application to mineral deposits |
|---|---|---|---|---|---|---|---|
| Zircon | $ZrSiO_4$ | All type of intermediate to acidic magmatism, differentiate products of mafic to ultramafic magmatism, Porphyry-systems (incl. Epithermal, Skarn), VMS, … | Magmatic, hydrothermal, detrital provenance and deposition, metamorphic | Can present very complex zoning patterns with several age domains | Limited common Pb. Chemical abrasion is possible | XXX | Most of the references provided for the other minerals also present zircon U–Pb dating |
| Wolframite | $(Fe^{2+}, Mn)WO_4$ | Granite-related W ± Sn ± Mo deposits, greisen, skarn, lodes and pegmatite | Hydrothermal activity | Low to moderate amount of common Pb; no matrix-matched standard available; Possible alteration of the mineral; Prone to host fluid and mineral inclusions | | X | Romer and Lüders (2006); Pfaff et al. (2009); Lecumberri-Sanchez et al. (2014); Harlaux et al. (2017) |
| Other minerals: (urano) thorite, vesuvianite, bastnaesite, polycrase, coffinite, … | | U deposits; REE deposits; … | Hydrothermal activity; Metamorphism; Supergene alteration | – | – | – | Romer (1992); Romer (1996); Rasmussen et al. (2008); Dill et al. (2010, 2013); Wu et al. (2011); Bergen and Fayek (2012); Cottle (2014); Downes et al. (2016) |

[a]XXX: Low common Pb, high U and structurally robust minerals; XX: Moderate common Pb, low U and structurally robust minerals; X: Common Pb-rich, low U, structurally and/or chemically weak minerals. This classification should only be taken as a 'rule of thumb' as each case would be different

[b]Refer to Fig. 4 to assess the magnitude of initial $^{230}Th$-disequilibrium of the expected age of the mineral

resistance in a range of extreme geological processes from the surface to the deep Earth crust and to the low diffusivity of U and Pb in its crystal lattice (Cherniak et al. 1997; Cherniak and Watson 2001, 2003; Harley and Kelly 2007). Importantly, zircon may contain tens to thousands of ppm of U (Hoskin and Schaltegger 2003) while essentially excluding initial Pb upon crystallization (Watson et al. 1997). This is mainly due to the large charge and ionic radius differences between $Pb^{2+}$ (1.26 Å) and $Zr^{4+}$ (0.84 Å) in eight-fold coordination in zircon. In fact, common Pb in zircon is often limited to small inclusions and to structurally damaged parts of the crystal which are readily removed with a chemical abrasion procedure while preserving the crystalline portion of the mineral (Mattinson 2005). The quality and ubiquity of this mineral has triggered most of the technical development of U–Pb geochronology including a wealth of international reference materials used for in-situ dating methods in all laboratories around the world.

Nevertheless, other minerals such as baddeleyite, columbite group minerals (columbo-tantalite), and rare earth element (REE)-phosphates (monazite and xenotime) present U enrichment and common Pb exclusion properties comparable to zircon. Despite their occurrence in the geological environment being more restricted than that of zircon, published data often show the same level of precision as for zircon, according to the analytical method used. Chemical abrasion techniques have been tested on these minerals but show contrasting behavior. In the case of monazite and baddeleyite, chemical abrasion has not shown any significant improvement in term of precision, reproducibility and concordance (Rioux et al. 2010; Peterman et al. 2012). This might be due to the fact that monazite and baddeleyite do not suffer metamictization (Seydoux-Guillaume et al. 2002, 2004; Trachenko, 2004). However, baddeleyite is suggested to become tetragonal at high ion radiation doses, a phase change that may facilitate radiogenic Pb mobility (Schaltegger and Davies 2017). Additionally, chemical abrasion has been successfully applied to columbo-tantalite minerals and improved the concordance of the data (Romer and Wright 1992). It is thought to remove small inclusions of Pb bearing minerals such as uraninite or secondary Nb- and Ta-bearing minerals (Romer et al. 1996).

## 5.2 Moderate Common Pb, Low U and Structurally Robust Minerals

Titanite, rutile and allanite represent very interesting properties for U–Pb dating. These accessory mineral species usually have low to moderate amounts of common Pb while being sufficiently enriched in U to allow precise dating in most cases. Analytical protocols and matrix-matched standards for in-situ dating have been developed and allow some labs to routinely date these mineral (Storey et al. 2006, 2007; Aleinikoff et al. 2007; Gregory et al. 2007; Luvizotto et al. 2009; Zack et al. 2011; Darling et al. 2012; Schmitt and Zack 2012; Smye et al. 2014). The use of titanite and especially rutile as geochronometers might be limited by their relatively lower closure temperature of the U–Pb system compared to zircon. Hydrothermal titanite (e.g., in skarn deposits) would crystallize near or just below its closure temperature allowing its use as a geochronometer (Chiaradia et al. 2008; Chelle-Michou et al. 2015), and helping to pinpoint antecrystic zircon growth (i.e., crystallized in earlier magma pulses and incorporated in a later pulse; Miller et al. 2007) in the skarn-forming magmatic intrusion. Rutile is involved in high temperature metamorphic reactions and can produce new zircon upon recrystallization at lower temperature and expulsion of Zr (e.g., Pape et al. 2016). Allanite may have exceedingly high Th/U ratios requiring a very careful approach for accurately correcting and interpreting initial $^{230}Th$ disequilibrium (Oberli et al. 2004).

## 5.3 Common Pb-Rich, Low U, Structurally and/or Chemically Weak Minerals

A wealth of other minerals can be used for U–Pb geochronology but tend (most of the time) to produce lower quality data than the minerals described above. This is mainly due to the high ratio of common to radiogenic lead in these mineral ($\gg$ 1 ppm) together with low U concentrations (< 10 ppm). This results in the chosen common Pb correction having a critical impact on the accuracy and precision of the dates. The best dates are usually obtained with the 3D isochron method or 238U/206Pb intercept ages of mixing lines (so-called "isochrons") in a Tera-Wasserburg concordia space from LA-ICP-MS dating (Schoene and Bowring 2006) and potential accompanied with the measurement of a cogenetic common Pb-rich phase (such as the magnetite-apatite geochronometer; Gelcich et al. 2005).

Furthermore, some species such as brannerite, calcite, uraninite, and, to a lesser extent, perovskite and wolframite are prone to resetting of the U–Pb system (Pb-loss), or even U mobility in the presence of hydrothermal fluids that may also promote dissolution/recrystallization of the mineral (e.g., Zartman and Smith 2009; Rasbury and Cole 2009; Ono and Fayek 2011; Bergen and Fayek 2012; Donnelly et al. 2012; Decree et al. 2014; Harlaux et al. 2017). This often results in markedly normally or inversely discordant common Pb-corrected data. Recent, advances in calcite U–Pb dating by LA-ICPMS and ID-TIMS make it possible to routinely achieve uncertainties on the order of 2–5% despite the high amount of common Pb (Li et al. 2014; Coogan et al. 2016; Roberts and Walker 2016; Burisch et al. 2017). Due to the ubiquity of calcite in vein, cement or replacement phase in mineral deposits, calcite U–Pb dating is expected to open to new opportunities for ore deposit research and to address the timing of crustal fluid flow through direct dating. Yet, the main difficulty of calcite dating is to correctly interpret the event being dated, or if unsure, allow for all reasonable possibilities (e.g., see the case of the Hamersley spherule beds, Australia; Woodhead et al. 1998; Rasmussen et al. 2005).

## 5.4 Choosing the Best Mineral for U–Pb Dating

The choice of the mineral targeted for U(–Th)–Pb dating should be dictated by the particular event or process of interest, cross-cutting and paragenetic information, and geochemical and/or structural data. Dating without consideration of the geological/petrographic context of the mineral will very likely lead to erroneous interpretation. One such example is the case of post-mineralization rhyodacite porphyry at the Corrocohuayco deposit, Peru. There, most zircon grains (11/13) from this post-mineralization porphyry were dated ~0.5 Ma older that the syn-mineralization porphyries it crosscuts (Chelle-Michou et al. 2014). This unambiguous field relationship shows that it could only be interpreted in the context of proto-pluton remelting, rather than as the age of magma emplacement.

Magmatism is arguably the most easily dated geological process. In the vast majority of cases zircon would be the mineral of choice. Even relatively mafic rocks can host zircon in the most differentiated 'melt pockets' (e.g. the Bushveld complex, South Africa; Zeh et al. 2015). In the cases where zircon is absent from the magmatic rock, usually in ultramafic, mafic or alkaline rocks, baddeleyite or perovskite present good alternatives. Finally, crust-derived granitoids often host zircon grains that are dominantly inherited from their source and minimally reflect new growth from the granitic liquid (e.g., Clemens 2003). In such cases, dating of monazite may be preferred. The main goal of dating these magmatic minerals is to constrain the age of magma emplacement in the crust or of volcanic eruption.

The increasing precision of zircon dates achievable with the CA-ID-TIMS method sheds new light on the long-lived history of magmatic systems. At the sample scale, more than 0.1 Ma of protracted zircon crystallization has been documented at a number of silicic systems, some

of which are associated with porphyry copper mineralization (Schütte et al. 2010; Wotzlaw et al. 2013; Chelle-Michou et al. 2014; Barboni et al. 2015; Buret et al. 2017). When combined with complimentary geochemical data, zircon crystallization ages can provide valuable insights into the specific petrological processes responsible the transition from barren to ore-producing intrusions (Chelle-Michou et al. 2014; Tapster et al. 2016; Buret et al. 2016).

Despite its common usage in ore deposit research, the dating of magma intrusion only rarely dates the mineralization itself. In fact, this is only restricted to places where the ore minerals have crystallized under magmatic conditions such as the magmatic Ni–Cu–Cr(±Au ± PGE) deposits and possibly some magmatic REE deposits as well. If appropriate crosscutting relationship with the mineralization can be observed, dating magmatic intrusions can elegantly bracket the timing of ore deposition (e.g., von Quadt et al. 2011). In the case of porphyry, greisen, or volcanogenic massive sulfide (VMS) deposits the age of the ore-related intrusion or of the associated volcanics may often provide a good, if not excellent, approximation for age of the mineralization. Yet, this approach requires much caution as even in classical magmatic-hydrothermal deposits such as W–Sn granite deposits or porphyry Cu deposits, the mineralization can have been sourced by a hidden intrusion at depth while being hosted in a previously emplaced one (e.g., Schaltegger et al. 2005). However, for deposits where the relationship between ore formation and a particular magma intrusion is ambiguous (e.g., iron oxide copper–gold (IOCG) deposits, orogenic Au deposit, epithermal deposits, distal skarns) or even totally absent (e.g., Mississippi Valley-type (MVT) deposits) it is much more advantageous to determine directly the timing of hydrothermal fluid circulation and/or of ore deposition. The list of ore minerals suitable for U–Pb dating include cassiterite (for Sn deposits), wolframite (for W deposits) columbo-tantalite (in some rare-metal granite, greisen and pegmatite deposits), rutile (for Ti deposits), and minerals associated with U deposits (e.g., uraninite, brannerite). This restricts the types of ore that can dated with the U–Pb method. Alternatively, several gangue mineral species can be used to date hydrothermal fluid circulation, metasomatism and metamorphism. Their relevance for the genesis or reworking of the studied ore deposit is fundamentally linked to their position in the paragenetic sequence with respect to the ore minerals. REE-phosphates such as monazite and xenotime are common in a wide variety of hydrothermal systems ranging from granite-related rare metal deposits to MVT deposits (Table 2) and, if available, would be the ideal minerals to date hydrothermal processes. In few cases, hydrothermal zircons at skarn (Niiranen et al. 2007; Wan et al. 2012; Deng et al. 2015c), IOCG (Valley et al. 2009), orogenic Au (Kerrich and Kyser 1994; Pelleter et al. 2007), and alkaline/carbonatite magmatism related rare-metal deposits (Yang et al. 2013; Campbell et al. 2014) have been reported and can date hydrothermal activity and metasomatism. However, in the absence of these hydrothermal minerals (which is not uncommon), other minerals listed in Table 2 with non-negligible amounts of common Pb can be called on. Titanite or allanite can provide excellent dates for skarn (Chiaradia et al. 2008; Deng et al. 2014, 2015b; Chelle-Michou et al. 2015) and IOCG deposits (Skirrow et al. 2007; Smith et al. 2009; De Haller et al. 2011). Ore-stage calcite or apatite may sometimes represent the only minerals suitable for U–Pb dating at MVT deposits (Grandia et al. 2000) or some REE-P deposits (Huston et al. 2016). The ability of apatite to keep record of Cl, F, OH and $SO_4^{2-}$ of the hydrothermal fluid (or magma) from which it crystallizes (Webster and Piccoli 2015; Harlov 2015) coupled with the possibility to date it with the U–Pb method (Chew and Spikings 2015) opens interesting opportunities to refine ore forming models. Finally, U–Pb minerals such as rutile, apatite and/or titanite can provide invaluable thermochronological information on the thermal evolution of the studied ore deposit during and after its genesis.

## 6 Case Studies of Applications of U–Pb Dating to Mineral Deposits

In the following section, we present two case studies that make very distinct use of U–Pb geochronology. The first one focuses on the Witwatersrand gold deposits, South Africa, and illustrates how geochronology based on several mineral species can be used to bracket the age of multiple geological events over long timescales (> 10 Ma). The second one discusses how rather than the absolute age, the duration of the mineralizing event at porphyry copper deposits can help understand the ore-forming processes and the main controls on the size (metal content) of the deposits. These two examples embody different timescales of reasoning, different precision, accuracy and spatial resolution requirements, and different uses of the geochronological data.

### 6.1 Input of Multi-mineral U–Pb Dating for Understanding Gold Deposition and Remobilization in the Witwatersrand Basin, South Africa

About 32% of all gold ever mined and about the same proportion of known gold resources comes from deposits hosted in the Witwatersrand Basin, South Africa (Frimmel and Hennigh 2015), a Mesoarchean detrital sedimentary basin deposited on the Kaapvaal Craton (Fig. 9). The genesis of this enormous accumulation of gold in the crust has triggered one of the "*greatest debate in the history of economic geology*" (see summary in Muntean et al. 2005). Proposed models for the deposition of gold range from a modified paleoplacer to a purely hydrothermal origin. These disparate views arises from contradicting observations that are selectively put forward to favor either model (Frimmel et al. 2005; Law and Phillips 2005; Muntean et al. 2005). In fact, probably none of these end-member models can account for all the geological, chemical and isotopic observations. The most recent models rather consider the very peculiar conditions that prevailed in the Mesoarchean atmosphere, hydrosphere and biosphere (Frimmel and Hennigh 2015; Heinrich 2015). At this time, redox reations mediated by microbial life could have triggered the synsedimentary precipitation of the large quantities of gold dissolved in acidic and reduced meteoric and shallow sea waters.

U–Pb geochronology has been instrumental in the understanding of the formation Witwatersrand goldfields. It first played an essential role in calibrating the depositional age of the sediments (Fig. 9). One of the most significant contribution comes from Armstrong et al. (1991) who dated zircons from volcanic rocks distributed along the sedimentary pile of the basin. They constrained the deposition of the Witwatersrand Supergroup to within a timeframe of ca. 360 Ma from 3074 to 2714 Ma. Subsequent studies have focused on detrital zircon and xenotime from the main formations present along the stratigraphic column and intimately associated with the gold-bearing reefs (England et al. 2001; Kositcin and Krapež 2004; Koglin et al. 2010). These have confirmed the previous depositional ages but provide additional insight in the source of the detritus that filled the basin, as well as secular changes in the catchment area of the basin over time. Results show that the source area of detritus has an increasing age-range of rocks undergoing erosion over time. Apart from the lowermost part of the Witwatersrand Supergroup (Orange Formation, West Rand Group) which has dates clustering around 3.21 Ga, zircon dates from the West Rand Group cluster around 3.06 Ga, with only few older and younger dates (Fig. 9). Furthermore, zircon dates from the Central Rand Group shows additional peaks at 2.96–2.92 Ga and 3.44–3.43 Ga with several intervening dates in between these main peaks. Dates of detrital xenotime are mostly within the 3.1–2.9 Ga range but also extend as low as 2.8 Ga (Fig. 9). Koglin et al. (2010) and Ruiz et al. (2006) further link the gold-rich sediments to the presence of the 3.06 Ga zircon age peak. When compared with

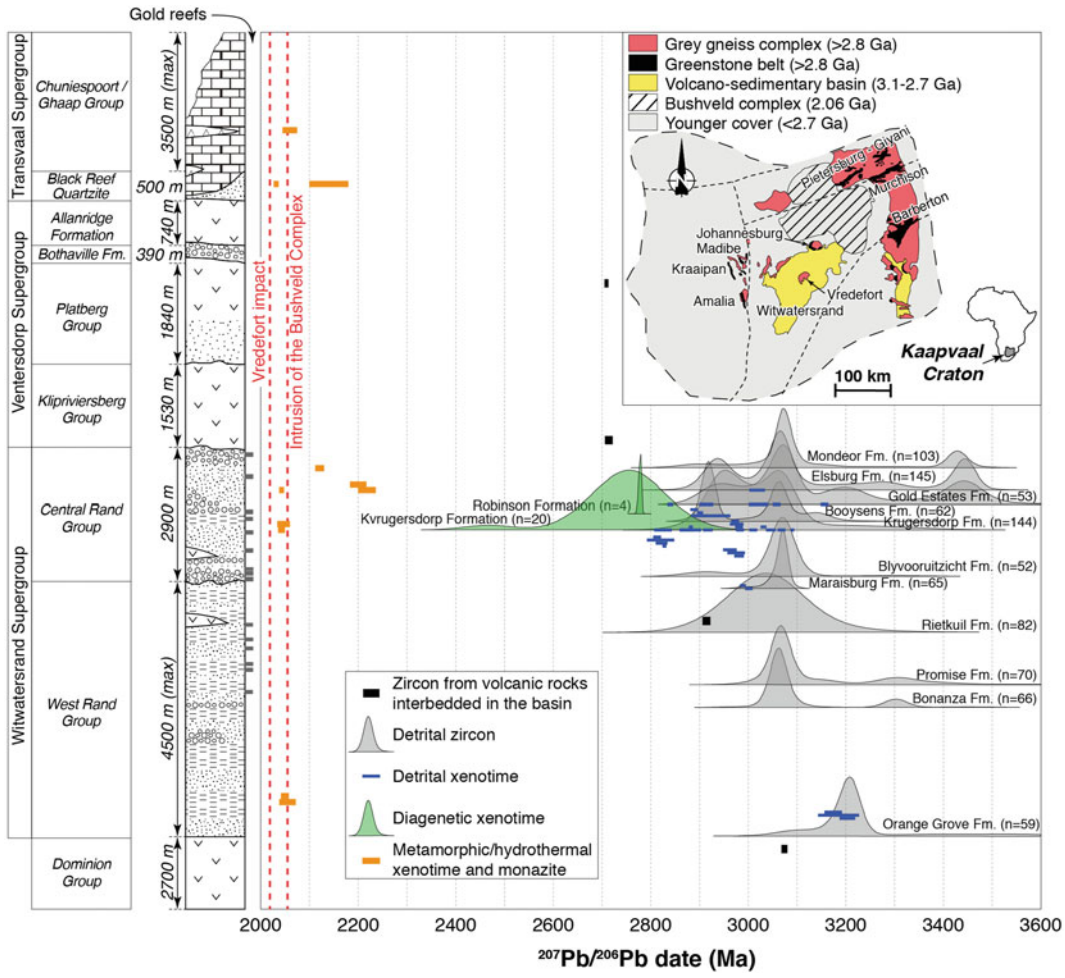


**Fig. 9** Compilation of available U–Pb data from the Witwatersrand basin plotted against the stratigraphic position of the sample. Stratigraphic column of the Archean to early Proterozoic succession in South Africa from Muntean et al. (2005). Data from the Witwatersrand basin are from Armstrong et al. (1991), England et al. (2001), Kositcin et al. (2003) Kositcin and Krapež (2004), Rasmussen et al. (2007a) and Koglin et al. (2010). Ages of the intrusion of the Bushveld Complex and of the Vredefort impact are from Zeh et al. (2015) and Moser (1997), respectively. Kernel density estimates (KDE) where obtained using DensityPlotter (Vermeesch 2012). Selected data are 95–105% concordant and data points are plotted at the 2σ uncertainty level. Inset map of the Kaapvaal craton is modified from Poujol (2007)

outcropping Archean terrains of the Kaapvaal Craton, these zircons could have originated from the greenstone belts west of the Witwatersrand basin (Madibe and Kraaipan), rocks in the immediate proximity of the basin (e.g., Johannesburg and Vrefefort Dome) or from equivalent units located northwest of the basin that might be present below the post-Witwatersrand cover (Koglin et al. 2010). More distal candidates such as the Murchison and the Barberton greenstone belts have also been proposed (Ruiz et al. 2006; Koglin et al. 2010). This interpretation is also compatible with paleocurrent directions and isotopic data (Koglin et al. 2010).

A paleoplacer model requires that all of the gold deposited in the basin originated from the same eroding massifs that sourced the sediments. However, such gigantic quantities of gold are two orders of magnitude in excess of all the gold ever mined and discovered in the potential

outcropping massifs that sourced the zircons. This observation has been a major argument against any sort of paleoplacer model (e.g., Phillips and Law 2000; Law and Phillips 2005; Frimmel and Hennigh 2015). The existence of a now vanished or buried, hypothetical massif as a source of this huge amount of gold would pose an equally important question about how this massif would have been exceptionally well endowed with gold.

An epigenetic (hydrothermal) origin of the gold is supported by several petrographic observations. Yet, cross-cutting relationship suggest that hydrothermal activity took place before deposition of the Platberg Group, that is, before ca. 2.7 Ga (e.g., Law and Phillips 2005; Meier et al. 2009). U–Pb dating of diagenetic xenotime have yielded a major peak between 2.78–2.72 Ga which could be related to a heating event and flood-basalt volcanism during the deposition of the Klipriviersberg Group, immediately following the deposition of the Witwatersrand Supergroup (Fig. 9; England et al. 2001; Kositcin et al. 2003). Although this timing for gold introduction would be consistent with temporal constrains, the association of gold with this 2.78–2.72 Ga xenotime has not been reported. Additionally, U–Pb dating of metamorphic-hydrothermal REE-phosphates (monazite and xenotime) paragenetically associated with some gold or unrelated to gold mostly records ages between 2.06 and 2.03 Ga throughout the stratigraphic succession from the Witwatersrand to the Transvaal Supergroups (Fig. 9; England et al. 2001; Kositcin et al. 2003; Rasmussen et al. 2007a). This age is consistent with the emplacement age 1of the Bushveld complex on the northern flank of the Witwatersrand Basin (Zeh et al. 2015) which most likely triggered fluid circulation, gold remobilization and peak greenschist metamorphic conditions in the basin (Rasmussen et al. 2007a).

While none of the available U–Pb data for the Witwatersrand basin (Fig. 9) can firmly date gold deposition, or conclusively explain how gold was deposited, they have provided the necessary temporal framework on which to challenge relative chronological data. They have brought significant arguments against each of the classical models invoked for the formation of this district (syngenetic vs epigenetic) while confirming that gold remobilization occurred long after the formation of the deposit and contributed to the emergence of new ore forming models (Frimmel and Hennigh 2015; Heinrich 2015). This example highlights the necessity to properly constrain each U–Pb date against paragenetic, cross-cutting and stratigraphic observations in order to draw meaningful conclusions. The Witwatersrand gold deposits result from a long-lived and multi-episodic geological history where U–Pb geochronology provided constraints on basin formation, sediment provenance, diagenesis and metamorphism. It is noteworthy that the different minerals that were dated (zircon, monazite, xenotime), individually record a limited portion of the multiple processes that shaped the Witwatersrand basin and proved to be highly complementary to each other. Unveiling this protracted history did not require particularly high-precision dating methods, as LA-ICPMS and SIMS instruments with high sample throughput (Table 1) proved very effective. Additionally, the very high spatial resolution achievable with a SIMS instrument was crucial in unlocking the U–Pb information in tiny xenotime and monazite crystals identified from thin sections.

## 6.2 Zircon U–Pb Insights into the Genesis on Porphyry Copper Deposits

Porphyry copper deposits (PCDs) typically form at convergent margins in association with subduction or post-subduction magmatism (e.g., Richards 2009). Metals and sulfur fixed in these deposits are thought to have been sourced from a cooling and degassing fluid-saturated magma body emplaced at shallow depths within the upper crust and transported to the site of deposition by magmatic-hydrothermal fluids (Hedenquist and Lowenstern 1994; Sillitoe 2010; Pettke et al. 2010; Simon and Ripley 2011; Richards

2011). Ultimately, very efficient fluid focusing and sulfide precipitation together with post-mineralization ore deposit preservation will favor the presence of economic porphyry deposits at erosion levels.

The USGS global database of PCDs shows that these deposits span more than four orders of magnitude in copper endowment (Singer et al. 2008; Fig. 10a). Yet, the specific factors that control the size of these deposits have remained speculative. Comparing 'standard' and 'giant' PCDs, Richards (2013) speculated that the formation of the largest deposits result from a combination of copper enrichment in the magma, the focusing of fluids in structural corridors and, long-lived hydrothermal activity may favor the formation of the largest deposits. Among these possible factors, the timescale of PCD formation may play a significant role in their size. Compiling geochronological data (U–Pb on zircon and Re–Os on molybdenite) from PCDs around the world, Chelle-Michou et al. (2017) and Chiaradia and Caricchi (2017) have highlighted a correlation between the duration of the mineralizing event and the total mass of copper deposited, suggesting an average copper deposition rate of about 40 Mt/Ma (Fig. 10b). This relationship probably reflects the mass balance requirement for a giant deposit to be sourced by a large body of magma, which is incrementally injected into the upper crust over long timescales (see Chelle-Michou et al. 2017).

Similar conclusions where reached by Caricchi et al. (2014) who suggested that magmatism associated with economic PCDs is distinguishable from background pluton-forming

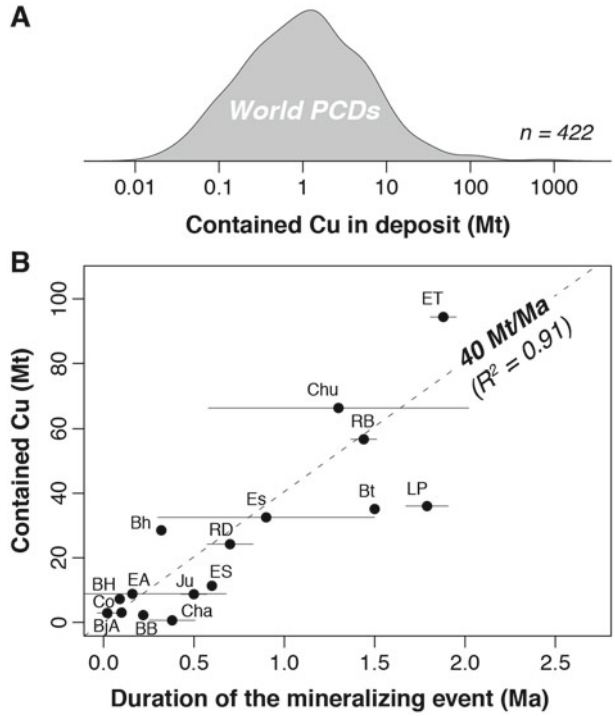


**Fig. 10** **a** probability density distribution of Cu endowment in global porphyry copper deposits (PCDs). Data from Singer et al. (2008). **b** Correlation between the duration of the mineralizing event and the total amount of Cu deposited (adapted from Chiaradia and Caricchi, 2017). BH: Batu Hijau (Indonesia), BjA: Bajo de la Alumbrera (Argentina), Co: Coroccohuayco (Peru), EA: El Abra (Chile), BB: Boyongan-Bayugo (Philippines)), Bh: Bingham (US), Cha: Chaucha (Ecuador), Ju: Junin (Ecuador), ES: El Salvador (Chile), Es: Escondida (Chile), LP: Los Pelambres (Chile), Chu: Chuquicamata (Chile), RB: Rio Blanco (Chile), Bt: Butte (US), ET: El Teniente (Chile), RD: Reko Diq (Pakistan)

magmatism and large-eruption-forming magmatism by large magma volumes emplaced at average rate of magma injection ($\sim$0.001 km$^3$/yr). This conclusion was drawn through inverse thermal modelling of high-precision CA-ID-TIMS U–Pb zircon age distributions.

While geochronology on PCDs has been mostly used to determine the formation age of these deposits, high-precision geochronological data can now be used to elucidate the duration of the ore-forming process. Figure 10b shows that the duration of ore-formation may be a significant control on their size (i.e., metal endowment) and, by inference, on the specific processes responsible for their formation. In addition, high-precision geochronological data may be able to help test the validity of numerical models of PCD formation (e.g., Weiss et al. 2012), or directly as input data into numerical models aiming at quantifying the time-volume-flux-geochemistry relationships of the magmatism associated with PCD genesis (e.g., Caricchi et al. 2014; Chelle-Michou et al. 2017; Chiaradia and Caricchi 2017). These studies only start to unearth the great potential of high-precision CA-ID-TIMS U–Pb dating for PCD exploration, and can also significantly contribute to a better understanding of PCD magmatic ore-forming processes.

## 7 Concluding Remarks

Over the past two decades U–Pb geochronology has become an essential tool for the study of ore deposits. After a century of development, more than 16 minerals can now be dated with the U–Pb technique allowing its use for most types of ore deposits. U–Pb dating is most commonly used to provide the age of a particular geological event related to a studied deposit (e.g., magmatism, hydrothermal activity, sedimentation, metamorphism, ore deposition and remobilization), depending on the mineral(s) available for dating. The choice of the mineral(s) and of the analytical technique (LA-ICPMS, SIMS or ID-TIMS) used for dating mainly depends on the scientific questions that need to be answered and on the opportunities offered by the studied deposit. This point is perhaps one of the main limitations of the U–Pb dating of ore deposits. For example, MVT deposits rarely contain minerals suitable for U–Pb dating (potentially calcite, provided it has low initial Pb), in which case the use of other isotopic systems will be necessary (e.g., Rb–Sr on sphalerite, Re–Os on sulfides). In addition, as we have seen in the case of the Witwatersrand basin, the spatial resolution required for the analysis may sometimes critically guide the choice of the analytical method.

Recent advances that combine numerical modelling with U–Pb geochronology for porphyry copper deposits suggest that high-precision zircon U–Pb data may also be used as a window to better understand the magmatic aspect of the ore-forming process (Caricchi et al. 2014) and to unravel the fundamental controls on the size of the deposit (Chelle-Michou et al. 2017; Chiaradia and Caricchi, 2017). Comparable studies on other deposit types could potentially advance our understanding of ore-forming processes and may generate innovative tools for mineral exploration.

A further important development of U–Pb geochronology concerns its coupling with textural and geochemical data (e.g., trace elements, Lu–Hf isotopes, O isotopes) obtained on the same grain or on the same spot as the U–Pb data. This is commonly referred to as 'petrochronology' and allows temporal information relative to the evolution and/or the source of the liquid (a magma or an aqueous fluid) from which the mineral precipitated and potentially the rate of its evolution (e.g., Ballard et al. 2002; Smith et al. 2009; Valley et al. 2010; Pal et al. 2011; Rao et al. 2013; Yang et al. 2013; Griffin et al. 2014; Rezeau et al. 2016; Poletti et al. 2016; Gardiner et al. 2017). In particular, high-precision petrochronology on zircon and baddeleyite can provide unprecedented insights into the processes at play during magma evolution, the potential turning point leading to mineralization, or, the link between small intrusive bodies (dykes or stocks) or volcanic products and their larger deep-seated plutonic source (e.g.,Wotzlaw et al. 2013, 2015; Chelle-Michou et al. 2014; Tapster

et al. 2016; Buret et al. 2016; 2017; Schaltegger and Davies, 2017).

The field of U–Pb geochronology is working towards a level of maturity whereby inter-laboratory reproducibility will be guaranteed in most labs around the world and where each date and its uncertainty can be fully traceable to SI units. This however, should not mask the high-level of competency and training required to certify the quality of the analysis, to maintain the lab at the best level (picogram levels of common Pb contaminations can be dramatic in a CA-ID-TIMS lab) and, very importantly, the interpretation of the dates into geologically relevant ages. As we have shown, there are numerous potential pitfalls that, if not carefully accounted for, can result in unsupported or even wrong conclusions.

The improving precision, accuracy and spatial resolution of analyses now achievable, challenges paradigms of ore-forming processes and will continue to contribute significant breakthroughs in ore deposit research and potentially also contribute to the development of new mineral exploration tools. The full added value of U–Pb geochronology will however only be assured through its coupling with geochemical data, high-quality field and petrographic observations and numerical modelling.

**Acknowledgements** We are grateful to the D. Huston for inviting us to write this chapter. Constructive reviews from Andrew Cross and Neal McNaughton significantly improved the clarity of the manuscript and were very much appreciated. C. Chelle-Michou acknowledges financial support from the European Commission and the Université Jean Monnet during the preparation of the manuscript. Both authors acknowledge the support of the Swiss National Science Foundation.

## References

Aleinikoff JN, Wintsch RP, Tollo RP, Unruh DM, Fanning CM, Schmitz MD (2007) Ages and origins of rocks of the Killingworth dome, south-central Connecticut: implications for the tectonic evolution of southern New England. Am J Sci 307:63–118. https://doi.org/10.2475/01.2007.04

Aleinikoff JN, Hayes TS, Evans KV, Mazdab FK, Pillers RM, Fanning CM (2012a) SHRIMP U–Pb Ages of xenotime and monazite from the Spar Lake red bed-associated Cu–Ag deposit, western Montana: implications for ore genesis. Econ Geol 107:1251–1274. https://doi.org/10.2113/econgeo.107.6.1251

Aleinikoff JN, Slack JF, Lund K, Evans KV, Fanning CM, Mazdab FK, Wooden JL, Pillers RM (2012b) Constraints on the timing of Co-Cu ± Au mineralization in the Blackbird District, Idaho, using SHRIMP U–Pb ages of monazite and xenotime plus zircon ages of related Mesoproterozoic orthogneisses and metasedimentary rocks. Econ Geol 107:1143–1175. https://doi.org/10.2113/econgeo.107.6.1143

Alexandre P, Kyser K, Thomas D, Polito P, Marlat J (2007) Geochronology of unconformity-related uranium deposits in the Athabasca Basin, Saskatchewan, Canada and their integration in the evolution of the basin. Miner Depos 44:41–59. https://doi.org/10.1007/s00126-007-0153-3

Allen CM, Campbell IH (2012) Identification and elimination of a matrix-induced systematic error in LA–ICP–MS $^{206}Pb/^{238}U$ dating of zircon. Chem Geol 332–333:157–165. https://doi.org/10.1016/j.chemgeo.2012.09.038

Amelin Y, Li C, Naldrett AJ (1999) Geochronology of the Voisey's Bay intrusion, Labrador, Canada, by precise U–Pb dating of coexisting baddeleyite, zircon, and apatite. Lithos 47:33–51

Amelin Y, Zaitsev AN (2002) Precise geochronology of phoscorites and carbonatites: the critical role of U-series disequilibrium in age interpretations. Geochim Cosmochim Acta 66:2399–2419. https://doi.org/10.1016/S0016-7037(02)00831-1

Anczkiewicz R, Oberli F, Burg JP, Villa IM, Günther D, Meier M (2001) Timing of normal faulting along the Indus suture in Pakistan Himalaya and a case of major $^{231}Pa/^{235}U$ initial disequilibrium in zircon. Earth Planet Sci Lett 191:101–114. https://doi.org/10.1016/S0012-821X(01)00406-X

Arevalo R Jr (2014) Laser ablation ICP-MS and laser fluorination GS-MS. In: Treatise on geochemistry. Elsevier, pp 425–441

Arevalo R, Bellucci J, McDonough WF (2010) GGR Biennial Review: advances in laser ablation and solution ICP-MS from 2008 to 2009 with particular emphasis on sensitivity enhancements, mitigation of fractionation effects and exploration of new applications. Geostand Geoanal 34:327–341. https://doi.org/10.1111/j.1751-908X.2010.00934.x

Armstrong RA, Compston W, Retief EA, Williams IS, Welke HJ (1991) Zircon ion microprobe studies bearing on the age and evolution of the Witwatersrand triad. Precambrian Res 53:243–266. https://doi.org/10.1016/0301-9268(91)90074-K

Aston FW (1929) The mass-spectrum of uranium lead and the atomic weight of protactinium. Nature 123:313. https://doi.org/10.1038/123313a0

Ballard J, Palin M, Campbell I (2002) Relative oxidation states of magmas inferred from Ce(IV)/Ce(III) in zircon: application to porphyry copper deposits of northern Chile. Contrib Mineral Petrol 144:347–364. https://doi.org/10.1007/s00410-002-0402-5

Ballard JR, Palin JM, Williams IS, Campbell IH, Faunes A (2001) Two ages of porphyry intrusion resolved for the super-giant Chuquicamata copper deposit of northern Chile by ELA-ICP-MS and SHRIMP. Geology 29:383–386. https://doi.org/10.1130/0091-7613(2001)029%3c0383:TAOPIR%3e2.0.CO;2

Barboni M, Annen C, Schoene B (2015) Evaluating the construction and evolution of upper crustal magma reservoirs with coupled U/Pb zircon geochronology and thermal modeling: a case study from the Mt. Capanne pluton (Elba, Italy). Earth Planet Sci Lett 432:436–448. https://doi.org/10.1016/j.epsl.2015.09.043

Baumgartner R, Romer RL, Moritz R, Sallet R, Chiaradia M (2006) Columbite–tantalite-bearing granitic pegmatites from the Seridó belt, northeastern Brazil: genetic constraints from U–Pb dating and Pb isotopes. Can Mineral 44:69–86. https://doi.org/10.2113/gscanmin.44.1.69

Becquerel H (1896a) Sur les radiations invisibles émises par les corps phosphorescents. C R Acad Sci Paris 122:501–503

Becquerel H (1896b) Sur les radiations invisibles émises par les sels d'uranium. C R Acad Sci Paris 122:689–694

Bergen L, Fayek M (2012) Petrography and geochronology of the Pele Mountain quartz-pebble conglomerate uranium deposit, Elliot Lake District, Canada. Am Min 97:1274–1283. https://doi.org/10.2138/am.2012.4040

Beyer C, Berndt J, Tappe S, Klemme S (2013) Trace element partitioning between perovskite and kimberlite to carbonatite melt: new experimental constraints. Chem Geol 353:132–139. https://doi.org/10.1016/j.chemgeo.2012.03.025

Bjärnborg K, Scherstén A, Söderlund U, Maier D, W, (2015) Geochronology and geochemical evidence for a magmatic arc setting for the Ni–Cu mineralised 1.79 Ga Kleva gabbro–diorite intrusive complex, southeast Sweden. GFF 137:83–101. https://doi.org/10.1080/11035897.2015.1015265

Black LP, Kamo SL, Allen CM, Davis DW, Aleinikoff JN, Valley JW, Mundil R, Campbell IH, Korsch RJ, Williams IS, Foudoulis C (2004) Improved $^{206}Pb/^{238}U$ microprobe geochronology by the monitoring of a trace-element-related matrix effect; SHRIMP, ID–TIMS, ELA–ICP–MS and oxygen isotope documentation for a series of zircon standards. Chem Geol 205:115–140. https://doi.org/10.1016/j.chemgeo.2004.01.003

Blackburn T, Bowring SA, Schoene B, Mahan K, Dudas F (2011) U–Pb thermochronology: creating a temporal record of lithosphere thermal evolution. Contrib Mineral Petrol 162:479–500. https://doi.org/10.1007/s00410-011-0607-6

Boltwood BB (1907) Ultimate disintegration products of the radioactive elements; Part II, Disintegration products of uranium. Am J Sci Series 4 23:78–88. https://doi.org/10.2475/ajs.s4-23.134.78

Bowring SA, Erwin D, Parrish R, Renne P (2005) EARTHTIME: a community-based effort towards high-precision calibration of earth history. Geochim Cosmochim Acta Supplement 69:A316

Bowring JF, McLean NM, Bowring SA (2011) Engineering cyber infrastructure for U–Pb geochronology: Tripoli and U–Pb_Redux. Geochem Geophys Geosyst 12:Q0AA19. https://doi.org/10.1029/2010GC003479

Brandt S, Schenk V, Raith MM, Appel P, Gerdes A, Srikantappa C (2011) Late Neoproterozoic P-T evolution of HP-UHT Granulites from the Palni Hills (South India): new constraints from phase diagram modelling, LA-ICP-MS zircon dating and in-situ EMP monazite dating. J Petrol 52:1813–1856. https://doi.org/10.1093/petrology/egr032

Brannon JC, Cole SC, Podosek FA, Ragan VM, Coveney RM, Wallace MW, Bradley AJ (1996) Th–Pb and U–Pb Dating of ore-stage calcite and Paleozoic fluid flow. Science 271:491–493. https://doi.org/10.1126/science.271.5248.491

Bucci LA, McNaughton NJ, Fletcher IR, Groves DI, Kositcin N, Stein HJ, Hagemann SG (2004) Timing and duration of high-temperature gold mineralization and spatially associated granitoid magmatism at Chalice, Yilgarn Craton, Western Australia. Econ Geol 99:1123–1144. https://doi.org/10.2113/gsecongeo.99.6.1123

Buret Y, von Quadt A, Heinrich C, Selby D, Wälle M, Peytcheva I (2016) From a long-lived upper-crustal magma chamber to rapid porphyry copper emplacement: reading the geochemistry of zircon crystals at Bajo de la Alumbrera (NW Argentina). Earth Planet Sci Lett 450:120–131. https://doi.org/10.1016/j.epsl.2016.06.017

Buret Y, Wotzlaw J-F, Roozen S, Guillong M, von Quadt A, Heinrich CA (2017) Zircon petrochronological evidence for a plutonic-volcanic connection in porphyry copper deposits. Geology 45:623–626. https://doi.org/10.1130/G38994.1

Burisch M, Gerdes A, Walter BF, Neumann U, Fettel M, Markl G (2017) Methane and the origin of five-element veins: mineralogy, age, fluid inclusion chemistry and ore forming processes in the Odenwald, SW Germany. Ore Geol Rev 81:42–61

Cabral AR, Zeh A (2015) Detrital zircon without detritus: a result of 496-Ma-old fluid–rock interaction during the gold-lode formation of Passagem, Minas Gerais, Brazil. Lithos 212–215:415–427. https://doi.org/10.1016/j.lithos.2014.10.011

Campbell LS, Compston W, Sircombe KN, Wilkinson CC (2014) Zircon from the East Orebody of the Bayan Obo Fe–Nb–REE deposit, China, and SHRIMP ages for carbonatite-related magmatism and REE mineralization events. Contrib Mineral Petrol 168:1041. https://doi.org/10.1007/s00410-014-1041-3

Caricchi L, Simpson G, Schaltegger U (2014) Zircons reveal magma fluxes in the Earth's crust. Nature 511:457–461. https://doi.org/10.1038/nature13532

Carl C, von Pechmann E, Höhndorf A, Ruhrmann G (2011) Mineralogy and U/Pb, Pb/Pb, and Sm/Nd

geochronology of the Key Lake uranium deposit, Athabasca Basin, Saskatchewan, Canada. Can J Earth Sci 29:879–895. https://doi.org/10.1139/e92-075

Carlson RW (2014) Thermal ionization mass spectrometry. In: Treatise on geochemistry. Elsevier, pp 337–354

Castillo-Oliver M, Galí S, Melgarejo JC, Griffin WL, Belousova E, Pearson NJ, Watangua M, O'Reilly SY (2016) Trace-element geochemistry and U–Pb dating of perovskite in kimberlites of the Lunda Norte province (NE Angola): Petrogenetic and tectonic implications. Chem Geol 426:118–134. https://doi.org/10.1016/j.chemgeo.2015.12.014

Catchpole H, Kouzmanov K, Bendezú A, Ovtcharova M, Spikings R, Stein H, Fontboté L (2015) Timing of porphyry (Cu–Mo) and base metal (Zn-Pb-Ag-Cu) mineralisation in a magmatic-hydrothermal system – Morococha district, Peru. Miner Depos 50:895–922. https://doi.org/10.1007/s00126-014-0564-x

Chakhmouradian AR, Reguir EP, Kamenetsky VS, Sharygin VV, Golovin AV (2013) Trace-element partitioning in perovskite: implications for the geochemistry of kimberlites and other mantle-derived undersaturated rocks. Chem Geol 353:112–131. https://doi.org/10.1016/j.chemgeo.2013.01.007

Che XD, Wu F-Y, Wang R-C, Gerdes A, Ji W-Q, Zhao Z-H, Yang J-H, Zhu Z-Y (2015) In situ U–Pb isotopic dating of columbite–tantalite by LA–ICP–MS. Ore Geol Rev 65:979–989. https://doi.org/10.1016/j.oregeorev.2014.07.008

Chelle-Michou C, Chiaradia M, Ovtcharova M, Ulianov A, Wotzlaw J-F (2014) Zircon petrochronology reveals the temporal link between porphyry systems and the magmatic evolution of their hidden plutonic roots (the Eocene Coroccohuayco deposit, Peru). Lithos 198–199:129–140. https://doi.org/10.1016/j.lithos.2014.03.017

Chelle-Michou C, Chiaradia M, Selby D, Ovtcharova M, Spikings RA (2015) High-resolution geochronology of the Coroccohuayco porphyry-skarn deposit, Peru: a rapid product of the Incaic Orogeny. Econ Geol 110:423–443. https://doi.org/10.2113/econgeo.110.2.423

Chelle-Michou C, Rottier B, Caricchi L, Simpson G (2017) Tempo of magma degassing and the genesis of porphyry copper deposits. Sci Rep 7:40566. https://doi.org/10.1038/srep40566

Chen WT, Zhou M-F (2014) Ages and compositions of primary and secondary allanite from the Lala Fe–Cu deposit, SW China: implications for multiple episodes of hydrothermal events. Contrib Mineral Petrol 168:1043. https://doi.org/10.1007/s00410-014-1043-1

Chen X-C, Hu R-Z, Bi X-W, Li H-M, Lan J-B, Zhao C-H, Zhu J-J (2014) Cassiterite LA-MC-ICP-MS U/Pb and muscovite $^{40}Ar/^{39}Ar$ dating of tin deposits in the Tengchong-Lianghe tin district, NW Yunnan, China. Miner Depos 49:843–860. https://doi.org/10.1007/s00126-014-0513-8

Cheng H, Lawrence Edwards R, Shen C-C, Polyak VJ, Asmerom Y, Woodhead J, Hellstrom J, Wang Y, Kong X, Spötl C, Wang X, Calvin Alexander E (2013) Improvements in $^{230}Th$ dating, $^{230}Th$ and $^{234}U$ half-life values, and U–Th isotopic measurements by multi-collector inductively coupled plasma mass spectrometry. Earth Planet Sci Lett 371:82–91. https://doi.org/10.1016/j.epsl.2013.04.006

Cherniak DJ, Watson EB (2001) Pb diffusion in zircon. Chem Geol 172:5–24. https://doi.org/10.1016/S0009-2541(00)00233-3

Cherniak DJ, Watson EB (2003) Diffusion in Zircon. Rev Mineral Geochem 53:113–143. https://doi.org/10.2113/0530113

Cherniak DJ, Hanchar JM, Watson EB (1997) Diffusion of tetravalent cations in zircon. Contrib Mineral Petrol 127:383–390. https://doi.org/10.1007/s004100050287

Cherniak DJ, Watson EB, Grove M, Harrison TM (2004) Pb diffusion in monazite: a combined RBS/SIMS study. Geochim Cosmochim Acta 68:829–840. https://doi.org/10.1016/j.gca.2003.07.012

Chew DM, Spikings RA (2015) Geochronology and thermochronology using apatite: time and temperature, lower crust to surface. Elements 11:189–194. https://doi.org/10.2113/gselements.11.3.189

Chew DM, Sylvester PJ, Tubrett MN (2011) U–Pb and Th–Pb dating of apatite by LA-ICPMS. Chem Geol 280:200–216. https://doi.org/10.1016/j.chemgeo.2010.11.010

Chiaradia M, Vallance J, Fontboté L, Stein H, Schaltegger U, Coder J, Richards J, Villeneuve M, Gendall I (2008) U–Pb, Re–Os, and $^{40}Ar/^{39}Ar$ geochronology of the Nambija Au-skarn and Pangui porphyry Cu deposits, Ecuador: implications for the Jurassic metallogenic belt of the Northern Andes. Miner Depos 44:371–387. https://doi.org/10.1007/s00126-008-0210-6

Chiaradia M, Caricchi L (2017) Stochastic modelling of deep magmatic controls on porphyry copper deposit endowment. Sci Rep 7:44523. https://doi.org/10.1038/srep44523

Chiaradia M, Schaltegger U, Spikings R, Wotzlaw JF, Ovtcharova M (2013) How accurately can we date the duration of magmatic-hydrothermal events in porphyry systems? An invited paper. Econ Geol 108:565–584. https://doi.org/10.2113/econgeo.108.4.565

Chiaradia M, Schaltegger U, Spikings RA (2014) Time scales of mineral systems—advances in understanding over the past decade. Soc Econ Geol Spec Publ 18:37–58

Clemens J (2003) S-type granitic magmas—petrogenetic issues, models and evidence. Earth Sci Rev 61:1–18. https://doi.org/10.1016/S0012-8252(02)00107-1

Cochrane R, Spikings RA, Chew DM, Wotzlaw J-F, Chiaradia M, Tyrrell S, Schaltegger U, van der Lelij R (2014) High temperature (> 350 °C) thermochronology and mechanisms of Pb loss in apatite. Geochim Cosmochim Acta 127:39–56. https://doi.org/10.1016/j.gca.2013.11.028

Condomines M, Gauthier P-J, Sigmarsson O (2003) Timescales of magma chamber processes and dating of young volcanic rocks. Rev Mineral Geochem 52:125–174. https://doi.org/10.2113/0520125

Condon DJ, Schoene B, McLean NM, Bowring SA, Parrish RR (2015) Metrology and traceability of U–Pb isotope dilution geochronology (EARTHTIME Tracer Calibration Part I). Geochim Cosmochim Acta 164:464–480. https://doi.org/10.1016/j.gca.2015.05.026

Coogan LA, Parrish RR, Roberts NMW (2016) Early hydrothermal carbon uptake by the upper oceanic crust: insight from in situ U–Pb dating. Geology 44:147–150. https://doi.org/10.1130/G37212.1

Corfu F (2013) A century of U–Pb geochronology: the long quest towards concordance. Geol Soc Am Bull 125:33–47. https://doi.org/10.1130/B30698.1

Corfu F, Lightfoot PC (1996) U–Pb geochronology of the sublayer environment, Sudbury igneous complex, Ontario. Econ Geol 91:1263–1269. https://doi.org/10.2113/gsecongeo.91.7.1263

Corfu F, Muir TL (1989) The Hemlo-Heron Bay greenstone belt and Hemlo Au-Mo deposit, Superior Province, Ontario, Canada 2. Timing of metamorphism, alteration and Au mineralization from titanite, rutile, and monazite U–Pb geochronology. Chem Geol 79:201–223. https://doi.org/10.1016/0168-9622(89)90030-4

Cottle JM (2014) In-situ U–Th/Pb geochronology of (urano)thorite. Am Min 99:1985–1995. https://doi.org/10.2138/am-2014-4920

Coveney RM, Ragan VM, Brannon JC (2000) Temporal benchmarks for modeling Phanerozoic flow of basinal brines and hydrocarbons in the southern Midcontinent based on radiometrically dated calcite. Geology 28:795–798. https://doi.org/10.1130/0091-7613(2000)028%3c0795:tbfmpf%3e2.3.co;2

Crowley Q, Heron K, Riggs N, Kamber B, Chew D, McConnell B, Benn K (2014) Chemical abrasion applied to LA-ICP-MS U–Pb zircon geochronology. Minerals 4:503–518

Curie P, Curie M, Bémont G (1898) Sur une nouvelle substance fortement radio-active contenue dans la pechblende. C R Acad Sci Paris 127:1215–1217

Curie P, Skolodowska Curie M (1898) Sur une substance nouvelle radioactive, contenue dans la pechblende. C R Acad Sci Paris 127:175–178

Dahl PS (1997) A crystal-chemical basis for Pb retention and fission-track annealing systematics in U-bearing minerals, with implications for geochronology. Earth Planet Sci Lett 150:277–290. https://doi.org/10.1016/S0012-821X(97)00108-8

Darling JR, Storey CD, Engi M (2012) Allanite U–Th–Pb geochronology by laser ablation ICPMS. Chem Geol 292–293:103–115

Davis DW, Krogh TE, Williams IS (2003) Historical development of zircon geochronology. Rev Mineral Geochem 53:145–181. https://doi.org/10.2113/0530145

De Haller A, Corfú F, Fontboté L, Schaltegger U, Barra F, Chiaradia M, Frank M, Alvarado JZ (2006) Geology, geochronology, and Hf and Pb isotope data of the Raúl-Condestable iron oxide-copper-gold deposit, central coast of Peru. Econ Geol 101:281–310. https://doi.org/10.2113/gsecongeo.101.2.281

De Haller A, Tarantola A, Mazurek M, Spangenberg J (2011) Fluid flow through the sedimentary cover in northern Switzerland recorded by calcite–celestite veins (Oftringen borehole, Olten). Swiss J Geosci 104:493–506. https://doi.org/10.1007/s00015-011-0085-x

de Ronde CEJ, Spooner ETC, de Wit MJ, Bray CJ (1992) Shear zone-related, Au quartz vein deposits in the Barberton greenstone belt, South Africa; field and petrographic characteristics, fluid properties, and light stable isotope geochemistry. Econ Geol 87:366–402. https://doi.org/10.2113/gsecongeo.87.2.366

Decree S, Deloule É, De Putter T, Dewaele S, Mees F, Baele J-M, Marignac C (2014) Dating of U-rich heterogenite: new insights into U deposit genesis and U cycling in the Katanga Copperbelt. Precambrian Res 241:17–28

Deng X-D, Li J-W, Wen G (2014) Dating iron skarn mineralization using hydrothermal allanite-(La) U–Th–Pb isotopes by laser ablation ICP-MS. Chem Geol 382:95–110

Deng X-D, Li J-W, Zhao X-F, Wang H-Q, Qi L (2015a) Re–Os and U–Pb geochronology of the Laochang Pb–Zn–Ag and concealed porphyry Mo mineralization along the Changning-Menglian suture, SW China: implications for ore genesis and porphyry Cu–Mo exploration. Miner Depos 51:237–248. https://doi.org/10.1007/s00126-015-0606-z

Deng X-D, Li J-W, Zhou M-F, Zhao X-F, Yan D-R (2015b) In-situ LA-ICPMS trace elements and U–Pb analysis of titanite from the Mesozoic Ruanjiawan W–Cu–Mo skarn deposit, Daye district, China. Ore Geol Rev 65:990–1004. https://doi.org/10.1016/j.oregeorev.2014.08.011

Deng XD, Li JW, Wen G (2015c) U–Pb geochronology of hydrothermal zircons from the Early Cretaceous iron skarn deposits in the Handan-Xingtai district, North China Craton. Econ Geol 110:2159–2180. https://doi.org/10.2113/econgeo.110.8.2159

Dewaele S, Henjes-Kunst F, Melcher F, Sitnikova M, Burgess R, Gerdes A, Fernandez MA, Clercq FD, Muchez P, Lehmann B (2011) Late Neoproterozoic overprinting of the cassiterite and columbite-tantalite bearing pegmatites of the Gatumba area, Rwanda (Central Africa). J Afr Earth Sci 61:10–26. https://doi.org/10.1016/j.jafrearsci.2011.04.004

DeWolf CP, Halliday AN (1991) U–Pb dating of a remagnetized Paleozoic limestone. Geophys Res Lett 18:1445–1448. https://doi.org/10.1029/91GL01278

Dieng S, Kyser K, Godin L (2013) Tectonic history of the North American shield recorded in uranium deposits in the Beaverlodge area, northern Saskatchewan, Canada. Precambrian Res 224:316–340

Dill HG, Gerdes A, Weber B (2010) Age and mineralogy of supergene uranium minerals — Tools to unravel geomorphological and palaeohydrological processes in granitic terrains (Bohemian Massif, SE Germany).

Geomorphology 117:44–65. https://doi.org/10.1016/j.geomorph.2009.11.005

Dill HG, Hansen BT, Weber B (2013) U/Pb age and origin of supergene uranophane-beta from the Borborema Pegmatite mineral province, Brazil. J South Am Earth Sci 45:160–165. https://doi.org/10.1016/j.jsames.2013.03.014

Donnelly CL, Griffin WL, Yang J-H, O'Reilly SY, Li Q-L, Pearson NJ, Li X-H (2012) In situ U–Pb dating and Sr–Nd isotopic analysis of perovskite: constraints on the age and petrogenesis of the Kuruman Kimberlite province, Kaapvaal Craton, South Africa. J Petrol 53:2497–2522. https://doi.org/10.1093/petrology/egs057

Downes PJ, Dunkley DJ, Fletcher IR, McNaughton NJ, Rasmussen B, Jaques AL, Verrall M, Sweetapple MT (2016) Zirconolite, zircon and monazite-(Ce) U–Th–Pb age constraints on the emplacement, deformation and alteration history of the Cummins Range carbonatite complex, Halls Creek Orogen, Kimberley region, Western Australia. Miner Petrol 110:199–222. https://doi.org/10.1007/s00710-015-0418-y

Drake H, Tullborg E-L, MacKenzie AB (2009) Detecting the near-surface redox front in crystalline bedrock using fracture mineral distribution, geochemistry and U-series disequilibrium. Appl Geochem 24:1023–1039. https://doi.org/10.1016/j.apgeochem.2009.03.004

Dziggel A, Poujol M, Otto A, Kisters AFM, Trieloff M, Schwarz WH, Meyer FM (2010) New U–Pb and $^{40}Ar/^{39}Ar$ ages from the northern margin of the Barberton greenstone belt, South Africa: implications for the formation of Mesoarchaean gold deposits. Precambrian Res 179:206–220. https://doi.org/10.1016/j.precamres.2010.03.006

Eichhorn R, Schärer U, Höll R (1995) Age and evolution of scheelite-hosting rocks in the Felbertal deposit (Eastern Alps): U–Pb geochronology of zircon and titanite. Contrib Mineral Petrol 119:377–386. https://doi.org/10.1007/BF00286936

England GL, Rasmussen B, McNaughton NJ, Fletcher IR, Groves DI, Krapež B (2001) SHRIMP U–Pb ages of diagenetic and hydrothermal xenotime from the Archaean Witwatersrand Supergroup of South Africa. Terra Nova 13:360–367. https://doi.org/10.1046/j.1365-3121.2001.00363.x

Fayek M, Harrison TM, Grove M, Coath CD (2000) A rapid in situ method for determining the ages of uranium oxide minerals: evolution of the Cigar Lake deposit, Athabasca Basin. Int Geol Rev 42:163–171

Fisher CM, Longerich HP, Jackson SE, Hanchar JM (2010) Data acquisition and calculation of U–Pb isotopic analyses using laser ablation (single collector) inductively coupled plasma mass spectrometry. J Anal at Spectrom 25:1905–1920. https://doi.org/10.1039/C004955G

Fletcher IR, McNaughton NJ, Aleinikoff JA, Rasmussen B, Kamo SL (2004) Improved calibration procedures and new standards for U–Pb and Th–Pb dating of Phanerozoic xenotime by ion microprobe. Chem Geol 209:295–314. https://doi.org/10.1016/j.chemgeo.2004.06.015

Fletcher IR, McNaughton NJ, Davis WJ, Rasmussen B (2010) Matrix effects and calibration limitations in ion probe U–Pb and Th–Pb dating of monazite. Chem Geol 270:31–44

Frei R (1996) The extent of inter-mineral isotope equilibrium: a systematic bulk U–Pb and Pb step leaching (PbSL) isotope study of individual minerals from the Tertiary granite of Jerissos (northern Greece). Eur J Mineral 8:1175–1190. https://doi.org/10.1127/ejm/8/5/1175

Frimmel HE, Hennigh Q (2015) First whiffs of atmospheric oxygen triggered onset of crustal gold cycle. Miner Depos 50:5–23. https://doi.org/10.1007/s00126-014-0574-8

Frimmel HE, Groves DI, Kirk J, Ruiz J, Chesley J, Minter WEL (2005) The formation and preservation of the Witwatersrand goldfields, the world's largest gold province. Econ Geol 100th Anniv:769–797

Froude DO, Ireland TR, Kinny PD, Williams IS, Compston W, Williams IR, Myers JS (1983) Ion microprobe identification of 4100–4200 Myr-old terrestrial zircons. Nature 304:616–618. https://doi.org/10.1038/304616a0

Fryer BJ, Jackson SE, Longerich HP (1993) The application of laser ablation microprobe-inductively coupled plasma-mass spectrometry (LAM-ICP-MS) to in situ (U)–Pb geochronology. Chem Geol 109:1–8. https://doi.org/10.1016/0009-2541(93)90058-Q

Fu Y, Sun X, Zhou H, Lin H, Yang T (2016) In-situ LA–ICP–MS U–Pb geochronology and trace elements analysis of polygenetic titanite from the giant Beiya gold–polymetallic deposit in Yunnan Province, Southwest China. Ore Geol Rev 77:43–56

Gardiner NJ, Hawkesworth CJ, Robb LJ, Whitehouse MJ, Roberts NMW, Kirkland CL, Evans NJ (2017) Contrasting granite metallogeny through the zircon record: a case study from Myanmar. Sci Rep 7:748. https://doi.org/10.1038/s41598-017-00832-2

Gehrels GE, Valencia VA, Ruiz J (2008) Enhanced precision, accuracy, efficiency, and spatial resolution of U–Pb ages by laser ablation–multicollector–inductively coupled plasma–mass spectrometry. Geochem Geophys Geosyst 9:Q03017. https://doi.org/10.1029/2007GC001805

Geisler T, Schaltegger U, Tomaschek F (2007) Re-equilibration of zircon in aqueous fluids and melts. Elements 3:43–50. https://doi.org/10.2113/gselements.3.1.43

Gelcich S, Davis DW, Spooner ETC (2005) Testing the apatite-magnetite geochronometer: U–Pb and $^{40}Ar/^{39}Ar$ geochronology of plutonic rocks, massive magnetite-apatite tabular bodies, and IOCG mineralization in northern Chile. Geochim Cosmochim Acta 69:3367–3384. https://doi.org/10.1016/j.gca.2004.12.020

Glodny J, Grauert B, Fiala J, Vejnar Z, Krohe A (1998) Metapegmatites in the western Bohemian massif: ages of crystallisation and metamorphic overprint, as

constrained by U–Pb zircon, monazite, garnet, columbite and Rb–Sr muscovite data. Geol Rundsch 87:124–134. https://doi.org/10.1007/s005310050194

Grandia F, Asmerom Y, Getty S, Cardellach E, Canals A (2000) U–Pb dating of MVT ore-stage calcite: implications for fluid flow in a Mesozoic extensional basin from Iberian Peninsula. J Geochem Explor 69–70:377–380. https://doi.org/10.1016/S0375-6742(00)00030-3

Gregory CJ, Rubatto D, Allen CM, Williams IS, Hermann J, Ireland T (2007) Allanite microgeochronology: a LA-ICP-MS and SHRIMP U–Th–Pb study. Chem Geol 245:162–182. https://doi.org/10.1016/j.chemgeo.2007.07.029

Griffin WL, Batumike JM, Greau Y, Pearson NJ, Shee SR, O'Reilly SY (2014) Emplacement ages and sources of kimberlites and related rocks in southern Africa: U–Pb ages and Sr–Nd isotopes of groundmass perovskite. Contrib Mineral Petrol 168:1032. https://doi.org/10.1007/s00410-014-1032-4

Guillong M, Horn I, Günther D (2003) A comparison of 266 nm, 213 nm and 193 nm produced from a single solid state Nd:YAG laser for laser ablation ICP-MS. J Anal at Spectrom 18:1224–1230. https://doi.org/10.1039/B305434A

Gulson BL, Jones MT (1992) Cassiterite: potential for direct dating of mineral deposits and a precise age for the Bushveld Complex granites. Geology 20:355–358. https://doi.org/10.1130/0091-7613(1992)020%3c0355:CPFDDO%3e2.3.CO;2

Günther D, Frischknecht R, Heinrich CA, Kahlert H-J (1997) Capabilities of an argon fluoride 193 nm excimer laser for laser ablation inductively coupled plasma mass spectometry microanalysis of geological materials. J Anal at Spectrom 12:939–944. https://doi.org/10.1039/A701423F

Harlaux M, Romer RL, Mercadier J, Morlot C, Marignac C, Cuney M (2017) 40 Ma years of hydrothermal W mineralization during the Variscan orogenic evolution of the French Massif Central revealed by U–Pb dating of wolframite. Miner Depos 334:1–31. https://doi.org/10.1007/s00126-017-0721-0

Harley SL, Kelly NM (2007) Zircon tiny but timely. Elements 3:13–18. https://doi.org/10.2113/gselements.3.1.13

Harlov DE (2015) Apatite: a fingerprint for metasomatic processes. Elements 11:171–176. https://doi.org/10.2113/gselements.11.3.171

Harris AC, Allen CM, Bryan SE, Campbell IH, Holcombe RJ, Palin MJ (2004) ELA-ICP-MS U–Pb zircon geochronology of regional volcanism hosting the Bajo de la Alumbrera Cu–Au deposit: implications for porphyry-related mineralization. Miner Depos 39:46–67. https://doi.org/10.1007/s00126-003-0381-0

Harris AC, Dunlap WJ, Reiners PW, Allen CM, Cooke DR, White NC, Campbell IH, Golding SD (2008) Multimillion year thermal history of a porphyry copper deposit: application of U–Pb, $^{40}Ar/^{39}Ar$ and (U–Th)/He chronometers, Bajo de la Alumbrera copper-gold deposit, Argentina. Miner Depos 43:295–314. https://doi.org/10.1007/s00126-007-0151-5

Heaman L (2003) The timing of kimberlite magmatism in North America: implications for global kimberlite genesis and diamond exploration. Lithos 71:153–184

Heaman LM (2009) The application of U–Pb geochronology to mafic, ultramafic and alkaline rocks: an evaluation of three mineral standards. Chem Geol 261:43–52. https://doi.org/10.1016/j.chemgeo.2008.10.021

Heaman LM, LeCheminant AN (2001) Anomalous U–Pb systematics in mantle-derived baddeleyite xenocrysts from Île Bizard: evidence for high temperature radon diffusion? Chem Geol 172:77–93. https://doi.org/10.1016/S0009-2541(00)00237-0

Heaman LM, Pell J, Grütter HS, Creaser RA (2015) U–Pb geochronology and Sr/Nd isotope compositions of groundmass perovskite from the newly discovered Jurassic Chidliak kimberlite field, Baffin Island, Canada. Earth Planet Sci Lett 415:183–199. https://doi.org/10.1016/j.epsl.2014.12.056

Hedenquist JW, Lowenstern JB (1994) The role of magmas in the formation of hydrothermal ore deposits. Nature 370:519–527. https://doi.org/10.1038/370519a0

Heinrich CA (2015) Witwatersrand gold deposits formed by volcanic rain, anoxic rivers and Archaean life. Nature Geosci 8:206–209. https://doi.org/10.1038/ngeo2344

Hiess J, Condon DJ, McLean N, Noble SR (2012) $^{238}U/^{235}U$ systematics in terrestrial uranium-bearing minerals. Science 335:1610–1614. https://doi.org/10.1126/science.1215507

Hinthorne JR, Andersen CA, Conrad RL, Lovering JF (1979) Single-grain $^{207}Pb/^{206}Pb$ and U/Pb age determinations with a 10-μm spatial resolution using the ion microprobe mass analyzer (IMMA). Chem Geol 25:271–303. https://doi.org/10.1016/0009-2541(79)90061-5

Hinton RW, Long JVP (1979) High-resolution ion-microprobe measurement of lead isotopes: variations within single zircons from Lac Seul, northwestern Ontario. Earth Planet Sci Lett 45:309–325. https://doi.org/10.1016/0012-821X(79)90132-8

Hofmann B, Eikenberg J (1991) The Krunkelbach uranium deposit, Schwarzwald, Germany; correlation of radiometric ages (U–Pb, U–Xe–Kr, K–Ar, $^{230}Th$–$^{234}U$). Econ Geol 86:1031–1049. https://doi.org/10.2113/gsecongeo.86.5.1031

Hofmann BA, Knill MD (1996) Geochemistry and genesis of the Lengenbach Pb–Zn–As–Tl–Ba-mineralisation, Binn Valley, Switzerland. Miner Depos 31:319–339. https://doi.org/10.1007/BF02280795

Holden NE (1990) Total half-lives for selected nuclides. Pure Appl Chem 62:941–958. https://doi.org/10.1351/pac199062050941

Holmes A (1911) The association of lead with uranium in rock-minerals, and its application to the measurement

of geological time. Proc R Soc Lond A 85:248–256. https://doi.org/10.1098/rspa.1911.0036

Holmes A (1913) The age of the Earth. Harper and Brothers, London and New York

Holmes A (1954) The oldest dated minerals of the Rhodesian Shield. Nature 173:612–614

Horn I, Rudnick RL, McDonough WF (2000) Precise elemental and isotope ratio determination by simultaneous solution nebulization and laser ablation-ICP-MS: application to U–Pb geochronology. Chem Geol 164:281–301

Horstwood MSA, Košler J, Gehrels G, Jackson SE, McLean NM, Paton C, Pearson NJ, Sircombe K, Sylvester P, Vermeesch P, Bowring JF, Condon DJ, Schoene B (2016) Community-derived standards for LA-ICP-MS U–(Th–)Pb geochronology - uncertainty propagation, age interpretation and data reporting. Geostand Geoanal Res 40:311–332. https://doi.org/10.1111/j.1751-908X.2016.00379.x

Hoskin PWO, Schaltegger U (2003) The composition of zircon and igneous and metamorphic petrogenesis. Rev Mineral Geochem 53:27–62. https://doi.org/10.2113/0530027

Huston DL, Maas R, Cross A, Hussey KJ, Mernagh TP, Fraser G, Champion DC (2016) The Nolans Bore rare-earth element-phosphorus-uranium mineral system: geology, origin and post-depositional modifications. Miner Depos 51:797–822. https://doi.org/10.1007/s00126-015-0631-y

Ireland TR (2014) Ion microscopes and microprobes. Treatise on geochemistry. Elsevier, Amsterdam, pp 385–409

Ireland TR, Williams IS (2003) Considerations in zircon geochronology by SIMS. Rev Mineral Geochem 53:215–241. https://doi.org/10.2113/0530215

Jaffey AH, Flynn KF, Glendenin LE, Bentley WC, Essling AM (1971) Precision measurement of half-lives and specific activities of $^{235}$U and $^{238}$U. Phys Rev C 4:1889–1906

Jung S, Mezger K (2003) U–Pb garnet chronometry in high-grade rocks – case studies from the central Damara orogen (Namibia) and implications for the interpretation of Sm–Nd garnet ages and the role of high U–Th inclusions. Contrib Mineral Petrol 146:382–396. https://doi.org/10.1007/s00410-003-0506-6

Kelly NM, Harley SL (2005) An integrated microtextural and chemical approach to zircon geochronology: refining the Archaean history of the Napier Complex, east Antarctica. Contrib Mineral Petrol 149:57–84. https://doi.org/10.1007/s00410-004-0635-6

Kempe U, Lehmann B, Wolf D, Rodionov N, Bombach K, Schwengfelder U, Dietrich A (2008) U–Pb SHRIMP geochronology of Th-poor, hydrothermal monazite: an example from the Llallagua tin-porphyry deposit, Bolivia. Geochim Cosmochim Acta 72:4352–4366. https://doi.org/10.1016/j.gca.2008.05.059

Kerrich R, Kyser TK (1994) 100 Ma timing paradox of Archean gold, Abitibi greenstone belt (Canada): new evidence from U–Pb and Pb–Pb evaporation ages of hydrothermal zircons. Geology 22:1131–1134. https://doi.org/10.1130/0091-7613(1994)022%3c1131:MTPOAG%3e2.3.CO;2

Klemme S, Meyer H-P (2003) Trace element partitioning between baddeleyite and carbonatite melt at high pressures and high temperatures. Chem Geol 199:233–242

Klemme S, Prowatke S, Hametner K, Günther D (2005) Partitioning of trace elements between rutile and silicate melts: implications for subduction zones. Geochim Cosmochim Acta 69:2361–2371. https://doi.org/10.1016/j.gca.2004.11.015

Klötzli U, Klötzli E, Günes Z, Košler J (2009) Accuracy of laser ablation U–Pb zircon dating: results from a test using five different reference zircons. Geostand Geoanal Res 33:5–15. https://doi.org/10.1111/j.1751-908X.2009.00921.x

Koglin N, Zeh A, Frimmel HE, Gerdes A (2010) New constraints on the auriferous Witwatersrand sediment provenance from combined detrital zircon U–Pb and Lu–Hf isotope data for the Eldorado Reef (Central Rand Group, South Africa). Precambrian Res 183:817–824

Kooijman E, Mezger K, Berndt J (2010) Constraints on the U–Pb systematics of metamorphic rutile from in situ LA-ICP-MS analysis. Earth Planet Sci Lett 293:321–330. https://doi.org/10.1016/j.epsl.2010.02.047

Kositcin N, Krapež B (2004) Relationship between detrital zircon age-spectra and the tectonic evolution of the Late Archaean Witwatersrand Basin, South Africa. Precambrian Res 129:141–168. https://doi.org/10.1016/j.precamres.2003.10.011

Kositcin N, McNaughton NJ, Griffin BJ, Fletcher IR, Groves DI, Rasmussen B (2003) Textural and geochemical discrimination between xenotime of different origin in the Archaean Witwatersrand Basin, South Africa. Geochim Cosmochim Acta 67:709–731. https://doi.org/10.1016/S0016-7037(02)01169-9

Košler J, Wiedenbeck M, Wirth R, Hovorka J, Sylvester P, Míková J (2005) Chemical and phase composition of particles produced by laser ablation of silicate glass and zircon—implications for elemental fractionation during ICP-MS analysis. J Anal at Spectrom 20:402–409. https://doi.org/10.1039/B416269B

Košler J, Sláma J, Belousova E, Corfú F, Gehrels GE, Gerdes A, Horstwood MSA, Sircombe KN, Sylvester PJ, Tiepolo M, Whitehouse MJ, Woodhead JD (2013) U–Pb detrital zircon analysis—results of an inter-laboratory comparison. Geostand Geoanal Res 37:243–259. https://doi.org/10.1111/j.1751-908X.2013.00245.x

Kouzmanov K, Moritz R, von Quadt A, Chiaradia M, Peytcheva I, Fontignie D, Ramboz C, Bogdanov K (2009) Late Cretaceous porphyry Cu and epithermal Cu–Au association in the southern Panagyurishte district, Bulgaria: the paired Vlaykov Vruh and Elshitsa deposits. Miner Depos 44:611–646. https://doi.org/10.1007/s00126-009-0239-1

Krogh TE (1973) A low-contamination method for hydrothermal decomposition of zircon and extraction of U and Pb for isotopic age determinations. Geochim Cosmochim Acta 37:485–494. https://doi.org/10.1016/0016-7037(73)90213-5

Krogh TE (1982) Improved accuracy of U–Pb zircon ages by the creation of more concordant systems using an air abrasion technique. Geochim Cosmochim Acta 46:637–649. https://doi.org/10.1016/0016-7037(82)90165-X

Krogh TE, Davis GL (1975) The production and preparation of $^{205}$Pb for use as a tracer for isotope dilution analyses. Carnegie Institute of Washington, Yearbook 74:416–417

Kröner A, Kovach VP, Kozakov IK, Kirnozova T, Azimov P, Wong J, Geng HY (2015) Zircon ages and Nd–Hf isotopes in UHT granulites of the Ider complex: a cratonic terrane within the Central Asian Orogenic Belt in NW Mongolia. Gondwana Res 27:1392–1406. https://doi.org/10.1016/j.gr.2014.03.005

Kryza R, Crowley QG, Larionov A, Pin C, Oberc-Dziedzic T, Mochnacka K (2012) Chemical abrasion applied to SHRIMP zircon geochronology: an example from the Variscan Karkonosze Granite (Sudetes, SW Poland). Gondwana Res 21:757–767. https://doi.org/10.1016/j.gr.2011.07.007

Lancelot J, Vitrac A, Allegre CJ (1976) Uranium and lead isotopic dating with grain-by-grain zircon analysis: a study of complex geological history with a single rock. Earth Planet Sci Lett 29:357–366. https://doi.org/10.1016/0012-821X(76)90140-0

Larsen ES, Keevil NB, Harrison HC (1952) Method for determining the age of igneous rocks using the accessory minerals. Geol Soc Am Bull 63:1045–1052. https://doi.org/10.1130/0016-7606(1952)63[1045:MFDTAO]2.0.CO;2

Law JDM, Phillips GN (2005) Hydrothermal replacement model for Witwatersrand gold. Econ Geol 100th Anniv:799–811

Lecumberri-Sanchez P, Romer RL, Lüders V, Bodnar RJ (2014) Genetic relationship between silver–lead–zinc mineralization in the Wutong deposit, Guangxi Province and Mesozoic granitic magmatism in the Nanling belt, southeast China. Miner Depos 49:353–369. https://doi.org/10.1007/s00126-013-0494-z

Lehmann B, Burgess R, Frei D, Belyatsky B, Mainkar D, Rao NVC, Heaman LM (2010) Diamondiferous kimberlites in central India synchronous with Deccan flood basalts. Earth Planet Sci Lett 290:142–149. https://doi.org/10.1016/j.epsl.2009.12.014

Li XH, Su L, Chung SL, Li ZX, Liu Y, Song B, Liu DY (2005) Formation of the Jinchuan ultramafic intrusion and the world's third largest Ni–Cu sulfide deposit: associated with the ~825 Ma south China mantle plume? Geochem Geophys Geosyst 6:Q11004. https://doi.org/10.1029/2005GC001006

Li J-W, Deng X-D, Zhou M-F, Liu Y-S, Zhao X-F, Guo J-L (2010) Laser ablation ICP-MS titanite U–Th–Pb dating of hydrothermal ore deposits: a case study of the Tonglushan Cu–Fe–Au skarn deposit, SE Hubei Province, China. Chem Geol 270:56–67. https://doi.org/10.1016/j.chemgeo.2009.11.005

Li Q, Parrish RR, Horstwood MSA, McArthur JM (2014) U–Pb dating of cements in Mesozoic ammonites. Chem Geol 376:76–83. https://doi.org/10.1016/j.chemgeo.2014.03.020

Li C-Y, Zhang R-Q, Ding X, Ling M-X, Fan W-M, Sun W-D (2016) Dating cassiterite using laser ablation ICP-MS. Ore Geol Rev 72:313–322. https://doi.org/10.1016/j.oregeorev.2015.07.016

Lobato LM, Santos JOS, McNaughton NJ, Fletcher IR, Noce CM (2007) U–Pb SHRIMP monazite ages of the giant Morro Velho and Cuiabá gold deposits, Rio das Velhas greenstone belt, Quadrilátero Ferrífero, Minas Gerais, Brazil. Ore Geol Rev 32:674–680. https://doi.org/10.1016/j.oregeorev.2006.11.007

Ludwig KR (1980) Calculation of uncertainties of U–Pb isotope data. Earth Planet Sci Lett 46:212–220

Ludwig KR (1998) On the treatment of concordant uranium-lead ages. Geochim Cosmochim Acta 62:665–676. https://doi.org/10.1016/S0016-7037(98)00059-3

Ludwig KR (2012) Isoplot 3.75, a geochronological toolkit for Microsoft Excel. Berkeley Geochronology Center Special Publication 75

Ludwig KA, Shen C-C, Kelley DS, Cheng H, Edwards RL (2011) U–Th systematics and $^{230}$Th ages of carbonate chimneys at the Lost City hydrothermal field. Geochim Cosmochim Acta 75:1869–1888. https://doi.org/10.1016/j.gca.2011.01.008

Luo J-C, Hu R-Z, Fayek M, Li C-S, Bi X-W, Abdu Y, Chen Y-W (2015) In-situ SIMS uraninite U–Pb dating and genesis of the Xianshi granite-hosted uranium deposit, South China. Ore Geol Rev 65:968–978. https://doi.org/10.1016/j.oregeorev.2014.06.016

Luvizotto GL, Zack T, Meyer HP, Ludwig T, Triebold S, Kronz A, Münker C, Stöckli DF, Prowatke S, Klemme S, Jacob DE, von Eynatten H (2009) Rutile crystals as potential trace element and isotope mineral standards for microanalysis. Chem Geol 261:346–369. https://doi.org/10.1016/j.chemgeo.2008.04.012

Marillo-Sialer E, Woodhead J, Hergt J, Greig A, Guillong M, Gleadow A, Evans N, Paton C (2014) The zircon "matrix effect": evidence for an ablation rate control on the accuracy of U–Pb age determinations by LA-ICP-MS. J Anal at Spectrom 29:981–989. https://doi.org/10.1039/C4JA00008K

Mattinson JM (1972) Preparation of hydrofluoric, hydrochloric, and nitric acids at ultralow lead levels. Anal Chem 44:1715–1716. https://doi.org/10.1021/ac60317a032

Mattinson JM (1994) A study of complex discordance in zircons using step-wise dissolution techniques. Contrib Mineral Petrol 116:117–129. https://doi.org/10.1007/BF00310694

Mattinson JM (2005) Zircon U–Pb chemical abrasion ("CA-TIMS") method: combined annealing and multi-step partial dissolution analysis for improved precision

and accuracy of zircon ages. Chem Geol 220:47–66. https://doi.org/10.1016/j.chemgeo.2005.03.011

Mattinson JM (2013) Revolution and evolution: 100 years of U–Pb geochronology. Elements 9:53–57. https://doi.org/10.2113/gselements.9.1.53

McKinney ST, Cottle JM, Lederer GW (2015) Evaluating rare earth element (REE) mineralization mechanisms in Proterozoic gneiss, Music Valley, California. Geol Soc Am Bull 127:1135–1152. https://doi.org/10.1130/B31165.1

McLean NM, Bowring JF, Bowring SA (2011) An algorithm for U–Pb isotope dilution data reduction and uncertainty propagation. Geochem Geophys Geosyst 12:Q0AA18. https://doi.org/10.1029/2010GC003478

McLean NM, Condon DJ, Schoene B, Bowring SA (2015) Evaluating uncertainties in the calibration of isotopic reference materials and multi-element isotopic tracers (EARTHTIME Tracer Calibration Part II). Geochim Cosmochim Acta 164:481–501. https://doi.org/10.1016/j.gca.2015.02.040

McLean NM, Bowring JF, Gehrels G (2016) Algorithms and software for U–Pb geochronology by LA-ICPMS. Geochem Geophys Geosyst 17. https://doi.org/10.1002/2015GC006097

McNaughton NJ, Rasmussen B, Fletcher IR (1999) SHRIMP uranium-lead dating of diagenetic xenotime in siliciclastic sedimentary rocks. Science 285:78–80. https://doi.org/10.1126/science.285.5424.78

Meier DL, Heinrich CA, Watts MA (2009) Mafic dikes displacing Witwatersrand gold reefs: evidence against metamorphic-hydrothermal ore formation. Geology 37:607–610. https://doi.org/10.1130/G25657A.1

Meinhold G (2010) Rutile and its applications in earth sciences. Earth Sci Rev 102:1–28. https://doi.org/10.1016/j.earscirev.2010.06.001

Melcher F, Graupner T, Gäbler HE, Sitnikova M, Henjes-Kunst F, Oberthür T, Gerdes A, Dewaele S (2015) Tantalum–(niobium–tin) mineralisation in African pegmatites and rare metal granites: constraints from Ta–Nb oxide mineralogy, geochemistry and U–Pb geochronology. Ore Geol Rev 64:667–719. https://doi.org/10.1016/j.oregeorev.2013.09.003

Melleton J, Gloaguen E, Frei D, Novák M, Breiter K (2012) How are the emplacement of rare-element pegmatites, regional metamorphism and magmatism interrelated in the Moldanubian domain of the Variscan Bohemian Massif, Czech Republic? Can Mineral 50:1751–1773. https://doi.org/10.3749/canmin.50.6.1751

Mezger K, Hanson GN, Bohlen SR (1989) U–Pb systematics of garnet: dating the growth of garnet in the late Archean Pikwitonei granulite domain at Cauchon and Natawahunan lakes, Manitoba, Canada. Contrib Mineral Petrol 101:136–148. https://doi.org/10.1007/BF00375301

Michael Meyer F, Kolb J, Sakellaris GA, Gerdes A (2006) New ages from the Mauritanides Belt: recognition of Archean IOCG mineralization at Guelb Moghrein, Mauritania. Terra Nova 18:345–352. https://doi.org/10.1111/j.1365-3121.2006.00698.x

Michard-Vitrac A, Lancelot J, Allegre CJ, Moorbath S (1977) U–Pb ages on single zircons from the early Precambrian rocks of West Greenland and the Minnesota River Valley. Earth Planet Sci Lett 35:449–453. https://doi.org/10.1016/0012-821X(77)90077-2

Miller JS, Matzel JEP, Miller CF, Burgess SD, Miller RB (2007) Zircon growth and recycling during the assembly of large, composite arc plutons. J Volcanol Geotherm Res 167:282–299. https://doi.org/10.1016/j.jvolgeores.2007.04.019

Möller A, O'Brien PJ, Kennedy A, Kröner A (2003) Linking growth episodes of zircon and metamorphic textures to zircon chemistry: an example from the ultrahigh-temperature granulites of Rogaland (SW Norway). Geol Soc Spec Pub 220:65–81. https://doi.org/10.1144/GSL.SP.2003.220.01.04

Moreto CPN, Monteiro LVS, Xavier RP, Creaser RA, DuFrane SA, Melo GHC, da Silva MAD, Tassinari CCG, Sato K (2014) Timing of multiple hydrothermal events in the iron oxide–copper–gold deposits of the Southern Copper Belt, Carajás Province, Brazil. Miner Depos 50:517–546. https://doi.org/10.1007/s00126-014-0549-9

Morisset C-E, Scoates JS, Weis D, Friedman RM (2009) U–Pb and $^{40}Ar/^{39}Ar$ geochronology of the Saint-Urbain and Lac Allard (Havre-Saint-Pierre) anorthosites and their associated Fe–Ti oxide ores, Québec: evidence for emplacement and slow cooling during the collisional Ottawan Orogeny in the Grenville Province. Precambrian Res 174:95–116. https://doi.org/10.1016/j.precamres.2009.06.009

Moser DE (1997) Dating the shock wave and thermal imprint of the giant Vredefort impact, South Africa. Geology 25:7–10. https://doi.org/10.1130/0091-7613(1997)025%3c0007:DTSWAT%3e2.3.CO;2

Moser DE, Davis WJ, Reddy SM, Flemming RL, Hart RJ (2009) Zircon U–Pb strain chronometry reveals deep impact-triggered flow. Earth Planet Sci Lett 277:73–79. https://doi.org/10.1016/j.epsl.2008.09.036

Mosoh Bambi CK, Frimmel HE, Zeh A, Suh CE (2013) Age and origin of Pan-African granites and associated U-Mo mineralization at Ekomédion, southwestern Cameroon. J Afr Earth Sci 88:15–37. https://doi.org/10.1016/j.jafrearsci.2013.08.005

Mueller AG, Campbell IH, Schiotte L, Sevigny JH, Layer PW (1996) Constraints on the age of granitoid emplacement, metamorphism, gold mineralization, and subsequent cooling of the Archean greenstone terrane at Big Bell, Western Australia. Econ Geol 91:896–915. https://doi.org/10.2113/gsecongeo.91.5.896

Mueller AG, Hall GC, Nemchin AA, Stein HJ, Creaser RA, Mason DR (2007) Archean high-Mg monzodiorite–syenite, epidote skarn, and biotite–sericite gold lodes in the Granny Smith-Wallaby district, Australia: U–Pb and Re–Os chronometry of two intrusion-related hydrothermal systems. Miner Depos 43:337–362. https://doi.org/10.1007/s00126-007-0164-0

Muhling JR, Fletcher IR, Rasmussen B (2012) Dating fluid flow and Mississippi Valley type base-metal mineralization in the Paleoproterozoic Earaheedy Basin, Western Australia. Precambrian Res 212–213:75–90. https://doi.org/10.1016/j.precamres.2012.04.016

Müller SG, Krapež B, Barley ME, Fletcher IR (2005) Giant iron-ore deposits of the Hamersley province related to the breakup of Paleoproterozoic Australia: new insights from in situ SHRIMP dating of baddeleyite from mafic intrusions. Geology 33:577–580. https://doi.org/10.1130/G21482.1

Muntean JL, Frimmel HE, Phillips N, Law J, Myers R (2005) Controversies on the origin of world-class gold deposits, Part II: Witwatersrand gold deposits. Soc Econ Geol Newsl 60:7–12–19

Niiranen T, Poutiainen M, Mänttäri I (2007) Geology, geochemistry, fluid inclusion characteristics, and U–Pb age studies on iron oxide–Cu–Au deposits in the Kolari region, northern Finland. Ore Geol Rev 30:75–105. https://doi.org/10.1016/j.oregeorev.2005.11.002

Norcross C, Davis DW, Spooner E, Rust A (2000) U–Pb and Pb–Pb age constraints on Paleoproterozoic magmatism, deformation and gold mineralization in the Omai area, Guyana Shield. Precambrian Res 102:69–86. https://doi.org/10.1016/s0301-9268(99)00102-3

Oberli F, Meier M, Berger A, Rosenberg CL, Gieré R (2004) U–Th–Pb and $^{230}Th/^{238}U$ disequilibrium isotope systematics: precise accessory mineral chronology and melt evolution tracing in the Alpine Bergell intrusion. Geochim Cosmochim Acta 68:2543–2560. https://doi.org/10.1016/j.gca.2003.10.017

Oberthür T, Melcher F, Henjes-Kunst F, Gerdes A, Stein H, Zimmerman A, El Ghorfi M (2009) Hercynian age of the cobalt-nickel-arsenide-(gold) ores, Bou Azzer, Anti-Atlas, Morocco: Re–Os, Sm–Nd, and U–Pb age determinations. Econ Geol 104:1065–1079. https://doi.org/10.2113/econgeo.104.7.1065

Ono S, Fayek M (2011) Decoupling of O and Pb isotope systems of uraninite in the early Proterozoic conglomerates in the Elliot Lake district. Chem Geol 288:1–13. https://doi.org/10.1016/j.chemgeo.2010.03.015

Pal DC, Chaudhuri T, McFarlane C, Mukherjee A, Sarangi AK (2011) Mineral chemistry and in situ dating of allanite, and geochemistry of its host rocks in the Bagjata uranium mine, Singhbhum Shear Zone, India—implications for the chemical evolution of REE mineralization and mobilization. Econ Geol 106:1155–1171. https://doi.org/10.2113/econgeo.106.7.1155

Pape J, Mezger K, Robyr M (2016) A systematic evaluation of the Zr-in-rutile thermometer in ultra-high temperature (UHT) rocks. Contrib Mineral Petrol 171:44. https://doi.org/10.1007/s00410-016-1254-8

Paquette JL, Tiepolo M (2007) High resolution (5 μm) U–Th–Pb isotope dating of monazite with excimer laser ablation (ELA)-ICPMS. Chem Geol 240:222–237. https://doi.org/10.1016/j.chemgeo.2007.02.014

Parrish RR (1987) An improved micro-capsule for zircon dissolution in U–Pb geochronology. Chem Geol 66:99–102. https://doi.org/10.1016/0168-9622(87)90032-7

Parrish RR (1990) U–Pb dating of monazite and its application to geological problems. Can J Earth Sci 27:1431–1450. https://doi.org/10.1139/e90-152

Parrish RR, Noble SR (2003) Zircon U–Th–Pb geochronology by isotope dilution—thermal ionization mass spectrometry (ID-TIMS). Rev Mineral Geochem 53:183–213. https://doi.org/10.2113/0530183

Pelleter E, Cheilletz A, Gasquet D, Mouttaqi A, Annich M, El Hakour A, Deloule É, Féraud G (2007) Hydrothermal zircons: a tool for ion microprobe U–Pb dating of gold mineralization (Tamlalt–Menhouhou gold deposit—Morocco). Chem Geol 245:135–161. https://doi.org/10.1016/j.chemgeo.2007.07.026

Peterman EM, Mattinson JM, Hacker BR (2012) Multi-step TIMS and CA-TIMS monazite U–Pb geochronology. Chem Geol 312–313:58–73

Petersson J, Whitehouse MJ, Eliasson T (2001) Ion microprobe U–Pb dating of hydrothermal xenotime from an episyenite: evidence for rift-related reactivation. Chem Geol 175:703–712. https://doi.org/10.1016/S0009-2541(00)00338-7

Pettke T, Oberli F, Heinrich CA (2010) The magma and metal source of giant porphyry-type ore deposits, based on lead isotope microanalysis of individual fluid inclusions. Earth Planet Sci Lett 296:267–277. https://doi.org/10.1016/j.epsl.2010.05.007

Pfaff K, Romer RL, Markl G (2009) U–Pb ages of ferberite, chalcedony, agate, "U-mica" and pitchblende: constraints on the mineralization history of the Schwarzwald ore district. Eur J Mineral 21:817–836. https://doi.org/10.1127/0935-1221/2009/0021-1944

Philippe S, Lancelot JR, Clauer N, Pacquet A (2011) Formation and evolution of the Cigar Lake uranium deposit based on U–Pb and K–Ar isotope systematics. Can J Earth Sci 30:720–730. https://doi.org/10.1139/e93-058

Phillips GN, Law JDM (2000) Witwatersrand gold fields; geology, genesis, and exploration. Rev Econ Geol 13:439–500

Pigois J-P, Groves DI, Fletcher IR, McNaughton NJ, Snee LW (2003) Age constraints on Tarkwaian palaeoplacer and lode-gold formation in the Tarkwa-Damang district, SW Ghana. Miner Depos 38:695–714. https://doi.org/10.1007/s00126-003-0360-5

Poletti JE, Cottle JM, Hagen-Peter GA, Lackey JS (2016) Petrochronological constraints on the origin of the Mountain Pass ultrapotassic and carbonatite intrusive suite, California. J Petrol 57:1555–1598. https://doi.org/10.1093/petrology/egw050

Polito PA, Kyser TK, Thomas D, Marlatt J, Drever G (2005) Re-evaluation of the petrogenesis of the Proterozoic Jabiluka unconformity-related uranium deposit, Northern Territory, Australia. Miner Depos 40:257–288. https://doi.org/10.1007/s00126-005-0007-9

Porcelli D, Swarzenski PW (2003) The behavior of U- and Th-series nuclides in groundwater. Rev Mineral Geochem 52:317–361. https://doi.org/10.2113/0520317

Poujol M (2007) An overview of the Pre-Mesoarchean rocks of the Kaapvaal Craton, South Africa. Dev Precambrian Geol 15:453–463. https://doi.org/10.1016/S0166-2635(07)15051-9

Prowatke S, Klemme S (2005) Effect of melt composition on the partitioning of trace elements between titanite and silicate melt. Geochim Cosmochim Acta 69:695–709. https://doi.org/10.1016/j.gca.2004.06.037

Prowatke S, Klemme S (2006) Trace element partitioning between apatite and silicate melts. Geochim Cosmochim Acta 70:4513–4527. https://doi.org/10.1016/j.gca.2006.06.162

Rao NVC, Wu F-Y, Mitchell RH, Li Q-L, Lehmann B (2013) Mesoproterozoic U–Pb ages, trace element and Sr–Nd isotopic composition of perovskite from kimberlites of the eastern Dharwar craton, southern India: distinct mantle sources and a widespread 1.1 Ga tectonomagmatic event. Chem Geol 353:48–64. https://doi.org/10.1016/j.chemgeo.2012.04.023

Rasbury ET, Cole JM (2009) Directly dating geologic events: U–Pb dating of carbonates. Rev Geophys 47: RG3001. https://doi.org/10.1029/2007RG000246

Rasmussen B, Blake TS, Fletcher IR (2005) U–Pb zircon age constraints on the Hamersley spherule beds: evidence for a single 2.63 Ga Jeerinah-Carawine impact ejecta layer. Geology 33:725–728. https://doi.org/10.1130/G21616.1

Rasmussen B, Fletcher IR, Muhling JR, Mueller AG, Hall GC (2007a) Bushveld-aged fluid flow, peak metamorphism, and gold mobilization in the Witwatersrand basin, South Africa: constraints from in situ SHRIMP U–Pb dating of monazite and xenotime. Geology 35:931–934. https://doi.org/10.1130/G23588A.1

Rasmussen B, Fletcher IR, Muhling JR, Thorne WS, Broadbent GC (2007b) Prolonged history of episodic fluid flow in giant hematite ore bodies: evidence from in situ U–Pb geochronology of hydrothermal xenotime. Earth Planet Sci Lett 258:249–259. https://doi.org/10.1016/j.epsl.2007.03.033

Rasmussen B, Mueller AG, Fletcher IR (2008) Zirconolite and xenotime U–Pb age constraints on the emplacement of the Golden Mile Dolerite sill and gold mineralization at the Mt Charlotte mine, Eastern Goldfields Province, Yilgarn Craton, Western Australia. Contrib Mineral Petrol 157:559–572. https://doi.org/10.1007/s00410-008-0352-7

Rezeau H, Moritz R, Wotzlaw J-F, Tayan R, Melkonyan R, Ulianov A, Selby D, D'Abzac F-X, Stern RA (2016) Temporal and genetic link between incremental pluton assembly and pulsed porphyry Cu–Mo formation in accretionary orogens. Geology 44:627–630. https://doi.org/10.1130/G38088.1

Richards JP (2009) Postsubduction porphyry Cu–Au and epithermal Au deposits: products of remelting of subduction-modified lithosphere. Geology 37:247–250. https://doi.org/10.1130/G25451A.1

Richards JP (2011) Magmatic to hydrothermal metal fluxes in convergent and collided margins. Ore Geol Rev 40:1–26. https://doi.org/10.1016/j.oregeorev.2011.05.006

Richards JP (2013) Giant ore deposits formed by optimal alignments and combinations of geological processes. Nature Geosci 6:911–916. https://doi.org/10.1038/ngeo1920

Rioux M, Bowring S, Dudás F, Hanson R (2010) Characterizing the U–Pb systematics of baddeleyite through chemical abrasion: application of multi-step digestion methods to baddeleyite geochronology. Contrib Mineral Petrol 160:777–801. https://doi.org/10.1007/s00410-010-0507-1

Robert J, Miranda CF, Muxart R (1969) Mesure de la période du protactinium 231 par microcalorimétrie. Radiochim Acta 11:104–108. https://doi.org/10.1524/ract.1969.11.2.104

Roberts NMW, Walker RJ (2016) U–Pb geochronology of calcite-mineralized faults: absolute timing of rift-related fault events on the northeast Atlantic margin. Geology 44:531–534. https://doi.org/10.1130/G37868.1

Romer RL (1992) Vesuvianite—new tool for the U–Pb dating of skarn ore deposits. Miner Petrol 46:331–341

Romer RL (1996) U–Pb systematics of stilbite-bearing low-temperature mineral assemblages from the Malmberget iron ore, northern Sweden. Geochim Cosmochim Acta 60:1951–1961. https://doi.org/10.1016/0016-7037(96)00066-X

Romer RL, Lüders V (2006) Direct dating of hydrothermal W mineralization: U–Pb age for hübnerite ($MnWO_4$), Sweet Home Mine, Colorado. Geochim Cosmochim Acta 70:4725–4733. https://doi.org/10.1016/j.gca.2006.07.003

Romer RL, Öhlander B (1994) U–Pb age of the Yxsjöberg tungsten-skarn deposit, Sweden. GFF 116:161–166. https://doi.org/10.1080/11035899409546179

Romer RL, Smeds S-A (1994) Implications of U–Pb ages of columbite-tantalites from granitic pegmatites for the Palaeoproterozoic accretion of 1.90–1.85 Ga magmatic arcs to the Baltic Shield. Precambrian Res 67:141–158. https://doi.org/10.1016/0301-9268(94)90008-6

Romer RL, Smeds S-A (1996) U–Pb columbite ages of pegmatites from Sveconorwegian terranes in southwestern Sweden. Precambrian Res 76:15–30. https://doi.org/10.1016/0301-9268(95)00023-2

Romer RL, Smeds S-A (1997) U–Pb columbite chronology of post-kinematic Palaeoproterozoic pegmatites in Sweden. Precambrian Res 82:85–99. https://doi.org/10.1016/S0301-9268(96)00050-2

Romer RL, Wright JE (1992) U–Pb dating of columbites: a geochronologic tool to date magmatism and ore deposits. Geochim Cosmochim Acta 56:2137–2142. https://doi.org/10.1016/0016-7037(92)90337-I

Romer RL, Martinsson O, Perdahl JA (1994) Geochronology of the Kiruna iron ores and hydrothermal alterations. Econ Geol 89:1249–1261. https://doi.org/10.2113/gsecongeo.89.6.1249

Romer RL, Smeds SA, Černý P (1996) Crystal-chemical and genetic controls of U–Pb systematics of columbite-tantalite. Miner Petrol 57:243–260. https://doi.org/10.1007/BF01162361

Rubatto D, Hermann J (2007) Experimental zircon/melt and zircon/garnet trace element partitioning and implications for the geochronology of crustal rocks. Chem Geol 241:38–61. https://doi.org/10.1016/j.chemgeo.2007.01.027

Ruiz J, Valencia VA, Chesley JT, Kirk J, Gehrels G, Frimmel HE (2006) The source of gold for the Witwatersrand from Re–Os and U–Pb detrital zircon geochronology. Geochim Cosmochim Acta 70:A543

Rutherford E (1906) Radioactive transformations. Yale University Press, New Haven

Rutherford E (1929) Origin of actinium and age of the Earth. Nature 123:313–314

Salier BP, Groves DI, McNaughton NJ, Fletcher IR (2004) The world-class Wallaby gold deposit, Laverton, Western Australia: an orogenic-style overprint on a magmatic-hydrothermal magnetite-calcite alteration pipe? Miner Depos 39:473–494. https://doi.org/10.1007/s00126-004-0425-0

Salier BP, Groves DI, McNaughton NJ, Fletcher IR (2005) Geochronological and stable isotope evidence for widespread orogenic gold mineralization from a deep-seated fluid source at ca 2.65 Ga in the Laverton gold province. Western Australia. Econ Geol 100:1363–1388. https://doi.org/10.2113/gsecongeo.100.7.1363

Sarma DS, Fletcher IR, Rasmussen B, McNaughton NJ, Mohan MR, Groves DI (2011) Archaean gold mineralization synchronous with late cratonization of the Western Dharwar Craton, India: 2.52 Ga U–Pb ages of hydrothermal monazite and xenotime in gold deposits. Miner Depos 46:273–288. https://doi.org/10.1007/s00126-010-0326-3

Schaltegger U, Davies JHFL (2017) Petrochronology of zircon and baddeleyite in igneous rocks: reconstructing magmatic processes at high temporal resolution. Rev Mineral Geochem 83:297–328. https://doi.org/10.2138/rmg.2017.83.10

Schaltegger U, Pettke T, Audétat A, Reusser E, Heinrich CA (2005) Magmatic-to-hydrothermal crystallization in the W–Sn mineralized Mole Granite (NSW, Australia). Chem Geol 220:215–235. https://doi.org/10.1016/j.chemgeo.2005.02.018

Schaltegger U, Schmitt AK, Horstwood MSA (2015) U–Th–Pb zircon geochronology by ID-TIMS, SIMS, and laser ablation ICP-MS: recipes, interpretations, and opportunities. Chem Geol 402:89–110. https://doi.org/10.1016/j.chemgeo.2015.02.028

Schärer U (1984) The effect of initial $^{230}$Th disequilibrium on young U–Pb ages: the Makalu case, Himalaya. Earth Planet Sci Lett 67:191–204. https://doi.org/10.1016/0012-821x(84)90114-6

Schärer U, Corfu F, Demaiffe D (1997) U–Pb and Lu–Hf isotopes in baddeleyite and zircon megacrysts from the Mbuji-Mayi kimberlite: constraints on the subcontinental mantle. Chem Geol 143:1–16. https://doi.org/10.1016/S0009-2541(97)00094-6

Schmitt AK (2007) Ion microprobe analysis of ($^{231}$Pa)/($^{235}$U) and an appraisal of protactinium partitioning in igneous zircon. Am Mineral 92:691–694. https://doi.org/10.2138/am.2007.2449

Schmitt AK, Zack T (2012) High-sensitivity U–Pb rutile dating by secondary ion mass spectrometry (SIMS) with an $O^{2+}$ primary beam. Chem Geol 332–333:65–73. https://doi.org/10.1016/j.chemgeo.2012.09.023

Schmitz MD, Bowring SA (2001) U–Pb zircon and titanite systematics of the Fish Canyon Tuff: an assessment of high-precision U–Pb geochronology and its application to young volcanic rocks. Geochim Cosmochim Acta 65:2571–2587

Schoene B (2014) U–Th–Pb geochronology. Treatise on geochemistry. Elsevier, Amsterdam, pp 341–378

Schoene B, Bowring SA (2006) U–Pb systematics of the McClure Mountain syenite: thermochronological constraints on the age of the $^{40}$Ar/$^{39}$Ar standard MMhb. Contrib Mineral Petrol 151:615–630. https://doi.org/10.1007/s00410-006-0077-4

Schoene B, Bowring SA (2007) Determining accurate temperature–time paths from U–Pb thermochronology: an example from the Kaapvaal craton, southern Africa. Geochim Cosmochim Acta 71:165–185. https://doi.org/10.1016/j.gca.2006.08.029

Schoene B, Crowley JL, Condon DJ, Schmitz MD, Bowring SA (2006) Reassessing the uranium decay constants for geochronology using ID-TIMS U–Pb data. Geochim Cosmochim Acta 70:426–445. https://doi.org/10.1016/j.gca.2005.09.007

Schütte P, Chiaradia M, Beate B (2010) Geodynamic controls on Tertiary arc magmatism in Ecuador: constraints from U–Pb zircon geochronology of Oligocene-Miocene intrusions and regional age distribution trends. Tectonophysics 489:159–176. https://doi.org/10.1016/j.tecto.2010.04.015

Seman S, Stöckli DF, McLean NM (2017) U–Pb geochronology of grossular-andradite garnet. Chem Geol 460:106–116. https://doi.org/10.1016/j.chemgeo.2017.04.020

Seo J, Choi S-G, Kim DW, Park J-W, Oh CW (2015) A new genetic model for the Triassic Yangyang iron-oxide–apatite deposit, South Korea: constraints from in situ U–Pb and trace element analyses of accessory minerals. Ore Geol Rev 70:110–135. https://doi.org/10.1016/j.oregeorev.2015.04.009

Seydoux-Guillaume AM, Wirth R, Nasdala L, Gottschalk M, Montel JM, Heinrich W (2002) An XRD, TEM and Raman study of experimentally annealed natural monazite. Phys Chem Min 29:240–253. https://doi.org/10.1007/s00269-001-0232-4

Seydoux-Guillaume A-M, Wirth R, Deutsch A, Schärer U (2004) Microstructure of 24–1928 Ma concordant monazites; implications for geochronology and nuclear waste deposits. Geochim Cosmochim Acta

68:2517–2527. https://doi.org/10.1016/j.gca.2003.10.042

Shi G, Li X, Li Q, Chen Z, Deng J, Liu Y, Kang Z, Pang E, Xu Y, Jia X (2012) Ion microprobe U–Pb age and Zr-in-rutile thermometry of rutiles from the Daixian rutile deposit in the Hengshan Mountains, Shanxi Province, China. Econ Geol 107:525–535. https://doi.org/10.2113/econgeo.107.3.525

Sillitoe RH (2010) Porphyry copper systems. Econ Geol 105:3–41. https://doi.org/10.2113/gsecongeo.105.1.3

Simon AC, Ripley EM (2011) The role of magmatic sulfur in the formation of ore deposits. Rev Mineral Geochem 73:513–578. https://doi.org/10.2138/rmg.2011.73.16

Singer DA, Berger VI, Moring BC (2008) Porphyry copper deposits of the world: database and grade and tonnage models. US Geol Surv Open File Rep:2008–1155

Skirrow RG, Bastrakov EN, Barovich K, Fraser GL, Creaser RA, Fanning CM, Raymond OL, Davidson GJ (2007) Timing of iron oxide Cu–Au–(U) hydrothermal activity and Nd isotope constraints on metal sources in the Gawler Craton, South Australia. Econ Geol 102:1441–1470

Skirrow RG, Mercadier J, Armstrong R, Kuske T, Deloule É (2016) The Ranger uranium deposit, northern Australia: timing constraints, regional and ore-related alteration, and genetic implications for unconformity-related mineralisation. Ore Geol Rev 76:463–503. https://doi.org/10.1016/j.oregeorev.2015.09.001

Skolodowska Curie M (1898) Rayons émis par les composés de l'uranium et du thorium. C R Acad Sci 126:1101–1103

Smith CB, Allsopp HL, Garvie OG, Kramers JD, Jackson PFS, Clement CR (1989) Note on the U–Pb perovskite method for dating kimberlites: examples from the Wesselton and De Beers mines, South Africa, and Somerset Island, Canada. Chem Geol 79:137–145. https://doi.org/10.1016/0168-9622(89)90016-X

Smith SR, Foster GL, Romer RL, Tindle AG, Kelley SP, Noble SR, Horstwood M, Breaks FW (2004) U–Pb columbite-tantalite chronology of rare-element pegmatites using TIMS and laser ablation-multi collector-ICP-MS. Contrib Mineral Petrol 147:549–564. https://doi.org/10.1007/s00410-003-0538-y

Smith MP, Storey CD, Jeffries TE, Ryan C (2009) In situ U–Pb and trace element analysis of accessory minerals in the Kiruna district, Norrbotten, Sweden: new constraints on the timing and origin of mineralization. J Petrol 50:2063–2094. https://doi.org/10.1093/petrology/egp069

Smye AJ, Roberts NMW, Condon DJ, Horstwood MSA, Parrish RR (2014) Characterising the U–Th–Pb systematics of allanite by ID and LA-ICPMS: implications for geochronology. Geochim Cosmochim Acta 135:1–28. https://doi.org/10.1016/j.gca.2014.03.021

Spandler C, Hammerli J, Sha P, Hilbert-Wolf H, Hu Y, Roberts E, Schmitz M (2016) MKED1: a new titanite standard for in situ analysis of Sm–Nd isotopes and U–Pb geochronology. Chem Geol 425:110–126. https://doi.org/10.1016/j.chemgeo.2016.01.002

Spencer CJ, Kirkland CL, Taylor RJM (2016) Strategies towards statistically robust interpretations of in situ U–Pb zircon geochronology. Geosci Front 7:581–589. https://doi.org/10.1016/j.gsf.2015.11.006

Stacey JS, Kramers JD (1975) Approximation of terrestrial lead isotope evolution by a two-stage model. Earth Planet Sci Lett 26:207–221. https://doi.org/10.1016/0012-821X(75)90088-6

Stelten ME, Cooper KM, Vazquez JA, Calvert AT, Glessner JJG (2015) Mechanisms and timescales of generating eruptible rhyolitic magmas at Yellowstone Caldera from zircon and sanidine geochronology and geochemistry. J Petrol 56:1607–1642. https://doi.org/10.1093/petrology/egv047

Stepanov AS, Hermann J, Rubatto D, Rapp RP (2012) Experimental study of monazite/melt partitioning with implications for the REE, Th and U geochemistry of crustal rocks. Chem Geol 300:200–220. https://doi.org/10.1016/j.chemgeo.2012.01.007

Storey CD, Jeffries TE, Smith M (2006) Common lead-corrected laser ablation ICP–MS U–Pb systematics and geochronology of titanite. Chem Geol 227:37–52

Storey CD, Smith MP, Jeffries TE (2007) In situ LA-ICP-MS U–Pb dating of metavolcanics of Norrbotten, Sweden: records of extended geological histories in complex titanite grains. Chem Geol 240:163–181. https://doi.org/10.1016/j.chemgeo.2007.02.004

Stosch H-G, Romer RL, Daliran F, Rhede D (2010) Uranium–lead ages of apatite from iron oxide ores of the Bafq District, East-Central Iran. Miner Depos 46:9–21. https://doi.org/10.1007/s00126-010-0309-4

Tallarico FHB, McNaughton NJ, Groves DI, Fletcher IR, Figueiredo BR, Carvalho JB, Rego JL, Nunes AR (2004) Geological and SHRIMP II U–Pb constraints on the age and origin of the Breves Cu–Au-(W–Bi–Sn) deposit, Carajás, Brazil. Miner Depos 39:68–86. https://doi.org/10.1007/s00126-003-0383-y

Tapster S, Condon DJ, Naden J, Noble SR, Petterson MG, Roberts NMW, Saunders AD, Smith DJ (2016) Rapid thermal rejuvenation of high-crystallinity magma linked to porphyry copper deposit formation; evidence from the Koloula Porphyry Prospect, Solomon Islands. Earth Planet Sci Lett 442:206–217. https://doi.org/10.1016/j.epsl.2016.02.046

Taylor RD, Goldfarb RJ, Monecke T, Fletcher IR, Cosca MA, Kelly NM (2015) Application of U–Th–Pb phosphate geochronology to young orogenic gold deposits: new age constraints on the formation of the Grass Valley gold district, Sierra Nevada Foothills Province, California. Econ Geol 110:1313–1337. https://doi.org/10.2113/econgeo.110.5.1313

Tera F, Wasserburg GJ (1972a) U–Th–Pb systematics in lunar highland samples from the Luna 20 and Apollo 16 missions. Earth Planet Sci Lett 17:36–51

Tera F, Wasserburg GJ (1972b) U–Th–Pb systematics in three Apollo 14 basalts and the problem of initial Pb in lunar rocks. Earth Planet Sci Lett 14:281–304. https://doi.org/10.1016/0012-821X(72)90128-8

Tiepolo M, Oberti R, Vannucci R (2002) Trace-element incorporation in titanite: constraints from experimentally determined solid/liquid partition coefficients. Chem Geol 191:105–119. https://doi.org/10.1016/S0009-2541(02)00151-1

Tilton GR (1960) Volume diffusion as a mechanism for discordant lead ages. J Geophys Res: Solid Earth 65:2933–2945. https://doi.org/10.1029/JZ065i009p02933

Tilton GR, Patterson C, Brown H, Inghram M, Hayden R, Hess D, Larsen E (1955) Isotopic composition and distribution of lead, uranium, and thorium in a Precambrian granite. Geol Soc Am Bull 66:1131–1148. https://doi.org/10.1130/0016-7606(1955)66[1131:ICADOL]2.0.CO;2

Tilton GR, Davis GL, Wetherill GW, Aldrich LT (1957) Isotopic ages of zircon from granites and pegmatites. Eos T Am Geophys Un 38:360–371. https://doi.org/10.1029/TR038i003p00360

Torrealday HI, Hitzman MW, Stein HJ, Markley RJ, Armstrong R, Broughton D (2000) Re–Os and U–Pb dating of the vein-hosted mineralization at the Kansanshi copper deposit, northern Zambia. Econ Geol 95:1165–1170. https://doi.org/10.2113/gsecongeo.95.5.1165

Trachenko K (2004) Understanding resistance to amorphization by radiation damage. J Phys: Condens Matter 16:R1491–R1515. https://doi.org/10.1088/0953-8984/16/49/R03

Valley PM, Hanchar JM, Whitehouse MJ (2009) Direct dating of Fe oxide-(Cu–Au) mineralization by U/Pb zircon geochronology. Geology 37:223–226. https://doi.org/10.1130/G25439A.1

Valley PM, Fisher CM, Hanchar JM, Lam R, Tubrett M (2010) Hafnium isotopes in zircon: a tracer of fluid-rock interaction during magnetite–apatite ("Kiruna-type") mineralization. Chem Geol 275:208–220. https://doi.org/10.1016/j.chemgeo.2010.05.011

Vallini DA, Groves DI, McNaughton NJ, Fletcher IR (2006) Uraniferous diagenetic xenotime in northern Australia and its relationship to unconformity-associated uranium mineralisation. Miner Depos 42:51–64. https://doi.org/10.1007/s00126-005-0012-z

Van Lichtervelde M, Grand'Homme A, de Saint Blanquat M, Olivier P, Gerdes A, Paquette J-L, Melgarejo JC, Druguet E, Alfonso P (2016) U–Pb geochronology on zircon and columbite-group minerals of the Cap de Creus pegmatites, NE Spain. Miner Petrol:1–21.https://doi.org/10.1007/s00710-016-0455-1

Vermeesch P (2012) On the visualisation of detrital age distributions. Chem Geol 312–313:190–194. https://doi.org/10.1016/j.chemgeo.2012.04.021

Vermeesch P (2018) IsoplotR: a free and open toolbox for geochronology. Geosci Front 9:1479–1493. https://doi.org/10.1016/j.gsf.2018.04.001

Vielreicher NM, Groves DI, Snee LW, Fletcher IR, McNaughton NJ (2010) Broad synchroneity of three gold mineralization styles in the Kalgoorlie Gold Field: SHRIMP, U–Pb, and $^{40}Ar/^{39}Ar$ geochronological evidence. Econ Geol 105:187–227. https://doi.org/10.2113/gsecongeo.105.1.187

Vielreicher N, Groves D, McNaughton N, Fletcher I (2015) The timing of gold mineralization across the eastern Yilgarn craton using U–Pb geochronology of hydrothermal phosphate minerals. Miner Depos 50:391–428. https://doi.org/10.1007/s00126-015-0589-9

von Grosse A (1932) On the origin of the actinium series of radioactive elements. Phys Rev 42:565–570. https://doi.org/10.1103/PhysRev.42.565

von Quadt A, Moritz R, Peytcheva I, Heinrich CA (2005) 3: Geochronology and geodynamics of Late Cretaceous magmatism and Cu–Au mineralization in the Panagyurishte region of the Apuseni–Banat–Timok–Srednogorie belt, Bulgaria. Ore Geol Rev 27:95–126. https://doi.org/10.1016/j.oregeorev.2005.07.024

von Quadt A, Erni M, Martinek K, Moll M, Peytcheva I, Heinrich CA (2011) Zircon crystallization and the lifetimes of ore-forming magmatic-hydrothermal systems. Geology 39:731–734. https://doi.org/10.1130/G31966.1

von Quadt A, Gallhofer D, Guillong M, Peytcheva I, Waelle M, Sakata S (2014) U–Pb dating of CA/non-CA treated zircons obtained by LA-ICP-MS and CA-TIMS techniques: impact for their geological interpretation. J Anal at Spectrom 29:1618–1629. https://doi.org/10.1039/C4JA00102H

Vry JK, Baker JA (2006) LA-MC-ICPMS Pb–Pb dating of rutile from slowly cooled granulites: confirmation of the high closure temperature for Pb diffusion in rutile. Geochim Cosmochim Acta 70:1807–1820. https://doi.org/10.1016/j.gca.2005.12.006

Wall CJ, Scoates JS (2016) High-precision U–Pb zircon-baddeleyite dating of the J-M reef platinum group element deposit in the Stillwater Complex, Montana (USA). Econ Geol 111:771–782. https://doi.org/10.2113/econgeo.111.3.771

Wan B, Xiao W, Zhang L, Han C (2012) Iron mineralization associated with a major strike–slip shear zone: radiometric and oxygen isotope evidence from the Mengku deposit, NW China. Ore Geol Rev 44:136–147. https://doi.org/10.1016/j.oregeorev.2011.09.011

Wanhainen C, Billström K, Martinsson O, Stein H, Nordin R (2005) 160 Ma of magmatic/hydrothermal and metamorphic activity in the Gällivare area: Re–Os dating of molybdenite and U–Pb dating of titanite from the Aitik Cu–Au–Ag deposit, northern Sweden. Miner Depos 40:435–447

Watson EB, Chemiak DJ, Hanchar JM, Harrison TM, Wark DA (1997) The incorporation of Pb into zircon. Chem Geol 141:19–31. https://doi.org/10.1016/S0009-2541(97)00054-5

Webber GR, Hurley PM, Fairbairn HW (1956) Relative ages of eastern Massachusetts granites by total lead ratios in zircon. Am J Sci 254:574–583. https://doi.org/10.2475/ajs.254.9.574

Webster JD, Piccoli PM (2015) Magmatic apatite: a powerful, yet deceptive, mineral. Elements 11:177–182. https://doi.org/10.2113/gselements.11.3.177

Weis P, Driesner T, Heinrich CA (2012) Porphyry-copper ore shells form at stable pressure-temperature fronts within dynamic fluid plumes. Science 338:1613–1616. https://doi.org/10.1126/science.1225009

Wendt I (1984) A three-dimensional U–Pb discordia plane to evaluate samples with common lead of unknown isotopic composition. Chem Geol 46:1–12. https://doi.org/10.1016/0009-2541(84)90162-1

Wendt I, Carl C (1991) The statistical distribution of the mean squared weighted deviation. Chem Geol 86:275–285. https://doi.org/10.1016/0168-9622(91)90010-T

Wetherill GW (1956) Discordant uranium-lead ages, I. Eos T Am Geophys Un 37:320–326. https://doi.org/10.1029/TR037i003p00320

White LT, Ireland TR (2012) High-uranium matrix effect in zircon and its implications for SHRIMP U–Pb age determinations. Chem Geol 306–307:78–91. https://doi.org/10.1029/2011GC003726

Widmann P, Davies JHFL, Schaltegger U (2019) Calibrating chemical abrasion_ Its effects on zircon crystal structure, chemical composition and UPb age. Chem Geol 511:1–10. https://doi.org/10.1016/j.chemgeo.2019.02.026

Wingate MTD, Compston W (2000) Crystal orientation effects during ion microprobe U–Pb analysis of baddeleyite. Chem Geol 168:75–97. https://doi.org/10.1016/S0009-2541(00)00184-4

Woodhead JD, Hergt JM, Simonson BM (1998) Isotopic dating of an Archean bolide impact horizon, Hamersley basin, Western Australia. Geology 26:47–50. https://doi.org/10.1130/0091-7613(1998)026%3c0047:IDOAAB%3e2.3.CO;2

Wotzlaw JF, Schaltegger U, Frick DA, Dungan MA, Gerdes A, Günther D (2013) Tracking the evolution of large-volume silicic magma reservoirs from assembly to supereruption. Geology 41:867–870. https://doi.org/10.1130/G34366.1

Wotzlaw J-F, Bindeman IN, Watts KE, Schmitt AK, Caricchi L, Schaltegger U (2014) Linking rapid magma reservoir assembly and eruption trigger mechanisms at evolved Yellowstone-type supervolcanoes. Geology 42:807–810

Wotzlaw J-F, Bindeman IN, Stern RA, D'Abzac F-X, Schaltegger U (2015) Rapid heterogeneous assembly of multiple magma reservoirs prior to Yellowstone supereruptions. Sci Rep 5:14026. https://doi.org/10.1038/srep14026

Wu F-Y, Yang Y-H, Li Q-L, Mitchell RH, Dawson JB, Brandl G, Yuhara M (2011) In situ determination of U–Pb ages and Sr–Nd–Hf isotopic constraints on the petrogenesis of the Phalaborwa carbonatite Complex, South Africa. Lithos 127:309–322

Wu F-Y, Arzamastsev AA, Mitchell RH, Li Q-L, Sun J, Yang Y-H, Wang R-C (2013a) Emplacement age and Sr–Nd isotopic compositions of the Afrikanda alkaline ultramafic complex, Kola Peninsula, Russia. Chem Geol 353:210–229. https://doi.org/10.1016/j.chemgeo.2012.09.027

Wu F-Y, Mitchell RH, Li Q-L, Sun J, Liu C-Z, Yang Y-H (2013b) In situ U–Pb age determination and Sr–Nd isotopic analysis of perovskite from the Premier (Cullinan) kimberlite, South Africa. Chem Geol 353:83–95. https://doi.org/10.1016/j.chemgeo.2012.06.002

Yang W-B, Niu H-C, Shan Q, Sun W-D, Zhang H, Li N-B, Jiang Y-H, Yu X-Y (2013) Geochemistry of magmatic and hydrothermal zircon from the highly evolved Baerzhe alkaline granite: implications for Zr–REE–Nb mineralization. Miner Depos 49:451–470. https://doi.org/10.1007/s00126-013-0504-1

York D (1968) Least squares fitting of a straight line with correlated errors. Earth Planet Sci Lett 5:320–324. https://doi.org/10.1016/S0012-821X(68)80059-7

Yuan S, Peng J, Hao S, Li H, Geng J, Zhang D (2011) In situ LA-MC-ICP-MS and ID-TIMS U–Pb geochronology of cassiterite in the giant Furong tin deposit, Hunan Province, South China: new constraints on the timing of tin–polymetallic mineralization. Ore Geol Rev 43:235–242. https://doi.org/10.1016/j.oregeorev.2011.08.002

Zack T, Stockli DF, Luvizotto GL, Barth MG, Belousova E, Wolfe MR, Hinton RW (2011) In situ U–Pb rutile dating by LA-ICP-MS: $^{208}$Pb correction and prospects for geological applications. Contrib Mineral Petrol 162:515–530. https://doi.org/10.1007/s00410-011-0609-4

Zartman RE, Smith JV (2009) Mineralogy and U–Th–Pb age of a uranium-bearing jasperoid vein, Sunshine Mine, Coeur d'Alene district, Idaho, USA. Chem Geol 261:185–195. https://doi.org/10.1016/j.chemgeo.2008.09.006

Zeh A, Ovtcharova M, Wilson AH, Schaltegger U (2015) The Bushveld Complex was emplaced and cooled in less than one million years—results of zirconology, and geotectonic implications. Earth Planet Sci Lett 418:103–114. https://doi.org/10.1016/j.epsl.2015.02.035

Zhang D, Zhang Z, Santosh M, Cheng Z, He H, Kang J (2013) Perovskite and baddeleyite from kimberlitic intrusions in the Tarim large igneous province signal the onset of an end-Carboniferous mantle plume. Earth Planet Sci Lett 361:238–248. https://doi.org/10.1016/j.epsl.2012.10.034

Zhang D, Peng J, Coulson IM, Hou L, Li S (2014) Cassiterite U–Pb and muscovite $^{40}$Ar–$^{39}$Ar age constraints on the timing of mineralization in the Xuebaoding Sn–W–Be deposit, western China. Ore Geol Rev 62:315–322. https://doi.org/10.1016/j.oregeorev.2014.04.011

Zi J-W, Rasmussen B, Muhling JR, Fletcher IR, Thorne AM, Johnson SP, Cutten HN, Dunkley DJ, Korhonen FJ (2015) In situ U–Pb geochronology of xenotime and monazite from the Abra polymetallic deposit in the Capricorn Orogen, Australia: dating hydrothermal mineralization and fluid flow in a long-lived crustal structure. Precambrian Res 260:91–112. https://doi.org/10.1016/j.precamres.2015.01.010